BIFURCATION AND STABILITY ANALYSIS OF MULTIPLE MOLAR VOLUME ROOTS FOR STATISTICAL ASSOCIATING FLUID THEORY

BY

Isa Ataallah Saeed Al Aslani

A Thesis Presented to the
DEANSHIP OF GRADUATE STUDIES

KING FAHD UNIVERSITY OF PETROLEUM & MINERALS

DHAHRAN, SAUDI ARABIA

In Partial Fulfillment of the
Requirements for the Degree of

MASTER OF SCIENCE

In

CHEMICAL ENGINEERING

May 2015

KING FAHD UNIVERSITY OF PETROLEUM & MINERALS

DHAHRAN- 31261, SAUDI ARABIA

DEANSHIP OF GRADUATE STUDIES

This thesis, written by **Isa Ataallah Saeed Al Aslani** under the direction his thesis advisor and approved by his thesis committee, has been presented and accepted by the Dean of Graduate Studies, in partial fulfillment of the requirements for the degree of **MASTER OF SCIENCE IN CHEMICAL ENGINEERING.**

Dr. Nayef M. Al-Saifi
(Advisor)

Dr. Mohammed Ba-Shammakh
Department Chairman

Dr. Housam Binous
(Member)

Dr. Salam A. Zummo
Dean of Graduate Studies

Dr. Nabeel Salim M. Abo-Ghander
(Member)

27/12/15

Date

Dedicated to my parents

and

to my wife

ACKNOWLEDGMENTS

I express my deep acknowledgment to my master thesis advisor Dr. Nayef Al-Saifi for his guidance throughout the whole work. I appreciate his teaching of statistical association fluid theory and improving of my technical writing skills. He encouraged me to do my best in each part of my thesis. I also appreciate Dr. Housam Binous for his valuable information regarding the application of arc-length continuation method using Mathematica©. I would like to thank Dr. Nabeel Abo-Ghander for his valuable comments in the bifurcation analysis and the write-up of my thesis.

I am grateful to the Deanship of Graduate Studies at King Fahd University of Petroleum and Minerals for its scholarship to do my master degree.

I would like to thank all the faculty members of chemical engineering department for their cooperation and encouragement. I also thank all of my colleagues for nice study environment.

TABLE OF CONTENTS

LIST OF TABLES

LIST OF FIGURES

NOMENCLATURE

Abbreviations

CK-SAFT	Chen and Kreglewski SAFT
PC-SAFT	Perturbed-Chain SAFT
SAFT	statistical association fluid theory
EOS	equation of state

Symbols

a	energy term parameter or Helmholtz energy
b	co-volume parameter (l/mol)
d	temperature dependent parameter
g	radial distribution function
K	chemical equilibrium constant
m	segment number
N_A	Avogadro's number
n_T	true number of moles
n_0	apparent number of moles
P	pressure (bar)
Q	partition function
R	gas constant (atm cm^3/mol/K)
T	temperature (K)
V	molar volume (cm^3/mol)

X_A	fraction of not bonded molecules
v^{00}	segment volume (ml/mol)
k	Boltzmann constant (J/K)

Greek letters

$\Gamma(r)$	potential energy distance function
Δ	association strength
ε	dispersion energy parameter
ζ	partial volume fraction
η	reduced density
κ	association volume
ρ	molar density (mol/cm^3)
σ	segment diameter
ω	acentric factor

Superscripts

A	site A
B	site B
hc	hard chain
hs	hard sphere
i	component index
j	component index
ref	reference
res	residual

rep	repulsive
sat	saturated
seg	segment

Subscripts

c	critical

ABSTRACT

Full Name : Isa Ataallah Saeed Al Aslani

Thesis Title : BIFURCATION AND STABILITY ANALYSIS OF MULTIPLE MOLAR VOLUME ROOTS FOR STATISTICAL ASSOCIATING FLUID THEORY

Major Field : Chemical Engineering

Date of Degree : May 2015

The determination of correct stable molar volume roots is a crucial step in the calculations of thermodynamic properties and phase behavior. Many theory-based EOSs exhibit more than three molar volume roots at specific state condition. The main challenge is not only limited on how to determine and test the stability of the multiple density roots but also on how to provide a simple procedure that is practical to implement into process simulators. In this study, the locus of all multiple molar volume roots of CK-SAFT, simplified SAFT, soft SAFT and PC-SAFT EOSs is investigated over a broad range of temperatures and pressures. This thesis illustrates how the number of multiple molar volume roots varies when the chain term is added to the model. It is illustrated that the number of multiple molar volume roots could exceed the number reported in previous studies. This thesis reveals that it is possible to avoid the complication arising in the calculation of multiple molar volume roots in PC-SAFT EOS without the need to determine all multiple molar volume roots.

ملخص الرسالة

الاسم الكامل: عيسى عطاالله سعيد العصلاني

عنوان الرسالة: التحليل التفريعي والاستقراري لتعدد حلول الحجم المولي في نظرية الترابط الإحصائي للموائع

التخصص: الهندسة الكيميائية

تاريخ الدرجة العلمية: مايو 2015

يعتبر تحديد الحلول الصحيحة والمستقرة للحجم المولي خطوة حاسمة لحساب خصائص الديناميكا الحرارية وحسابات السلوك المرحلي. العديد من المعادلات النظرية للحالة تعرض أكثر من ثلاثة حلول للحجم المولي في ظروف محددة. التحدي الأهم لا يكمن في كيفية حساب ومعرفة الحل الصحيح للحجم المولي ولكن في تقديم طريقة مبسطة وقابلة للتطبيق في برامج المحاكاة تسهل الوصول للحل الصحيح للحجم المولي بدون الحاجة إلى معرفة كل الحلول ومن ثم معرفة الحل الصحيح باستخدام التحليل الاستقراري. في هذه الدراسة، تم تتبع كل الحلول المتعددة للحجم المولي في معادلات الحالة CK-SAFT و soft SAFT و simplified SAFT و PC-SAFT على مدى واسع من درجات الحرارة والضغط. تم توضيح كيفية تأثر الحلول عند إضافة الحد التسلسلي للمعادلة. تم أيضاً توضيح إمكانية تجاوز عدد حلول الحجم المولي للرقم الموثق في بعض الدراسات المنشورة. تم كشف إمكانية تجاوز الصعوبات الحاصلة بسبب تعدد حلول الحجم المولي بدون الحاجة لتحديد كل الحلول في معادلة الحالة PC-SAFT .

CHAPTER 1

INTRODUCTION

1.1 Motivation

The thermodynamic properties and phase behavior of simple fluids have extensively been studied during the last fifty years because of their importance in chemical industry. They are called “simple” because the only dominant forces acting among their molecules are dispersion and repulsion (Muller and Gubbins, 2001). These accurate properties are vital for the optimization of industrial processes and newly designed equipment as more novel process and materials are being developed (Economou, 2002). There are many engineering EOSs that could be applied for simple fluids such as Peng-Robinson EOS (Peng and Robinson, 1976). However, these EOSs cannot accurately predict the thermodynamic properties of many fluids such as polar solvents. This is because polar interactions and other intermolecular forces are not included in those equations. For this reason, a new approach is needed to account for various intermolecular forces to predict accurate properties (Muller and Gubbins, 2001).

The substantial improvement in statistical mechanics helps to determine accurate properties by studying various molecular interactions among molecules other than dispersion and repulsion. It has led also to a number of EOSs such as the lattice fluid theory (LFT) (Sanchez and Lacombe, 1976) and the perturbed hard-chain theory

(Donohue and Prausnitz, 1978). These EOSs are considerably more accurate when applied for complex fluids such as hydrogen bonding fluids, polymers, polar and supercritical fluids. However, these EOSs are more complex than cubic EOSs. Fortunately, the incredible rise of computing ability at reasonable costs made these EOSs promising for process simulation calculations (Economou, 2002).

One of the statistical mechanical theories that facilitates the study of different kinds of molecules is Wertheim's thermodynamic perturbation theory (Wertheim, 1984a; Wertheim, 1984b; Wertheim, 1986a; Wertheim, 1986b). Based on Wertheim first order thermodynamic perturbation theory, Chapman et al. (1988; 1989b; 1990) proposed statistical association fluid theory (SAFT) which is currently considered as one of the most popular EOSs. It gains wide acceptance in academic research and industry. Many SAFT versions have been proposed over the past years due to the selection of different pair potentials and perturbation terms in the EOS such as CK-SAFT (Haung and Radosz, 1990), simplified SAFT (Fu and Sandler, 1995), soft SAFT (Blas and Vega, 1997) and perturbed-chain SAFT (PC-SAFT) (Gross and Sadowski, 2001).

Although the SAFT EOS has illustrated noteworthy success in predicting thermodynamic properties, some problems have not been fully resolved. . For instance, some SAFT versions exhibit two phase-separation and three critical demixing regions (Yelash et al., 2005). The problem of multiple mechanically stable critical points was also noted by Segura et al (2003). Another problem is related to the accuracy of predicting the second derivative thermodynamic properties where the SAFT has illustrated incorrect physical behavior (Polishuk, 2011; Polishuk and Mulero, 2011). Furthermore, the SAFT

EOS experiences a problem in exhibiting non-physical multiple density roots at specific temperature and pressure as indicated by (Koak et al., 1999).

The resolution of all the previous problems is a challenging task and it depends on the utilized SAFT version. For example, some SAFT versions have not illustrated the two phase-separation problem (Lafitte et al., 2013). However, all SAFT versions exhibit unphysical multiple density roots. The selection of incorrect volume roots would lead to error in the calculation of phase equilibrium and thermodynamic properties. In order to implement SAFT in process simulator, it is very crucial to provide a reliable procedure for selecting the correct density roots. The work on this thesis sheds light on this problem.

The problem of multiple density roots problem exists in SAFT EOS due to the complex mathematical terms (Aslam and Sunol, 2006; Koak et al., 1999; Lucia and Luo, 2002; Xu et al., 2002). For instance, the dispersion term in CK-SAFT was constructed based on a power series of 28 terms. The unphysical density roots were attributed to this dispersion term (Koak et al., 1999). In the simplified SAFT, the mathematical form of the compressibility factor expression is a polynomial of order seven for pure components and nine for mixtures (Lucia and Luo, 2002). The complex mathematical expressions are also noted in PC-SAFT and soft-SAFT EOSs where empirical expressions were utilized to construct the dispersion terms which are function of density. The empirical nature of these terms would eventually lead to unphysical multiple density roots.

Several studies have been conducted to illustrate the multiplicity of roots for specific state conditions. Koak et al. (1999) was perhaps the first to address this problem.

Based on CK-SAFT EOS, they found that the SAFT EOS might exhibit more than three density roots and some of them exceed the maximum value of packing fraction which is 0.74048. Surprisingly, they also found that the non-physical density root might be mechanically stable. For associating mixtures, Xu et al. (2002) found that the CK-SAFT exhibits three density roots for 1-butanol-ethanol system at 343 K and 0.35 bar. When ethanol-acetic acid system was studied at 308 K and 0.02664 bar, the number of density roots was four. Privat et al. (2010) reported a maximum of five density roots using PC-SAFT EOS by studying n-decane at 135 K and 0.01 bar. As will be illustrated later in **Chapter 5**, the number of roots might reach nine with three negative roots at this state condition. This indicates that caution should be exercised if any method is utilized to determine the multiple density roots.

One proposed way to resolve the problem of multiple density roots is to utilize a reliable numerical technique that is capable to determine all roots. This method was reported in several studies (Alsaifi and Englezos, 2011; Aslam and Sunol, 2006; Lucia and Luo, 2002; Privat et al., 2010; Xu et al., 2002). Interval analysis method by Xu et al. (2002) is one example of such a method but it is not appropriate to use in process simulators because it needs special computing environment. Aslam and Sunol (2006) have used a global fixed-point homotopy continuation algorithm to find all roots. However, the use of a reliable numerical technique doesn't explain how the number of multiple roots changes when the state conditions of pressure and temperature vary. Aslam and Sunol (2006) stated that if continuation method is properly implemented, all the solutions on nonlinear equations will be computed. Privat et al. (2010) proposed a procedure to identify all the possible volume roots of EOSs. Then, the correct molar

volumes were selected based on stability tests. Although their study provided a valuable procedure to identify all multiple volumes, the procedure was limited to specific state conditions. Furthermore, as will be illustrated later, at some specific state conditions, the number of molar volumes might be higher than what was reported in their study.

Furthermore, the effect of each SAFT term on the number of molar volume roots has not been totally explored. The main focus was mainly on hard sphere, chain and dispersion terms. Polishuk (2010) investigated the effect of the chain term on the polynomial order for many versions of SAFT EOS. The number is increased by one in simplified SAFT, original SAFT and CK-SAFT EOSs after the chain term is added while the order number is found to be increased by 5 in simplified PC-SAFT EOS. In this thesis, different SAFT versions will be utilized with the emphasis on PC-SAFT EOS. Chapter 2 will give a detailed description of different SAFT versions.

In this work, a systematic study is conducted to study the effect of adding the chain term in the SAFT EOS and its effect on the multiple volume roots.

1.2 Thesis Objectives

The ultimate objective of the work is to contribute to the computation related to statistical association fluid theory EOS. The specific objectives of this work are: 1) To determine all solution branches of multiple volume roots of the PC-SAFT, CK-SAFT, soft SAFT and simplified SAFT EOSs using arc-length continuation method to generate bifurcation diagrams by showing how molar volumes vary with temperature at different constant pressures.

2) To study the bifurcation diagrams for PC-SAFT, CK-SAFT, soft SAFT and simplified SAFT EOSs to investigate the number of roots, branches and turning points.

3) To study the effect of adding the chain term on the zero-locus of multiple volume roots by generating bifurcation diagrams.

4) To study stability of bifurcation diagrams.

5) To construct a simple strategy that would assist in the determination of the number of multiple volume roots when state conditions of pressure and temperature are selected.

1.3 Thesis Organization

The thesis has six chapters. The purpose of each chapter is illustrated as follows:

Chapter 2 is dedicated to provide the needed theoretical and historical background of the presented models in this thesis.

Chapter 3 gives an introduction about the two types of analysis used in the thesis, namely, bifurcation and stability analysis.

Chapter 4 illustrates the results generated by the analysis described in **Chapter 3** for the case where the chain effect is neglected.

Chapter 5 presents the results in the same way of the **Chapter 4** but with taking the effect of the chain term.

In **Chapter 6**, simple guidelines are given to track the physical roots in PC-SAFT EOS.

CHAPTER 2

Statistical Association Fluid Theory

2.1 Introduction

In the first section of **Chapter 1**, the importance of developing new approaches for predicting accurate thermodynamic properties and phase behavior was presented. The role of statistical mechanics and computing ability in the existence of applicable complex models were illustrated. The theoretical foundation of SAFT EOSs was stated. Multiplicity of volume roots was raised as one of the problems needed to be solved in order to avoid the selection of unrealistic volume roots. The complexity of the mathematical terms was considered as the reason of this problem. Several studies were illustrated in which multiple roots were reported at specific state conditions. As illustrated in the previous chapter, some of these studies suggested using reliable numerical techniques to determine all the roots at any state condition. However, these techniques are unable to explain how the number of roots is changing with the change of temperature or pressure as was discussed. Moreover, the effect of each term on the number of roots is not totally explored as was stated.

In this chapter, historical and theoretical background for the models presented in this thesis is provided. In section 2.2, the development and formulation of EOSs is described starting by simple relationships among molar volume, pressure and temperature through cubic EOSs then ending by association theories. The first sub-section describes

the two simplest relationships of Boyles and Charles (Sandler, 1993). The second subsection is dedicated to show the formulation of cubic EOSs of van der Waals, Redlich-Kwong (Redlich and Kwong, 1949), Soave-Redlich-Kwong (Soave, 1972) and Peng-Robinson (Peng and Robinson, 1976). The last subsection described the association theories having three sub-sections for chemical association theory, quasi-chemical association theory and perturbation theory. The latter is the platform of SAFT. In section 2.3, SAFT terms and molecular shape are briefly introduced. In section 2.4, the adjustable parameters characterizing each component in SAFT EOSs are also briefly introduced. In section 2.5, the formulation of each SAFT term along with the differences among some popular SAFT versions is described. In section 2.5.1, the chain term is described. In section 2.5.2, the association term is described. In section 2.5.3, the segment term is described including the repulsive and attractive terms. In section 2.6, PC-SAFT EOS is emphasized because of its popularity. In section 2.7, the conclusion of this chapter is stated.

2.2 Equations of state

An equation of state (EOS) can be referred as the relationship among pressure, temperature and molar volume. It has a critical importance in chemical engineering design. To apply it for a mixture, a mixing rule should be used to take into account the new added variable which is the composition (Ramdharee et al., 2013).

2.2.1 Boyle and Charles Relationships

The first EOS was reported by Boyle in 1662 in which the relation between pressure and molar volume of the gas is an inversely proportional relation (Boyle, 1772; Ramdharee et al., 2013):

$$PV = constant \tag{2.1}$$

In 1787, a relation was developed to be proportional between the volume and temperature at fixed pressure by Charles (Ramdharee et al., 2013). These two equations were combined to form the ideal gas law relation (Sandler, 1993):

$$PV = RT \tag{2.2}$$

or

$$Z = \frac{PV}{RT} = 1 \tag{2.3}$$

where R is the gas constant and Z is the compressibility factor.

The previous equation is limited to low pressure and does not predict the saturation point where the two phases of vapor and liquid are present.

2.2.2 Cubic Equations of State

These EOSs are called “cubic” because when they are converted into polynomials, they show a polynomial of order of three in volume. The first cubic EOS which provides a major improvement was proposed by van der Waals in 1873. This EOS

was qualitatively able to describe the phase behavior of pure components and mixtures. The expression of this cubic EOS was given by van der Waals (1889):

$$P = \frac{RT}{(V-b)} - \frac{a}{V^2} \tag{2.4}$$

with

$$a = \frac{27}{64}\left(\frac{R^2\,T_c^2}{P_c}\right), b = \frac{1}{8}\left(\frac{RT_c}{P_c}\right) \tag{2.5}$$

where a is the attraction parameter and b is the repulsion parameter or the excluded volume which is the volume occupied by the other molecules (Ramdharee et al., 2013; Sandler, 1993).

Many modifications have been conducted on the previous expression to improve the accuracy of its prediction. The general form can be given by (Valderrama, 2003):

$$P = \frac{RT}{(V-b)} - P_{att}(T,V) \tag{2.6}$$

with

$$P_{att}(T,V) = \frac{a}{V(V+d)+c(V-d)} \tag{2.7}$$

where a, b, c and d are constants or it can be functions in terms of some fluid properties.

The most successful improvement after the van der Waals cubic EOS was proposed by Redlich and Kwong in 1949 with the introduction of a temperature dependent attraction parameter (Ramdharee et al., 2013). The Redlich-Kwong EOS is expressed as:

$$P = \frac{RT}{(V-b)} - \frac{a/\sqrt{T}}{V(V+b)} \tag{2.8}$$

with

$$a = 0.42748\left(\frac{R^2\,T_c^{2.5}}{P_c}\right), b = 0.08664\left(\frac{RT_c}{P_c}\right) \tag{2.9}$$

This EOS was formed primary to be accurate for gases only (Valderrama, 2003). To account of the non-spherical shape of molecules, Pitzer (1955) introduced the acentric factor. The acentric factor was implemented in the Redlich-Kwong cubic EOS by Soave (1972):

$$P = \frac{RT}{(V-b)} - \frac{a\,\alpha(T_r,\omega)}{V(V+b)} \tag{2.10}$$

with

$$a = 0.42748\left(\frac{R^2\,T_c^2\,\alpha(T_r,\omega)}{P_c}\right), b = 0.08664\left(\frac{RT_c}{P_c}\right) \tag{2.11}$$

where

$$\alpha(T_r,\omega) = \left(1+\kappa\left(1-\sqrt{T_r}\right)\right)^2, \kappa = 0.48 + 1.574\omega - 0.176\omega^2 \tag{2.12}$$

This cubic EOS can predict accurately the behavior of both vapor and liquid phases. It is a popular cubic EOS and applied successfully in hydrocarbon industry (Ramdharee et al., 2013; Valderrama, 2003).

Peng and Robinson (1976) improved the $\alpha(T_r,\omega)$ function and the volume dependency on the attraction term to give more accurate results; particularly for liquid

densities. The expression of Peng-Robinson cubic EOS is given by (Peng and Robinson, 1976; Valderrama, 2003):

$$P = \frac{RT}{(V-b)} - \frac{a\,\alpha(T_r,\omega)}{V(V+b)+b(V-b)} \tag{2.13}$$

with

$$a = 0.45724\left(\frac{R^2\,T_c^2\,\alpha(T_r,\omega)}{P_c}\right), b = 0.07780\left(\frac{RT_c}{P_c}\right) \tag{2.14}$$

where

$$\alpha(T_r,\omega) = \left(1+\kappa\left(1-\sqrt{T_r}\right)\right)^2, \kappa = 0.37464 + 1.54226\omega - 0.26992\omega^2 \tag{2.15}$$

In the previous models, all the modifications were concentrated on the attractive term in the EOSs. However, at high pressure, the repulsive effect is dominant and the van der Walls repulsive form is not accurate. A more accurate repulsive term was proposed by Carnhan-Starling (1969). It is the most well-known repulsive term and has a theory-based development:

$$Z^{rep} = \frac{1+y+y^2-y^3}{(1-y)^3} \tag{2.16}$$

where

$$y = \frac{b}{4\,V} \tag{2.17}$$

If Carnahan-Starling term is utilized to replace the repulsive term in cubic EOSs, the resulted equation is not any more cubic in molar volume.

2.2.3 Association Theories

2.2.3.1 Introduction

The prediction of the phase behavior and thermodynamic properties of associating species properties such as water, alcohols and amines cannot accurately be obtained by cubic EOSs. This is because cubic EOSs take into consideration only dispersion attractive forces. To account of associative interactions, two approaches are usually followed. The first approach is to adjust the form and/or parameters of non-associating fluid to be applicable for associating fluids then apply the mixing rules for mixtures. So, there is no prior estimation to the properties unless large and condition-dependent parameters are generated which is not always easy to do. The second recent approach is to show these chemical reactions and bond in an explicit way with little adjustable parameters. This approach is known by the "association theories" (Economou and Donohue, 1991; Economou and Donohue, 1996; Kontogeorgis and Folas, 2009; Sandler, 1993).

There are three types of associating theories. The first one deals with the hydrogen bonding as "new species" of more than one monomer to form dimer or oligomers which are formed as a function of composition, temperature, density and composition. This type is called "chemical" associating theory where the material balance equations are simultaneously solved with the chemical equilibrium. The extent of association is defined by the number of dimers or oligomers. The second approach is based on the lattice-fluid theory which is called "quasi-chemical" associating theory. It accounts for the number of chemical bonds among segment of different adjacent molecules sites. The extent of association is defined by the number of bonds. The third

one is based on the calculation of the total energy of the hydrogen bonding from statistical mechanics. This approach is done by solving many integral equations through potential functions that simulate the hydrogen bonding between two sites. A molecule is characterized by the number of bonding sites. The latter is called "perturbation" associating theory. The associating theories are expressing the compressibility factor often as follows (Economou and Donohue, 1991; Economou and Donohue, 1996; Kontogeorgis and Folas, 2009; Sandler, 1993):

$$Z = Z^{phys} + Z^{assoc} \tag{2.18}$$

2.2.3.2 Chemical Association Theory

As discussed before, this theory is based on the forming of new species and the extent of association which depends on the number of oligomers formed. To have a brief overlook to the formulation of this theory, assume a component M which has two bonding sites. Then the resulted form is a chain regardless of the numbers of monomers. The chemical equilibrium will be in the following form (Economou and Donohue, 1991):

$$M_1 + M_1 \leftrightarrow M_2$$

$$M_2 + M_1 \leftrightarrow M_3$$

$$\vdots$$

$$M_i + M_1 \leftrightarrow M_{i+1}$$

Hence, there will be two kinds of number of moles. The first kind is the true number of moles denoted by n_T which consider any collection of monomers as one species or

oligomer. The other kind is the superficial number of moles which is the number of moles in case of monomers only, i.e. with no association denoted by n_0 (Economou and Donohue, 1991). The two numbers of moles can be calculated through the following expressions:

$$n_T = n_1 + n_2 + n_3 + \cdots + n_i = \sum_i^{\infty} n_i \tag{2.19}$$

$$n_0 = n_1 + 2n_2 + 3n_3 + \cdots + in_i = \sum_i^{\infty} in_i \tag{2.20}$$

where n_i is the number of moles of oligomer of i monomers.

There are two approaches in the chemical associating theory. The first approach was done by Heidemann and Prausnitz (1976) and the other by Anderko (1991). In the latter approach, the compressibility factor is illustrated as follows (Kontogeorgis and Folas, 2009):

$$Z = Z^{phys} + Z^{assoc} = Z^{phys} + Z^{chem} - 1 = Z^{attr} + Z^{rep} + \frac{n_T}{n_0} - 1 \tag{2.21}$$

with

$$Z^{chem} = \frac{n_T}{n_0} = \frac{2}{1 + \sqrt{1 + 4\rho KRT}} \tag{2.22}$$

where T is the absolute temperature (K), ρ is the density, R is the gas constant and K is the equilibrium constant which is in the form of:

$$K = exp\left(-\frac{\Delta H^o}{RT} + \frac{\Delta S^o}{R}\right) \tag{2.23}$$

where ΔH^o is the standard enthalpy of association and ΔS^o is the standard entropy of association.

The repulsive and attraction terms are adopted from the three-parameter cubic EOS given by:

$$Z^{rep} = \frac{\eta}{1-\eta} \tag{2.24}$$

$$Z^{attr} = -\frac{a}{bRT}\frac{\eta}{1+\eta(d/b+3)+\eta^2\, d/b} \tag{2.25}$$

The other approach which is the Heidemann and Prausnitz one has the following expression of compressibility factor (Kontogeorgis and Folas, 2009):

$$Z = Z^{attr} + Z^{chem} Z^{rep} \tag{2.26}$$

where

$$Z^{chem} = \frac{n_T}{n_0} = \frac{2}{1+\sqrt{1+4\rho KRTe^g}} \tag{2.27}$$

with

$$g = \int_0^{\eta} \left(\frac{Z^{rep}-1}{\eta}\right) d\eta \tag{2.28}$$

where

$$\eta = \frac{b}{V} \tag{2.29}$$

In this approach, the repulsive term is the expression of Carnahan-Starling:

$$Z^{rep} = -\frac{\eta(4-2\eta)}{(1-\eta)^3} \tag{2.30}$$

The attraction term is the van der Waals attractive term:

$$Z^{attr} = -\frac{a}{bRT}\eta(1-4\eta) \tag{2.31}$$

2.2.3.3 Quasi-Chemical Association Theory

This approach was introduced first by Guggenheim in 1945, but the hydrogen bonding cannot be distinguished alone form the polar interactions in his EOS (Economou and Donohue, 1991; Guggenheim, 1945).

Panayiotou and Sanchez (1991) developed a statistical model which takes into account the hydrogen bonding separately. This model has a relationship between with the chemical and quasi-chemical associating theories. This model has divided the intermolecular forces into chemical (hydrogen bonding) and physical (van der Waals). This model can be described as (Economou and Donohue, 1991; Panayiotou and Sanchez, 1991):

$$Q = Q^{phys}Q^{assoc} \tag{2.32}$$

where Q is the partition function.

The physical term is adopted from the work of (Sanchez and Lacombe, 1976). The association term is calculated by knowing the total number of hydrogen bonds distribution (Economou and Donohue, 1991). For most cases, one proton acceptor and one proton donor are assumed (Kontogeorgis and Folas, 2009):

$$\frac{n_T}{n_0} = \frac{2}{1+\sqrt{1+4K\rho}} \tag{2.33}$$

The equilibrium constant is given by:

$$K = \frac{v^*}{r} exp\left(-\frac{\Delta G^{hb}}{RT}\right) \tag{2.34}$$

The expression for the EOS in terms of the compressibility factor is given by:

$$Z = \frac{PV}{RT} = 1 + Z^{assoc} + Z^{rep} + Z^{attr} \tag{2.35}$$

where

$$Z^{assoc} = \frac{n_T}{n_0} - 1 \tag{2.36}$$

$$Z^{rep} = r\left[-\frac{1}{\eta}\ln(1-\eta) - 1\right] \tag{2.37}$$

$$Z^{attr} = -\frac{r\eta}{T_r} \tag{2.38}$$

2.2.3.4 Perturbation Association Theory

In general, a perturbation theory is a mathematical theory for approximating the solution of mathematical problem. The solution starts from a known solution of a related problem that has an accurate solution. This term is called the reference term. Then, a perturbation term is added to approximate the deviation. This method has been utilized in thermodynamic modeling to approximate the behavior of fluids by exploiting the accurate related solution of hard sphere (repulsive term). Then, the attractive interactions have been added as perturbation terms. The famous contribution in perturbation

associating theory is the work of Wertheim which is the basis for the association term in many EOSs such as statistical associating fluid theory (SAFT). Wertheim developed a statistical thermodynamic theory for fluids which is based on an arbitrary reference term. The nature of association interactions has been considered in which one or more highly directional short range of the attractive sites exists (dispersion attraction) (Economou, 2002). In Wertheim's thermodynamic perturbation theory, the Helmholtz free energy was expanded into many integrals of association potential and molecular distribution functions. Wertheim made a simplified Helmholtz free energy expression after showing that many of those integrals are zeroes (Chapman et al., 1989b; Wertheim, 1984a; Wertheim, 1984b; Wertheim, 1986a; Wertheim, 1986b). This theory has many features over the previous ones. For instance, the theory proposed a new approach to account for association interactions which were not considered in the previous perturbation theories. Furthermore, the Wertheim thermodynamic perturbation theory is flexible in choosing the reference term and including any intermolecular interactions in terms of the Helmholtz free energy but not the intramolecular ones (Al-Saifi, 2011; Kontogeorgis and Folas, 2009).

The pair potential was defined by Wertheim with an arbitrary reference potential:

$$u_{ij}(12) = u_{ij}^{ref}(12) + \sum_{A\in\Gamma^{(i)}} \sum_{B\in\Gamma^{(i)}} u_{ij}^{qAB}(12) \qquad (2.39)$$

where the second term on the right hand side represents the association interactions in which $\Gamma^{(i)}$ is the group of all attraction sites (A, B …) which is on the perimeter of a molecule.

For the model to be applicable, a dispersion term is added as a perturbation. Wertheim developed his theory for only chain and tree shape associated molecule but no rings. The strength of the association is represented via a square-well potential and characterized by two parameters, the association energy and volume. The compressibility factor for the associating term for mixtures was derived by Chapman et al (1988):

$$Z^{assoc} = -\frac{1}{2}\left(1 + \rho\frac{\partial \ln g}{\partial \rho}\right)\sum_i x_i \sum_{A_i}\left(1 - X_{A_i}\right) \tag{2.40}$$

where in SAFT-type theory, the site fraction in the assumption of one proton acceptor and one proton donor is given by:

$$X_A = \frac{-1 + \sqrt{1 + 4\rho\Delta}}{2\rho\Delta} \tag{2.41}$$

where Δ is the association strength which is defined for SAFT EOS as follows:

$$\Delta^{A_iB_j} = d_{ij}^3 g_{ij}\left(d_{ij}\right)^{seg} \kappa^{A_iB_j}\left[exp\left(\frac{\varepsilon^{A_iB_j}}{kT}\right) - 1\right] \tag{2.42}$$

For the cubic plus association EOS the expression is given by (Kontogeorgis and Folas, 2009):

$$\Delta^{A_iB_j} = g(\rho)\left[exp\left(\frac{\varepsilon^{A_iB_j}}{RT}\right) - 1\right] b_{ij}\beta^{A_iB_j} \tag{2.43}$$

with

$$b_{ij} = \frac{b_i + b_j}{2} \tag{2.44}$$

where g is the radial distribution function.

2.3 Statistical Association Fluid Theory

As previously indicated, Chapman proposed an EOS based on Wertheim's thermodynamic perturbation theory in terms of residual Helmholtz free energy (a^{res}). It was originally given as the sum of four terms taking into account the contribution of different molecular forces:

$$a^{res} = a^{hs} + a^{disp} + a^{chain} + a^{assoc} \tag{2.45}$$

The first and the second terms represent hard sphere and dispersion Helmholtz free energies (a^{hs} and a^{disp}) which can be derived based on Lennard-Jones, square well or modified square well potentials. The third term (a^{chain}) represents the covalent bonds forming the chain-segment. The fourth term (a^{assoc}) accounts for association interactions like hydrogen bonding interactions. In terms of compressibility factor, SAFT could be given as:

$$Z = 1 + Z^{hs} + Z^{disp} + Z^{chain} + Z^{assoc} \tag{2.46}$$

The spherical segment is used to represent the molecules in the SAFT EOS even in the case of long chain molecules. It would be a chain of segments connected through sites. For the associating molecules, there would be some association sites on the outside perimeter through which the association interactions occur. The repulsion and dispersion forces occur between any two segments whether they are next to each other at a molecule chain or in separate molecules. The covalent bonding acts between any adjacent segments in the same chain. The polar forces are acting when some molecules have a dipole

moment. So if two molecules get dipole moments, their opposite charges will attract each other while the same charges repel each other. On the last segment of each chain, there are some sites which are available for association bonding with other chains such as hydrogen bonding. **Figure 2.1** illustrates the segments and sites of two molecules:

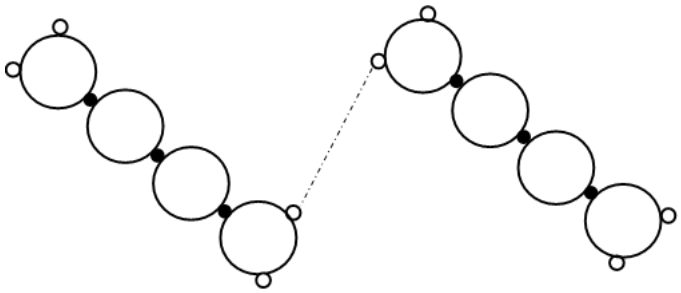

Figure 2.1 The segments (large open circles), chain sites (closed circles), associating sites (small open circles) and an associating force (dash line) of an associating molecule.

The sequence in forming the above picture starts by having the spherical segments first away from each other. Then, the dispersion forces bring those segments together. After that, the chains form for each molecule through chain sites. Finally, the association complexes form via the association sites (Kontogeorgis and Folas, 2009).

There are many versions of the SAFT EOSs. The most popular SAFT versions are listed in **Table 2.1**:

Table 2.1 Some of the most popular SAFT EOS versions (Kontogeorgis and Folas, 2009).

SAFT Version	Year	Authors
Original SAFT	1990	Chapman, Gubbins, Jackson and Radosz
Chen and Kreglewski SAFT (CK-SAFT)	1990	Huang and Radosz
Simplified SAFT	1995	Fu and Sandler
Soft SAFT	1997	Blas and Vega
Perturbed Chain SAFT (PC-SAFT)	2001	Gross and Sadowski

2.4 SAFT Adjustable Parameters

In general, to describe associating components, there are generally five adjustable parameters (Kontogeorgis and Folas, 2009):

1) The number of segments "m" which describe the length of the chain.

2) The segment size parameter which is given either as a diameter "σ" or a volume "v^{00}".

3) The segment energy parameter denoted by "ε" or "u^0".

4) The association volume "$\kappa^{A_iB_i}$".

5) The association energy "$\varepsilon^{A_iB_i}$".

where the last two parameters are used only in case of associating fluids. This indicates that, the SAFT needs only three parameters for non-association compounds.

2.5 Mathematical Representation of SAFT Terms

2.5.1 Chain Term

The chain term is given by the following expression:

$$\frac{a^{chain}}{RT} = \sum_{i=A}^{M} x_i \, (1 - m_i) \, \ln(g_{ii}(d_{ii})^{hs}) \tag{2.47}$$

where m_i is the number of segments in a molecule in the component i (Chapman et al., 1989a).

Most SAFT versions are using the same radial distribution function from the Carnahan-Starling EOS for a mixture of hard spheres (Carnahan and Starling, 1969; Kontogeorgis and Folas, 2009):

$$g_{ij}^{seg}(d_{ij}) \approx g_{ij}^{hs}(d_{ij}^{+}) = \frac{1}{1-\xi_3} + \left(\frac{d_i d_j}{d_i + d_j}\right)\frac{3\xi_2}{(1-\xi_3)^2} + \left(\frac{d_i d_j}{d_i + d_j}\right)\frac{2\xi_2^2}{(1-\xi_3)^3} \tag{2.48}$$

where ξ_k is a function of molar density:

$$\xi_k = \left(\frac{\pi N_{Av}}{6}\right)\rho \sum_i x_i m_i d_{ii}^k \tag{2.49}$$

where d is the effective segment diameter which depends on temperature.

The chain term in soft SAFT is given by (Blas and Vega, 1998):

$$\frac{a^{chain}}{N_m k_B T} = -\sum_{i=1}^{n} x_i \sum_{j=1}^{m_j - 1} \ln y_R\left(\sigma_{jj+1}{}^{(i)}\right) \tag{2.50}$$

where $x_i = N_m^{(i)} / N_m$ and $y_R\left(\sigma_{jj+1}{}^{(i)}\right)$ is the contact value of the cavity correlation function for spherical segments of species j and $j+1$ in the reference Lennard-Jones fluid.

2.5.2 Association Term

In most SAFT versions including simplified SAFT, CK-SAFT and PC-SAFT EOSs, the association term is represented as:

$$\frac{a^{assoc}}{RT} = \sum_i x_i \left[\sum_{A_i} \left[\ln X^{A_i} - \frac{X^{A_i}}{2} \right] + \frac{1}{2} M_i \right] \tag{2.51}$$

with

$$X^{A_i} = \left[1 + N_{A_i} \sum_j \sum_{B_j} \rho_j X^{B_j} \Delta^{A_i B_j} \right]^{-1} \tag{2.52}$$

where ρ_j is the molar density of component j given by:

$$\rho_j = X_j \rho_{mixture} \tag{2.53}$$

The association strength for mixtures is given by:

$$\Delta^{A_i B_j} = d_{ij}^3 g_{ij}\left(d_{ij}\right)^{seg} \kappa^{A_i B_j} \left[exp\left(\frac{\varepsilon^{A_i B_j}}{kT} \right) - 1 \right] \tag{2.54}$$

where k is the Boltzmann factor.

In the above equations, the effective segment diameter "d" is arbitrary defined by Barker-Henderson integral equation (Barker and Henderson, 1967; Kontogeorgis and Folas, 2009):

$$d = \int_0^{\sigma} \left[1 - exp\left(\frac{-u(r)}{kT}\right)\right] dr \tag{2.55}$$

The relation used in the original-SAFT as follows (Chapman et al., 1989; Kontogeorgis and Folas, 2009):

$$\frac{d}{\sigma} = \frac{1 + 0.2977\, kT/\varepsilon}{1 + 0.33163\, kT/\varepsilon + f(m)(kT/\varepsilon)^2} \tag{2.56}$$

with

$$f(m) = 0.0010477 + 0.25337\frac{m-1}{m} \tag{2.57}$$

where m is the number of segments.

There is another simplified form of the effective segment diameter proposed by Chen and Kreglewski (1977):

$$d = \sigma\left[1 - C\ exp\left(\frac{-3u^0}{kT}\right)\right] \tag{2.58}$$

where $u^0\ /\ k$ is the depth of the square-well potential and C is an integration constant.

In most of the SAFT EOSs versions, the "ε" symbol is used instead of "u^0". The latter symbol is used in the CK-SAFT and simplified SAFT EOSs. PC-SAFT EOS uses the temperature independent segment size parameter "σ" in the association strength equation instead of the temperature dependent segment size parameter "d". The physical significance in the latter parameter is that the segments are not exactly hard spheres but they have some overlap at high temperature, hence the effective segment diameter "d" is used which is smaller than the overall segment diameter. However, the effect of this different seems to be small in practical applications. In CK-SAFT and simplified SAFT,

the temperature independent segment volume "v^{00}" is used as one of the parameters characterizing size the components instead of the temperature independent segment diameter "σ". The relation among the last two parameters are obtained by (Kontogeorgis and Folas, 2009):

$$v^{00} = \frac{\pi N_{AV}}{6\tau}\sigma^3 \tag{2.59}$$

2.5.3 Segment Term

The segment term includes the repulsion and dispersion effects. The latter effect is the main difference among the SAFT EOS versions. The segment term can be described as (Kontogeorgis and Folas, 2009):

$$a^{seg} = a_0^{seg}\sum_i x_i m_i \tag{2.60}$$

with

$$a_0^{seg} = a_0^{hs} + a_0^{disp} \tag{2.61}$$

In original SAFT EOS, the Carnahan-Starling equation is used for the repulsive term in case of pure components and mixtures (Carnahan and Starling, 1969):

$$a_0^{hs} = \frac{4\eta - 3\eta^2}{(1-\eta)^2} \tag{2.62}$$

The dispersion term for the original SAFT EOS is given by:

$$a_0^{disp} = \frac{\varepsilon R}{k}\left(a_{01}^{disp} + \frac{a_{02}^{disp}}{T_R}\right) \tag{2.63}$$

with

$$a_{01}^{disp} = \rho_R[-0.85959 - 4.5424\rho_R - 2.1268\rho_R^2 + 10.285\rho_R^3] \quad (2.64)$$

$$a_{02}^{disp} = \rho_R[-1.9075 + 9.9724\rho_R - 22.216\rho_R^2 + 15.904\rho_R^3] \quad (2.65)$$

where $T_R = kT \,/\, \varepsilon$ and $\rho_R = [6/(2^{0.5}\,\pi)]\eta$

In the CK-SAFT, simplified SAFT and PC-SAFT EOSs, the full Carnahan-Starling hard sphere model is used for mixtures (Carnahan and Starling, 1969; Kontogeorgis and Folas, 2009):

$$\frac{a_0^{hs}}{RT} = \frac{1}{\xi_0}\left[\frac{3\xi_1\xi_2}{1-\xi_3} + \frac{\xi_2^3}{\xi_3(1-\xi_3)^2} + \left(\frac{\xi_2^3}{\xi_3^2} - \xi_0\right)\ln(1-\xi_3)\right] \quad (2.66)$$

In CK-SAFT EOS, the following polynomial expression originally proposed based on molecular dynamics simulation data for the square-well fluid. The dispersion term is given by (Alder et al., 1972):

$$\frac{a_0^{disp}}{RT} = \sum_{i=1}^{4}\sum_{j=1}^{9} D_{ij}\left(\frac{u}{kT}\right)^i\left(\frac{\eta}{\tau}\right)^j \quad (2.67)$$

where D_{ij} are universal constants, $\tau = 0.74048$, $u/k = (u^o/k)(1 + e/kT)$ and $e/k = 10\ K$ for all molecules with some exceptions.

In the simplified SAFT EOS, which is similar to the CK-SAFT except for the dispersion term which is given by (Kontogeorgis and Folas, 2009; Lee et al., 1985):

$$\frac{a_0^{disp}}{RT} = Z_m \ln\left(\frac{v_s}{v_s + v^*Y}\right) \quad (2.68)$$

with

$$Y = exp\left(\frac{u}{2kT}\right) - 1 \tag{2.69}$$

where Z_m is the maximum coordination number which is 36 as given by (Kim et al., 1986), v_s is molar volume of a segment, $v^* = N_{Av}d^3/\sqrt{2}$ is the closed-packed molar volume of a segment and u is the depth of the square-well potential.

In case of mixtures, the following expression is used:

$$\frac{a^{disp}}{RT} = mZ_m \ln\left(\frac{v_s}{v_s + v^*Y}\right) \tag{2.70}$$

with $v_s = 1/\rho m$, $m = \sum_i x_i m_i$ and v^*Y is given by the following expression:

$$v^*Y = \frac{N_{Av}\sum_i\sum_j x_i x_j m_i m_j \left(d_{ij}^3/\sqrt{2}\right)\left[exp\left(u_{ij}/kT\right) - 1\right]}{\sum_i\sum_j x_i x_j m_i m_j} \tag{2.71}$$

In PC-SAFT EOS, there is one main character in its dispersion term. The dispersion forces are considered to be among the whole chains rather than the individual segments. The dispersion term contribution to the Helmholtz free energy in PC-SAFT can be expressed as (Gross and Sadowski, 2001; Kontogeorgis and Folas, 2009):

$$\frac{a^{disp}}{kTN} = \frac{A_1}{kTN} + \frac{A_2}{kTN} \tag{2.72}$$

where

$$\frac{A_1}{kTN} = -2\pi\rho\bar{m}^2\left(\frac{\varepsilon_{ij}}{kT}\right)\sigma_{ij}^3 I_1 \tag{2.73}$$

$$\frac{A_2}{kTN} = -\pi\rho\bar{m}\left(1 + Z^{hs} + \rho\frac{\partial Z^{hc}}{\partial\rho}\right)^{-1}\bar{m}^2\left(\frac{\varepsilon_{ij}}{kT}\right)^2\sigma_{ij}^3\frac{\partial}{\partial\rho}[\rho I_2] \tag{2.74}$$

where $x = r/\sigma$ and $\tilde{u}(x) = u(x)/\varepsilon$ is the reduced intermolecular Lennard-Johns potential

with

$$\left(1 + Z^{hc} + \rho\frac{\partial Z^{hc}}{\partial \rho}\right)^{-1} =$$

$$\left(1 + \bar{m}\frac{8\eta - 2\eta^2}{(1-\eta)^4} + (1-\bar{m})\frac{20\eta - 27\eta^2 + 12\eta^3 - 2\eta^4}{\big((1-\eta)(2-\eta)\big)^2}\right) \tag{2.75}$$

The two integrals solutions are represented by a sextic polynomial:

$$I_1 = \int_1^\infty \tilde{u}(x) g^{hc}(\bar{m}; x\sigma/d)\, x^2 dx = \sum_{i=0}^{6} a_i \eta^i \tag{2.76}$$

$$I_2 = \frac{\partial}{\partial \rho}\left[\rho \int_1^\infty \tilde{u}(x)^2 g^{hc}(\bar{m}; x\sigma/d)\, x^2 dx\right] = \sum_{i=0}^{6} b_i \eta^i \tag{2.77}$$

where the expressions for a_i and b_i are given as:

$$a_i = a_{0i} + \frac{\bar{m}-1}{\bar{m}} a_{1i} + \frac{\bar{m}-1}{\bar{m}}\frac{\bar{m}-2}{\bar{m}} a_{2i}\,, i \in [\![0,6]\!] \tag{2.78}$$

$$b_i = b_{0i} + \frac{\bar{m}-1}{\bar{m}} b_{1i} + \frac{\bar{m}-1}{\bar{m}}\frac{\bar{m}-2}{\bar{m}} b_{2i}\,, i \in [\![0,6]\!] \tag{2.79}$$

with σ_{ij} and ε_{ij}/k_B given by combining rules as follows:

$$\sigma_{ij} = \frac{1}{2}\left(\sigma_i + \sigma_j\right) \tag{2.80}$$

$$\frac{\varepsilon_{ij}}{k_B} = \sqrt{\frac{\varepsilon_i}{k_B}\cdot\frac{\varepsilon_j}{k_B}}\left(1 - k_{ij}\right) \tag{2.81}$$

$\bar{m}$ is the mean segment number in mixtures defined by:

$$\bar{m} = \sum_{i=1}^{n_c} x_i \cdot m_i \tag{2.82}$$

The repulsive (hard-sphere) and dispersion forces in soft SAFT are proposed based on the Lennard-Johns potential:

$$\phi = 4 \sum_i \sum_j \varepsilon_{ij} \left[\left(\frac{\sigma_{ij}}{r} \right)^{12} - \left(\frac{\sigma_{ij}}{r} \right)^{6} \right] \tag{2.83}$$

The reader could consult Blas and Vega (1997) for the details of the derived equations for soft SAFT terms.

Table 2.2 highlights some of the main differences among CK-SAFT, simplified SAFT, soft SAFT and PC-SAFT in the SAFT segment term:

Table 2.2 Some of the main differences among CK-SAFT, simplified SAFT, soft SAFT and PC-SAFT in the SAFT segment term.

Model	**Repulsion between Segments**	**Attraction between Segments**	C	e/k
CK-SAFT (1990)	Carnahan and Starling Hard Sphere	Square-Well	0.12*	10*
Simplified SAFT (1995)	Carnahan and Starling Hard Sphere	Square-Well	0.333	-10
Soft SAFT (1997)	Lennard-Johns	Lennard-Johns	-	-
PC-SAFT (2001)	Carnahan and Starling Hard Sphere	Modified Square-Well	0.12*	-

*some compounds have different values, see the corresponding reference for these values.

2.6 Most Popular Version of SAFT

The most popular versions in the literature is probably the perturbed-chain SAFT (PC-SAFT) EOS (Gross and Sadowski, 2001). The PC-SAFT EOS was successfully applied to vapor-liquid equilibrium, liquid-liquid equilibrium, solubility prediction and thermodynamic properties. The applications cover a wide range of systems including polymers (Gross and Sadowski, 2002), complex fluids (Economou, 2002), ethylene based copolymer, copolymers consisting of polar and nonpolar repeat units (Gross et al., 2003), polar low-molecular components (Tumakaka and Sadowski, 2004), electrolyte systems (Cameretti et al., 2005), crude oil (Vargas et al., 2009), mixtures of hydrogen sulfide with hydrocarbons, mixtures of hydrogen sulfide with water, mixtures of CO_2 with hydrocarbons and mixtures of CO_2 with water (Tang and Gross, 2010). Due to the popularity of PC-SAFT, more emphasis will be given in this thesis to PC-SAFT as illustrated in **Chapter 6**.

2.7 Conclusion

In this chapter, the theoretical development for EOSs leading to the Statistical Associated Fluid Theory was covered. The first EOS formed after Boyle and Charles relationships was not able to show phase equilibria. After that, Van der Waals (1873) was able to show the two phase region with his celebrated cubic EOS considering repulsive and attractive forces. The accuracy of predicting phase equilibria was improved by several works. The most popular improvement was done by Peng and Robinson (1976). However, the latter EOS was not able to predict accurately the thermodynamic properties of associating mixtures. Three types of association theories were developed but the most

successful association theory was the Wertheim perturbation theory. Wertheim (1984) was able to describe the association forces among molecules by stating some reasonable assumptions. Chapman (1988) was able to describe the chain forces based on Wertheim work. The first version of SAFT was proposed by Chapman et al. (1990) representing the forces among molecules in terms of Helmholtz free energy. SAFT EOS has basically four terms rather than two after adding the chain and association terms. All of these terms are based on theory.

In this chapter, the formulation of the SAFT terms was also illustrated along with the differences among SAFT versions. In addition to the original SAFT version by Chapman et al. (1990), four more versions were described, namely: CK-SAFT (Huang and Radosz, 1990), simplified SAFT (Fu and Sandler, 1995), Soft SAFT (Blas and Vega, 1998) and PC-SAFT (Gross and Sadowski, 2001). The latter is the most popular version. The main differences among these versions are the use of different pair potential descriptions and defining the perturbation term.

Because of the mathematical complexity of the SAFT terms, an efficient method is required to analyze the model to understand the reason behind the multiple molar volume roots problem. In the next chapter, bifurcation and stability analysis are defined and discussed. The method of generating the bifurcation diagrams is explained. The components of a bifurcation diagrams are illustrated. Finally, the procedure of finding the physical root among all the roots is shown.

CHAPTER 3

Bifurcation and Stability Analysis

3.1 Introduction

In **Chapter 1**, the second objective of this thesis was to use bifurcation diagrams to determine the number of roots, branches and turning points for molar volume versus temperature at fixed pressures. The fourth objective was to use the stability analysis to determine the stable roots and branches. In the previous chapter, the mathematical formulation of SAFT was shown to be complex. This complexity makes the comprehension of the multiple molar volume roots problem so challenging. All the previous studies were limited to specific state conditions. In order to understand the general behavior of SAFT at any state condition, an efficient and comprehensive method of analysis is required.

The purpose of this chapter is to explain the two types of analysis which are applied in this thesis on SAFT EOSs in order to achieve the fifth objective discussed in **Chapter 1** which is to construct a simple strategy to select the realistic volume root among all the roots. Section 3.2 is dedicated to demonstrate the bifurcation analysis. This section has many sections. The importance and description of bifurcation diagrams are illustrated in the first section (3.2.1) with an example of van der Waals cubic EOS. The turning points in the bifurcation diagrams are explained in section 3.2.2 with the same example of van der Waals cubic EOS due to its simplicity. The analytical and numerical

methods of determining the turning points are explained in the third section (3.2.3). Section 3.2.4 is dedicated to show the method of determining the critical points while (3.2.5) demonstrates the issue of branches with an example of SAFT EOSs when more than one branch exists. The arc-length continuation method used to generate the bifurcation diagrams is discussed in section 3.2.6. Section 3.3 demonstrates that the correct stable molar volume roots are selected based on three aspects. These are based on avoiding the non-physical molar volume roots, testing the mechanical stability of the roots and selecting the minimum Gibbs free energy among the multiple molar volume roots. In section 3.4, the conclusion of this chapter is stated.

3.2 Bifurcation Analysis

The goal of bifurcation analysis is to show all physical and non-physical roots of any EOS at specific state conditions on one diagram.

3.2.1 Bifurcation Diagrams

A bifurcation diagram is a plot that is constructed to show the behavior of a curve which turns back at least once causing stability change (Sherman, 2011). The point at which the curve turns is called a turning point. The curve illustrates how the zero-locus of one variable behaves as a parameter varies. Constructing such diagrams is very valuable for studying multi-variable models. If the model contains more than one variable, the other variables could be fixed (Straty and Tsumura, 1976).

In thermodynamics, an EOS is the equation which relates temperature, pressure and molar volume. Most EOSs exhibit more than one volume root at fixed temperature

and pressure. Therefore, it is possible to generate a bifurcation diagram to show how the molar volume bifurcates as temperature varies at fixed pressure. To demonstrate how the molar volume behaves in the SAFT EOS, it would be wise to start with a simpler model such as van der Waals or Peng-Robinson cubic EOSs. It is known that cubic EOSs show a maximum of three volume roots at fixed temperature and pressure.

The method of constructing the bifurcation diagrams and turning points will be illustrated later. At this stage, bifurcation diagrams and turning points will be demonstrated to show how the number of molar volume roots varies with temperature at fixed pressure. **Figure 3.1** which is a bifurcation diagram illustrates how the molar volume varies with temperature for methane at 1 atm. The figure is constructed using van der Waals EOS.

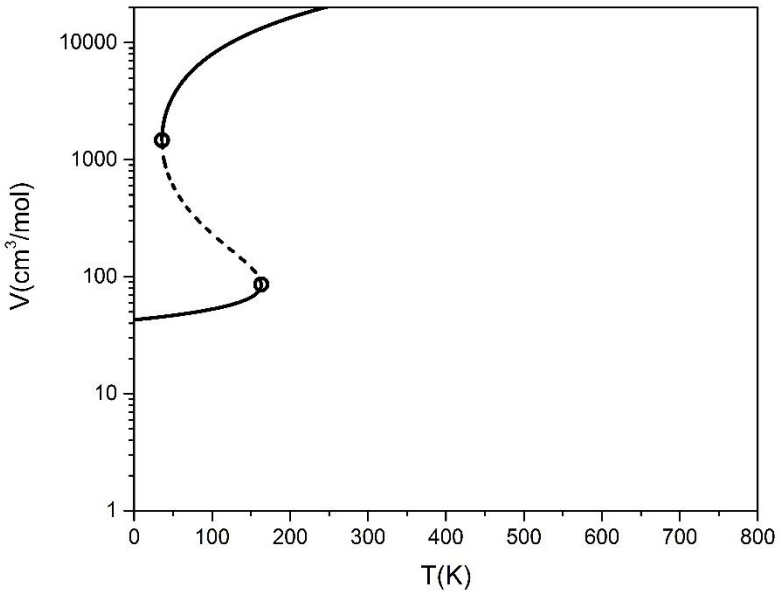

Figure 3.1 Molar volume of methane (cm^3/mol) (log-scale) versus temperature (K) at 1 atm using van der Waals cubic EOS. Dash curve indicates unstable region. Open circles indicate turning points.

It is apparent from the bifurcation diagram (**Figure 3.1**) that van der Waals exhibits three volume roots at 100 K. However, the diagram illustrates only one root at 250 K. In a similar manner, the diagram demonstrates one root at 50 K. Therefore, it is clear how the number of volume roots vary from 50 to 250 K. This behavior will be explained in details in the next section.

3.2.2 Turning points

An important feature of the bifurcation diagram is turning point. The truing point is the point at which the number of roots starts varying. The turning points are represented by open circles in **Figure 3.1**. In **Figure 3.1**, it is clear that how the number of roots changes suddenly for temperatures higher or lower than the turning point. It is also clear that **Figure 3.1** illustrates two turning points at 35.786 K and 163.11 K.

Thus, if any temperature is taken lower than 35.786 K, only one root is available. For simplicity, a vertical line will be utilized at any temperature to count the number of roots which will be represented by the number of the intersection points with the curve. For example, at 20 K, the number of roots is one as illustrated by the intersection of the vertical line with the curve. It is obvious that only one root exists at 20 K because it is lower than the turning point.

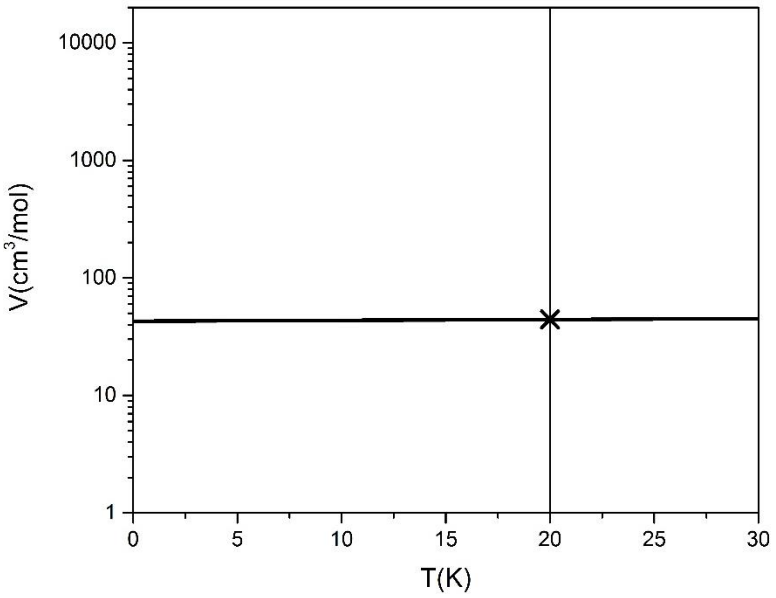

Figure 3.2 Molar volume of methane (cm^3/mol) (log-scale) versus temperature (K) at 1 atm using van der Waals cubic EOS. "×" indicates a molar volume root at 20 K.

Similarly, if any temperature is taken between the turning points of 35.786 and 163.11 K, the vertical line illustrates three intersection points as illustrated in **Figure 3.3** at 100 K.

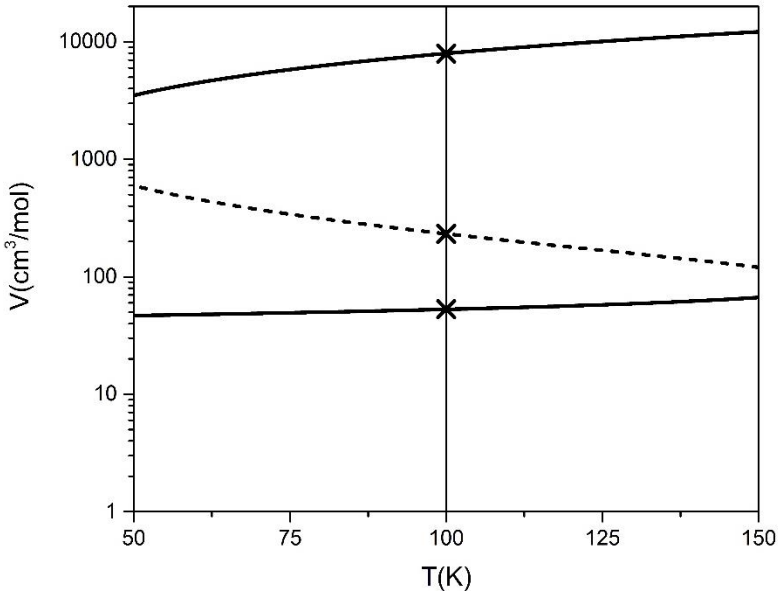

Figure 3.3 Molar volume of methane (cm^3/mol) (log-scale) versus temperature (K) at 1 atm using van der Waals cubic EOS. Dash curve indicates unstable region. "×" indicates molar volume roots at 100 K.

Finally, if any temperature is taken higher than the turning point of 163.11 K, the vertical line illustrates only one root. For example, **Figure 3.4** demonstrates the number of roots at 200 K. It is evident from the figure that the number of roots is one. It should be noted that the number roots at turning points is two. This indicates that cubic EOSs exhibits two real roots only if the given state conditions representing the turning points.

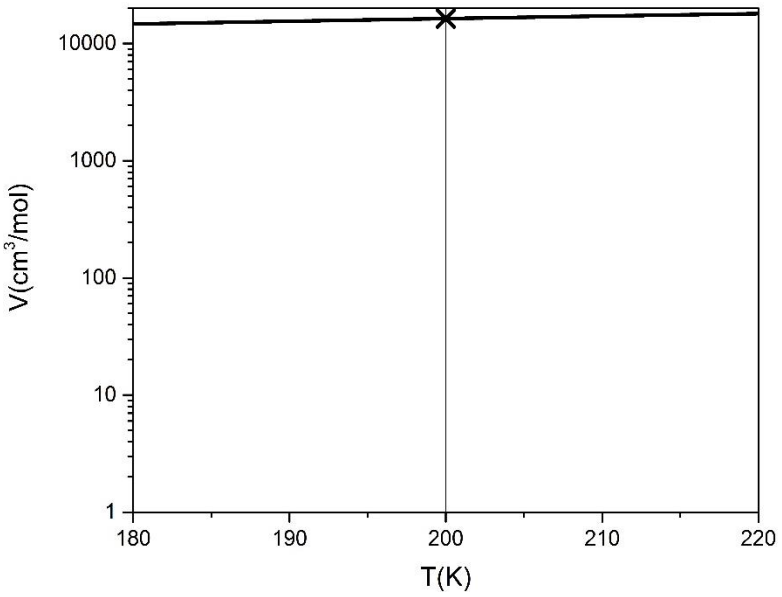

Figure 3.4 Molar volume of methane (cm^3/mol) (log-scale) versus temperature (K) at 1 atm using van der Waals cubic EOS. "×" indicates a molar volume root at 200 K.

Table 3.1 summarizes the previous figures regarding the number of turning points and roots. This elucidates that the bifurcation diagram is a valuable tool to demonstrate how the number of roots varies as temperature changes at fixed pressure. It also illustrates the importance of turning points which show precisely where the number of roots starts changing.

Table 3.1 The number of real molar volume roots for three temperature points before and after the two turning points

Temperature	**20 K**	**35.768 K (Turning Point)**	**100 K**	**163.11 K (Turning Point)**	**200 K**
Number of Molar Volume Roots	1	**2**	3	**2**	1

In case of a curve with no turning points, for example methane at 100 atm, the number of roots remains the same at any value of temperature. Figure 3.5 illustrates this point at 100, 200 and 300 K where only one root is available at each temperature.

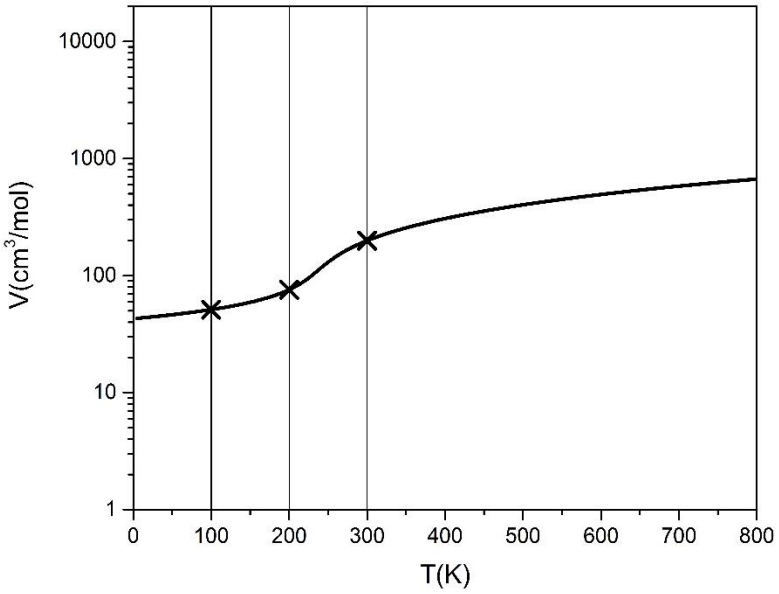

Figure 3.5 Molar volume of methane (cm^3/mol) (log-scale) versus temperature (K) at 100 atm using van der Waals cubic EOS. "×" indicates molar volume roots at 100, 200 and 300 K.

3.2.3 Determination of Bifurcation Diagrams and Turning points

In the previous section, the bifurcation diagrams and turning points were given without explaining how they were obtained. The method that could be utilized for this

purpose is either analytical or numerical method. For cubic EOSs, it is not possible to obtain the bifurcation diagrams analytically except for van der Waals EOS. For other equations of the state, the only way is to account on numerical methods.

3.2.3.1 Analytical Method

The analytical method could be explained by van der Waals cubic EOS:

$$P = \frac{RT}{V-b} - \frac{a}{V^2} \tag{3.1}$$

To generate the bifurcation diagram, the previous equation could be solved for temperature:

$$T = \left(P + \frac{a}{V^2}\right)\left(\frac{V-b}{R}\right) \tag{3.2}$$

From this equation, bifurcation diagrams could be generated for molar volume vs. temperature at different fixed pressures. The bifurcation diagram that was given in the previous section was generated using the above equation by fixing the pressure to 1 atm. It should be noted that it is sometimes convenient to replace the molar volume with compressibility factor (Z) or reduced density (η). For example, Figure 3.6 demonstrates a bifurcation diagram of reduced density vs. temperature for ethane at 2 atm.

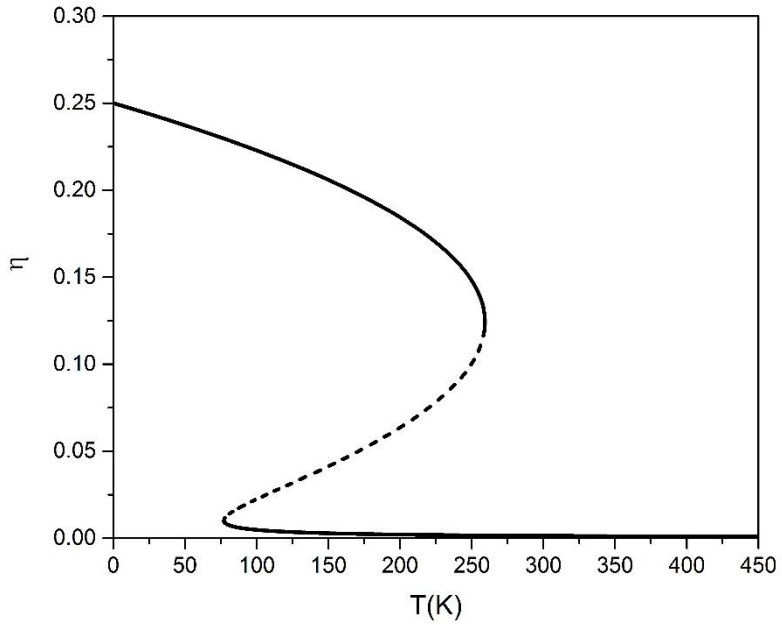

Figure 3.6 Reduced density versus temperature (K) for ethane at 2 atm using van der Waals cubic EOS. Dash curve indicates unstable region.

Figure 3.7 illustrates a bifurcation diagram of compressibility factor vs. temperature for ethane at 2 atm.

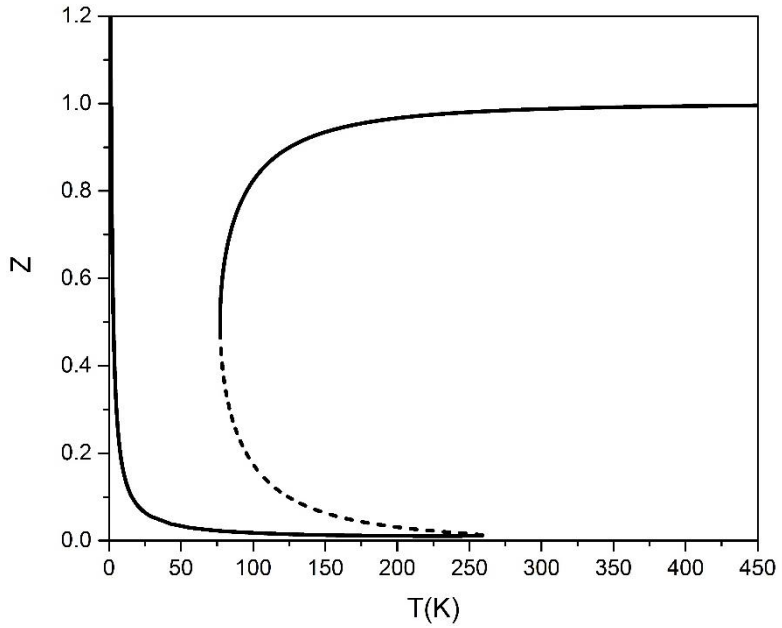

Figure 3.7 Compressibility factor versus temperature (K) for ethane at 2 atm using van der Waals cubic EOS. Dash curve indicates unstable region.

To find the turning points for ethane at 2 atm, the van der Waals cubic EOS should be recast in the following form:

$$f = P - \frac{RT}{V-b} - \frac{a}{V^2} \tag{3.3}$$

Then by differentiating the above function with respect to molar volume and making the derivative equals to zero:

$$\frac{\partial f}{\partial V} = 0 \tag{3.4}$$

$$\frac{\partial f}{\partial V} = \frac{RT}{(b-V)^2} - \frac{2a}{V^3} \tag{3.5}$$

solving for T:

$$T_{tp} = \frac{2a}{V^3}\frac{(b-V)^2}{R} \tag{3.6}$$

Equation 3.6 includes the value of temperature at which turning points take place. However, it is required to find the values of molar volume at which turning points occur. These values can be determined by inserting the temperature of equation 3.6 into equation 3.2 and solving for molar volume:

$$\left(P + \frac{a}{V^2}\right)\left(\frac{V-b}{R}\right) - \frac{2a}{V^3}\frac{(b-V)^2}{R} = 0 \tag{3.7}$$

It could alternatively be determined graphically by constructing a diagram of molar volume vs. temperature at a fixed pressure by using both **Equations 3.2 and 3.6** as illustrated in **Figure 3.8**. The intersection between the two curves represents the turning points.

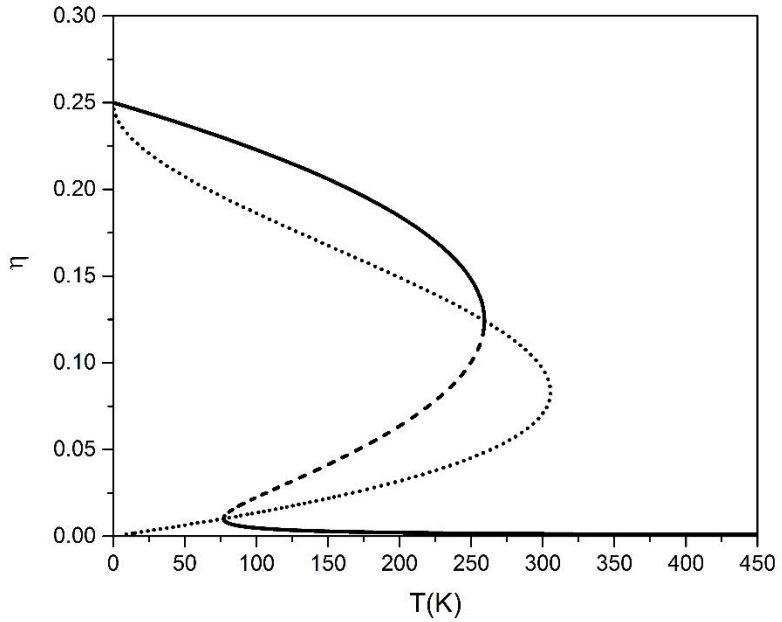

Figure 3.8 Reduced density versus temperature (K) for ethane at 2 atm using van der Waals cubic EOS. Dash curve indicates unstable region. Dot curve indicates the derivative solved for T_{tp}. The intersection points between the two curves indicate the turning points.

The same analysis can be applied to the compressibility factor as illustrated in **Figure 3.9**.

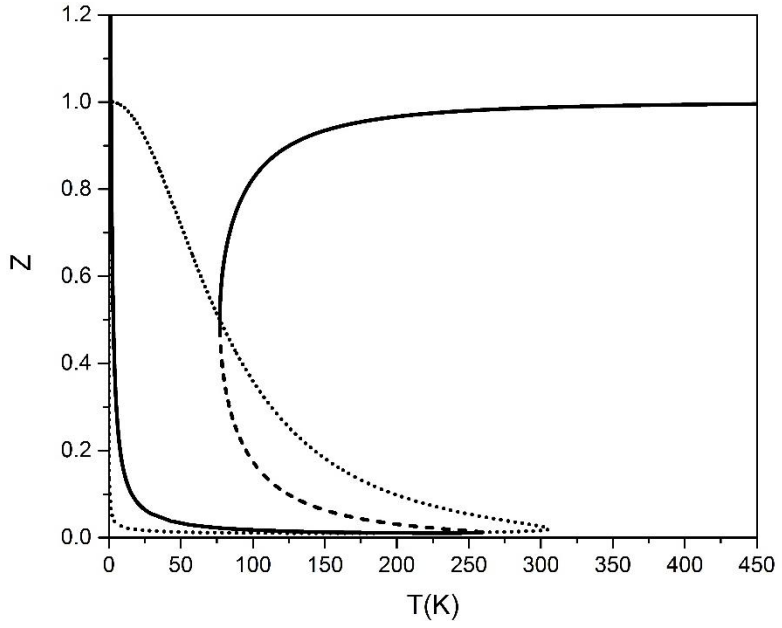

Figure 3.9 Compressibility factor versus temperature (K) for ethane at 2 atm using van der Waals cubic EOS. Dash curve indicates unstable region. Dot curve indicates the derivative solved for T_{tp}. The intersection points between the two curves indicate turning points.

3.2.3.2 Numerical Method

In fact, it is not possible to apply the analytical method to get the turning points for complex models such as SAFT EOS. That is why the numerical work is introduced. The classical numerical methods such as Newton's methods are not helpful and practical in generating bifurcation diagrams. All Newton methods such as Newton-Raphson, Gauss-Newton, Quasi-Newton would fail to locate all the roots. Even if they are successful at some state conditions, they don't add value to construct the complete picture of turning points and branches. This is why it is important to utilize an efficient numerical method that is capable to generate all roots, turning points and branches. One

of the techniques that could be used to achieve this objective is Newton continuation methods. In this work, the arc-length continuation method is utilized. The details of the method will be given in section 3.2.6.

3.2.4 Critical Points

A critical point which has the following coordination (T_c, P_c, V_c) should satisfy the following set of equations (Privat et al., 2010):

$$P(T_c, V_c) - P_c = 0 \tag{3.8}$$

$$(\partial P/\partial V)_T|_{T_c,V_c} = 0 \tag{3.9}$$

$$(\partial^2 P/\partial V^2)_T|_{T_c,V_c} = 0 \tag{3.10}$$

This system of equations can be solved using a numerical technique by selecting a good initial guess of T_c, P_c and V_c is provided. To select a good initial guess, it is important to understand how the bifurcation diagram behaves at and close to the critical point. To do so, it is good to build a bifurcation diagram for methane similar to the one given in **Figure 3.1. Figure 3.10** is plotted for molar volume vs. temperature at 45.99 atm. It is clear that the dashed line connected the two turning points became shorter and the two turning points got closer to each other. If the pressure is increased to a value that is very close to the critical pressure, the two turning points almost match. At the critical point, the two turning points become one. This turning point disappears at any pressure above the critical pressure. Therefore, the initial guess for the critical point could be selected from the bifurcation diagram where the two turning points are about to collide as illustrated in **Figure 3.10**.

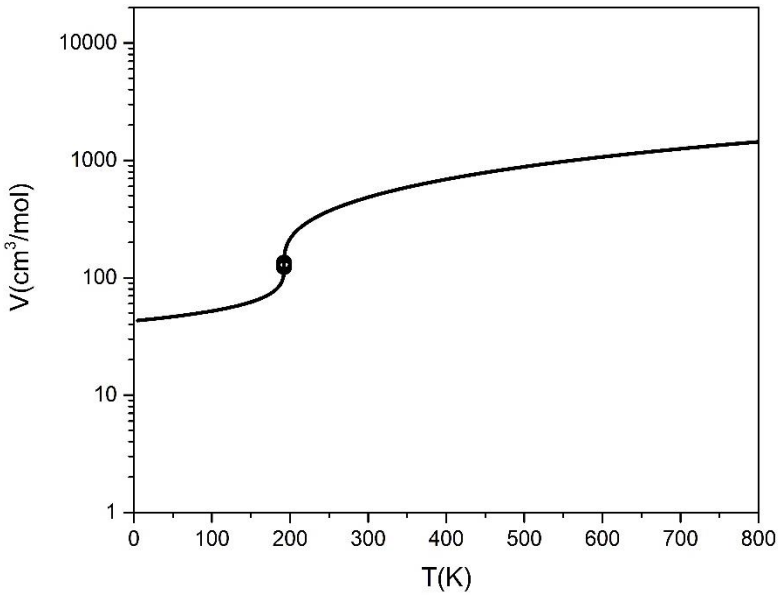

Figure 3.10 Molar volume of methane (cm^3/mol) (log-scale) versus temperature (K) at 45.99 atm using van der Waals cubic EOS. Open circles indicate turning points.

3.2.5 Branches

In the previous sections, the van der Waals EOS is utilized in constructing bifurcation diagram. It was clear that cubic EOSs have one curve. When a diagram has more than one curve starting from either the x-axis or y-axis, those curves are called "branches". The existence of more than one branch in a model might increase the number of roots at a given temperature. All cubic EOSs have only one branch with two turning points. As a result, the maximum number of roots for any cubic EOS is always three.

However, in some versions of SAFT EOS, it will be shown later that the maximum number of roots could exceed three. This would make it possible to have more than one branch. **Figure 3.11** illustrates a case where there is more than one branch. This bifurcation diagram of the simplified SAFT EOS was obtained for ethane at 1 atm. It is clear from the figure the existence of three branches. This would make the roots to

exceed three. For example, at 150 K, it is clear from the vertical line, the simplified SAFT EOS exhibits four roots. The behavior and the number of the branches might differ from one SAFT version to another. For example, the CK-SAFT EOS illustrates different behavior of the branches and number of roots. **Figure 3.12** illustrates the bifurcation diagram of ethane for the same conditions given in **Figure 3.11**. It is clear that different behavior is shown. In addition, from the vertical line at 150 K, it is clear that the number of roots is 5; it is obvious the difference in the number of roots between simplified SAFT and CK-SAFT EOSs. These will be discussed in detail in **Chapters 4 & 5**.

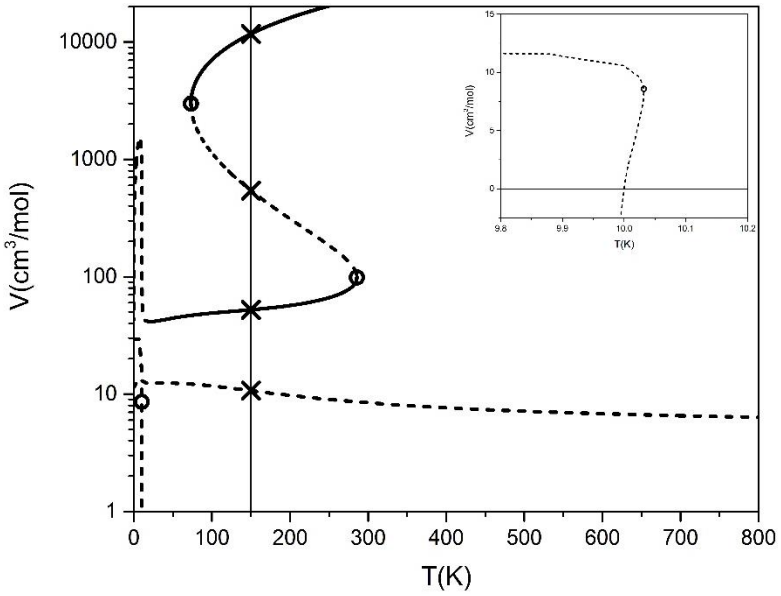

Figure 3.11 Molar volume of ethane (cm^3/mol) (log-scale) versus temperature (K) at 1 atm using simplified SAFT EOS. Dash curves indicate non-physical regions. Open circles indicate turning points. "×" indicates the molar volume roots at 150 K.

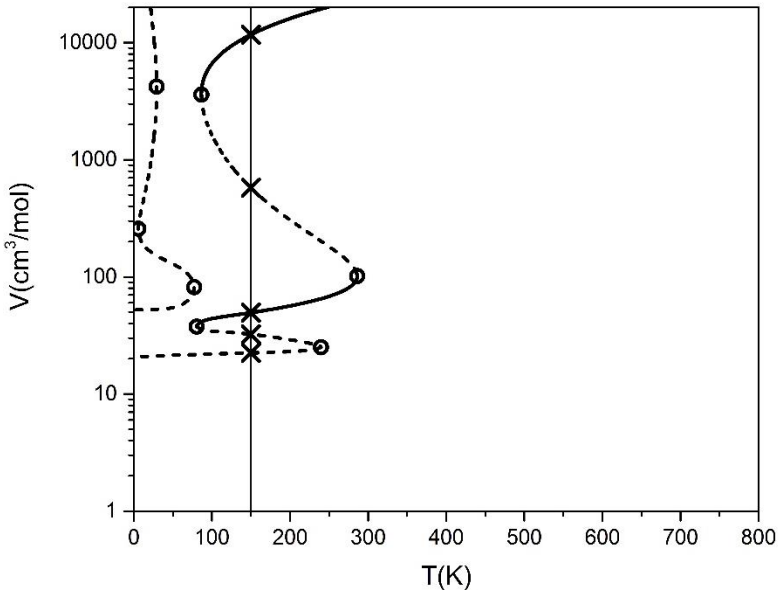

Figure 3.12 Molar volume of ethane (cm^3/mol) (log-scale) versus temperature (K) at 1 atm using CK-SAFT EOS. Dash curves indicate non-physical regions. Open circles indicate turning points. "×" indicates molar volume roots at 150 K.

3.2.6 Arc-Length Continuation Method

The are-length continuation method is among a class of path-following techniques that are widely utilized to obtain the variation of the solution paths for non-linear algebraic equations. The method is a valuable tool to compute available branches from the solution of non-linear algebraic equations. It has a broad use in chemical engineering subjects such as distillation, thermodynamics and reaction kinetics (Binous and Shaikh, 2014). To obtain the family of solutions using arc-length continuation method, the non-linear algebraic equations are converted into differential-algebraic equations. To explain the method clearly, it is important to represent it mathematically.

If the governing equations are a set of non-linear algebraic equations which can be expressed in the form:

$$f(x, \lambda) = 0 \tag{3.11}$$

where the components of the vectors f and x are $f = (f_1, f_2, \dots, f_N)$ and $x = (x_1, x_2, \dots, x_N)$ and λ is the dependent parameter. If there are other parameters, they should be fixed.

In multiple volume roots problems, x is considered to be molar volume, λ is the temperature and the pressure is fixed. A solution route of this equation is characterized by a curve to show how x varies with λ. For simplicity, the discussion will be focused on one algebraic equation. The solution could be initiated by assuming an initial guess x_0 for which $\lambda = \lambda_0$ and the non-linear equation could be given by:

$$f(x_0, \lambda_0) = 0 \tag{3.12}$$

Then, the solution originates from the above initial point where an arc-length segment is employed to move along the curve. Hence, it is illustrated by:

$$f\big(x(s), \lambda(s)\big) = 0 \tag{3.13}$$

To solve the above equation, an additional equation is needed. The relationship of λ and x with s can be formed by the defining an arc-length equation:

$$\frac{dx}{ds} \cdot \frac{dx}{ds} + \left(\frac{d\lambda}{ds}\right)^2 = 1 \tag{3.14}$$

The problem is clearly transformed from non-linear equations to a system of n+1 differential algebraic equations that could be solved to determine n+1 unknowns.

For any EOS, the function can be expressed in the following form:

$$f(V, P, T) = 0 \tag{3.15}$$

Compressibility factor or reduced density can be used instead of the compressibility factor as was previously illustrated. The bifurcation diagrams in the coming chapters are constructed with the arc-length continuation method.

3.3 Stability Analysis and Physical Roots

Once the bifurcation diagrams are constructed, it is crucial to test and study the stability of branches. The goal of the analysis is to determine the physical roots among all the roots appear in the bifurcation diagram. There are some tests that could easily be noticed. A root is said to be non-physical if it is not stable or the value of the reduced density is greater than the maximum number of packing fraction. A root is said to be mechanically stable if the change of pressure with the change in molar volume at fixed temperature is negative, i.e. when $(dP/dV)_T < 0$. No component can show an increase in volume while being pressurized at constant temperature.

If more than one root is mechanically stable and their reduced densities are less than the maximum value of packing fraction, then a second test is performed by calculating the Gibbs free energy for every root. If the Gibbs free energies for two roots are equal, then those two roots represent the saturation values. Among all the Gibbs free energy values, the root which has the smallest value is the stable or physical root.

3.4 Conclusion

In this chapter, the method for determining all the volume roots of SAFT EOSs is explained. The proposed analysis of studying the multiple volume roots problem was to utilize bifurcation diagrams. This is because the number of volume roots varies with the

change of state conditions. To obtain bifurcation diagrams, the arc-length continuation method was utilized in this work. Different branches were obtained by using different initial guesses. To study the stability of multiple volume roots, the mechanical stability of roots was first tested. The physical characteristics of the roots have been taken into considering by rejecting any root with a value higher than the maximum packing fraction. The last test to consider the stable root was carried out by determining the minimum values of the Gibbs free energies. Various examples of bifurcation disarms were given in this chapter for van der Waals, simplified SAFT and CK-SAFT EOSs.

CHAPTER 4

Bifurcation and Stability Analysis for Spherical Molecules using the SAFT EOS

4.1 Introduction

In this chapter, the bifurcation and stability analysis introduced in the previous chapter is extensively applied to spherical molecules which have the segment number "m" equals one. This value of segment number causes the chain term to vanish according to the chain terms introduced in **Chapter 2**. In this chapter, all multiple volume roots, turning points, branches and critical points will be determined for different SAFT versions. The bifurcation diagrams for PC-SAFT, CK-SAFT, soft-SAFT and simplified SAFT EOSs will be studied in five sections. Section 4.2 is dedicated for the general description of the bifurcation diagrams. This description includes the number of branches, turning points and molar volume roots. Section 4.3 is dedicated to illustrate the effect of increasing pressure on the behavior of branches, turning points and molar volume roots. Section 4.4 is dedicated to compare the bifurcation diagrams for different components to illustrate the effect of the SAFT parameters on the bifurcation diagrams. In addition, due to the role of critical points on bifurcation diagrams, the critical points are listed for each SAFT version in section 4.5. In the last section before stating the conclusions, a comparison among the studied SAFT versions in this chapter is going to be shown and discussed.

4.2 General Description of Bifurcation Diagrams of SAFT EOS

To explore how the multiple volume roots of any version of SAFT EOS behave, it is important to construct a bifurcation diagram that shows how the molar volume varies with temperature at constant pressure. The number of molar volume roots depends on how many branches and how they behave as explained in section 3.2.5. This section is going to cover PC-SAFT, CK-SAFT, soft SAFT and simplified SAFT EOSs.

Firstly, the PC-SAFT EOS in the case of methane has three branches in which only one of them includes the physical behavior which is the upper branch. This branch behaves similar to the one obtained from cubic EOS with a slight difference at low temperature where it represents non-physical behavior. Because there are several branches, the number of roots exceeds three at some state conditions.

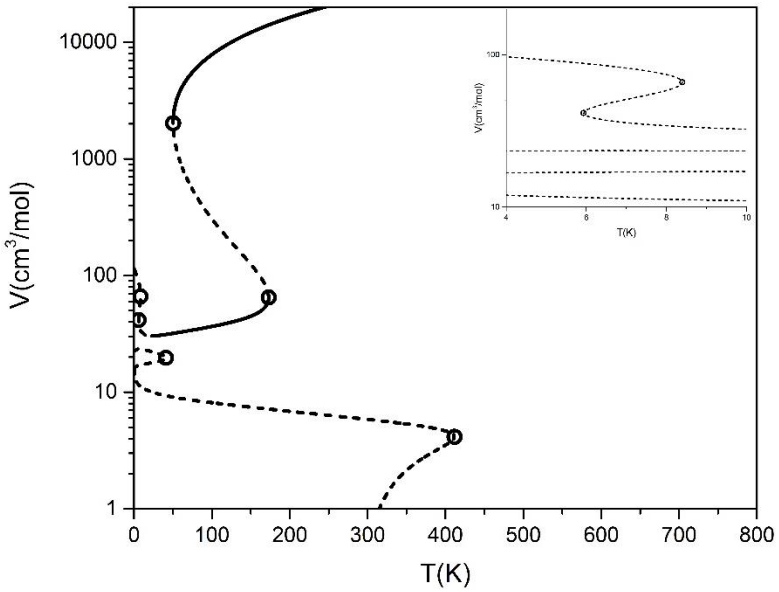

Figure 4.1 Molar volume of methane (cm^3/mol) (log-scale) versus temperature (K) at 1 atm using PC-SAFT EOS. Dash curves indicate non-physical regions. Open circles indicate turning points.

From the previous figure, it is obvious that the upper branch has four turning points while the lower and middle branches have only one turning point in the positive region of molar volumes. It should be noted that the lower branch extends to the negative region of molar volumes where two additional turning points exist (see **Figure 4.2**). The turning points with positive molar volumes exist at 5.93, 8.4, 41.04, 50.35, 173.01 and 411.65 K. This number of turning points would cause the availability of several roots starting from one up to 7 roots depending on the specified temperature. For example, at 7 K, the PC-SAFT exhibits 7 roots where one of them is a negative root as illustrated in **Figure 4.2**.

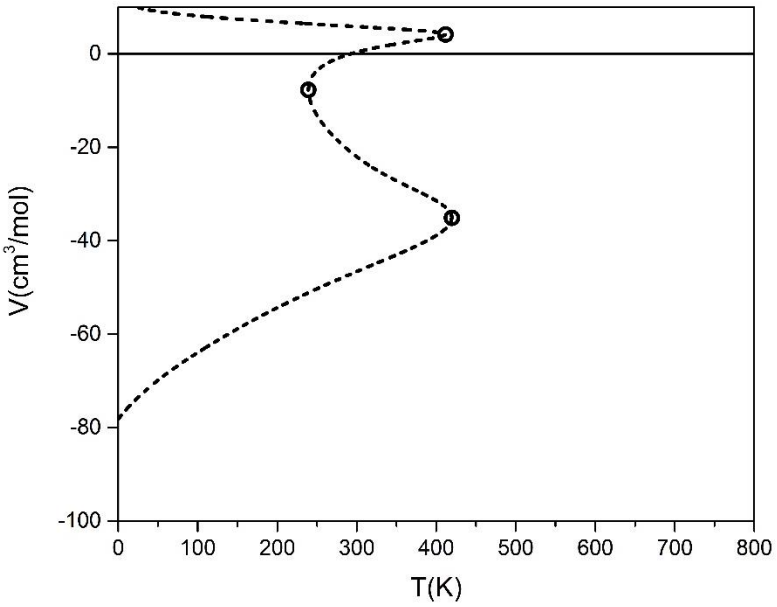

Figure 4.2 Lower branch molar volume region for methane (cm^3/mol) versus temperature (K) at 1 atm using PC-SAFT EOS. Dash curve indicate non-physical region. Open circles indicate turning points.

Figure 4.2 illustrates that the lower branch has three turning points. These turning points exist at 239.17, 411.65 and 419.65 K. **Table 4.1** lists the values of the seven roots at 7 K and 1 atm:

Table 4.1 Molar volume roots for methane at 7 K and 1 atm using PC-SAFT EOS.

Molar Volume Root Number	**Value (cm^3/mol)**
V_1	81.98
V_2	50.98
V_3	35.85
V_4	23.45
V_5	17.01
V_6	11.40
V_7	-76.74

In addition to the roots at 7 K, it is found that one pole (the denominator root) exists between V_5 and V_6 which has the value of 16.02 cm^3/mol. The number of roots might change depending on the selected temperature. For instance at 40 K, according to **Figures 4.1 & 4.2**, the number of roots is five. These roots are given in **Table 4.2** (31.16, 20.21, 19.27, 9.36 and -71.24 cm^3/mol). At this stage, it is important to shed light on which roots among these roots represent the physical behavior. For this reason, three tests are conducted to determine the physical roots. The three tests are added in **Table 4.2**. It is clear that the smallest root is negative which could be ignored. The mechanical stability would show that the second root (20.21 cm^3/mol) is not stable. If the reduced densities are obtained for the remaining roots, it would be clear that two roots (9.36 and 19.27 cm^3/mol) could also be ignored due to their values which are higher than the

maximum physical value. The minimum Gibbs free energy test would show that only one root is stable and physical. This root is 31.16 cm^3/mol.

Table 4.2 The analysis for finding the physical root for methane at 40 K and 1 atm using PC-SAFT EOS.

#	Value (cm^3/mol)	Mechanical Stability		Reduced Density		Gibbs Free Energy	
		Value	Result	Value	Result	Value	Result
V_1	31.16	-360.2	Stable	0.51	Physical	-17.4	Stable
V_2	20.21	3642.5	Unstable	-	-	-	-
V_3	19.27	-8245.5	Stable	0.83	Non-physical	-	-
V_4	9.36	$-1*10^8$	Stable	1.71	Non-physical	-	-
V_5	-71.24	-	-	-	-	-	-

In the previous table, it is clear that the physical root is available in the upper branch. Therefore, this indicates that the lower and middle branches are not physical branches.

Secondly, similar to PC-SAFT EOS, CK-SAFT EOS in the case of methane has also three branches, but it is unlike the PC-SAFT EOS where the upper branch is the physical branch. Also, the non-physical behavior of the physical branch is at higher temperature unlike in PC-SAFT EOS where it is at very low temperature. Moreover, the lower branch in case of CK-SAFT EOS is completely below the x-axis. The bifurcation diagram is generated for methane at 1 atm using CK-SAFT EOS.

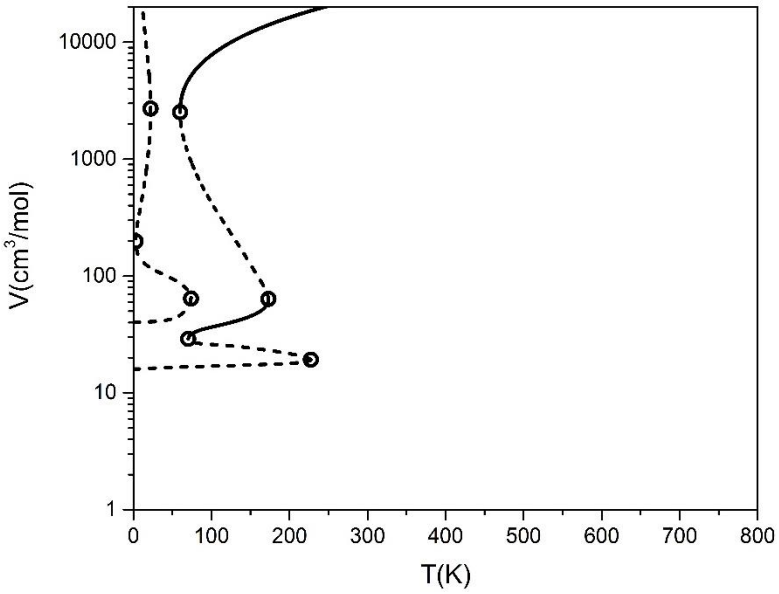

Figure 4.3 Molar volume of methane (cm^3/mol) (log-scale) versus temperature (K) at 1 atm using CK-SAFT EOS. Dash curves indicate non-physical regions. Open circles indicate turning points.

From the previous figure, it is obvious that the physical branch has four turning points while the upper branch has three turning points. These turning points exist at 2.86, 22.16, 59.76, 70.24, 73.92, 173.1, and 227.42 K. This number of turning points would cause the availability of several roots starting from one up to 9 depending on the specified temperature. For example, at 72 K, the CK-SAFT EOS exhibits 9 roots where two of them are negative roots as illustrated in **Figure 4.4**.

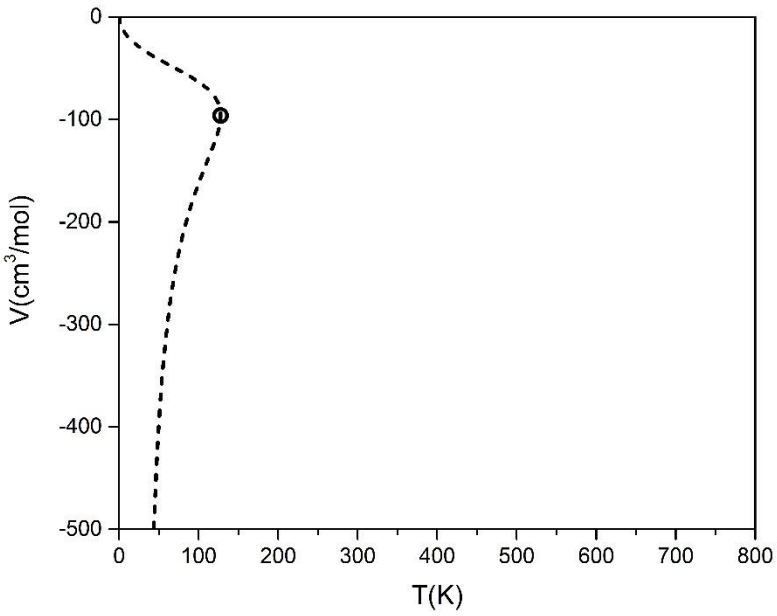

Figure 4.4 Negative region of molar volume for methane (cm^3/mol) versus temperature (K) at 1 atm using CK-SAFT EOS. Open circle indicates a turning point.

From the previous figure, the lower branch of CK-SAFT EOS has only one turning point at 127.75 K. **Table 4.3** lists the molar volume roots of methane at 72 K and 1 atm:

Table 4.3 Molar volume roots for methane at 72 K and 1 atm using CK-SAFT EOS.

Molar Volume Root Number	**Value (cm^3/mol)**
V_1	4952.4
V_2	1027.6
V_3	72.08
V_4	56.80
V_5	30.70
V_6	27.70
V_7	16.72
V_8	-50.65
V_9	-241.8

In addition to the previous roots, one pole exists between V_7 and V_8 which has the value of 15.97 cm^3/mol. The number of roots is not the same for all state conditions. Aslam and Sunol (2006) reported five reduced density roots for methane at 10 bar and 150 K as illustrated in **Table 4.4**. They reported also different number of reduced density roots for nitrogen at different state conditions as illustrated in **Tables 4.5 & 4.6**.

Table 4.4 A comparison of reduced density roots for methane at 10 bar and 150 K obtained in this work with the reported by Aslam and Sunol (2006).

Reduced Density Root Number	**(Aslam and Sunol, 2006)**	**This Work**	**Absolute Difference**
η_1	0.914	0.914	0.00%
η_2	0.654	0.654	0.00%
η_3	0.353	0.352	0.28%
η_4	0.070	0.099	41%
η_5	0.034	0.015	56%

From the previous table, the first three roots are similar in both studies but the last two have large difference. Koak et al. (1999) listed the mechanical stable molar volume roots for methane at 1.03070 MPa and 150 K as illustrated in **Table 4.5**. They called the lower molar volume root other than the two saturation molar volume roots as "V^{small}".

Table 4.5 A comparison of mechanically stable molar volume roots for methane at 1.03070 MPa and 150 K obtained in this work with the reported by Koak et al. (1999).

Mechanically Stable Molar Volume Root	**(Koak et al., 1999)**	**This Work**	**Absolute Difference**
V^{sat} (cm^3/mol)	990.414	990.423	0.00%
V^{sat} (cm^3/mol)	44.9901	44.9901	0.00%
V^{small} (cm^3/mol)	17.3397	17.3397	0.00%

From the previous table, the lower two molar volume roots are exactly same in both studies while for the first root the difference is very small. Koak et al. (1999) illustrate

that V^{small} has the lowest chemical potential than the other saturation roots. In addition, this root has a reduced density value of 0.91 which illustrates that this is not physical.

In case of nitrogen, Aslam and Sunol (2006) present two state conditions in which the first case gave five reduced density roots and the other gave three reduced density roots. The first case is at 80 K and 2 bar:

Table 4.6 A comparison of reduced density roots for nitrogen at 2 bar and 80 K obtained in this work with the reported by Aslam and Sunol (2006).

Reduced Density Root Number	**(Aslam and Sunol, 2006)**	**This Work**	**Absolute Difference**
η_1	0.931	0.931	0.00%
η_2	0.623	0.627	0.64%
η_3	0.406	0.406	0.00%
η_4	0.052	0.057	9.6%
η_5	0.008	0.005	40%
η_6	-	-0.130	-
η_7	-	-0.206	-

From the previous table, the first three roots are similar in the two studies but the next two roots are quite different especially the fifth root. Two more negative reduced density roots were not reported in their work which are located on the lower branch. In **Table 4.7**, the other case at 125 K and 30 bar is illustrated:

Table 4.7 A comparison of reduced density roots for nitrogen at 30 bar and 125 K obtained in this work with the reported by Aslam and Sunol (2006).

Reduced Density Root Number	**(Aslam and Sunol, 2006)**	**This Work**	**Absolute Difference**
η_1	0.883	0.885	0.23%
η_2	0.706	0.704	0.28%
η_3	0.264	0.0790	70.1%

In the previous table, the first two roots are similar in the two studies but the last roots are different.

Thirdly, for the case of soft SAFT EOS, methane has four branches. Two of them are located in the positive region of the molar volume while two of them are located in the negative region. One of the non-physical positive branches forms a shape of a closed loop. **Figure 4.5** illustrates the bifurcation diagram for the positive region of molar volume using soft SAFT generated for methane at 1 atm.

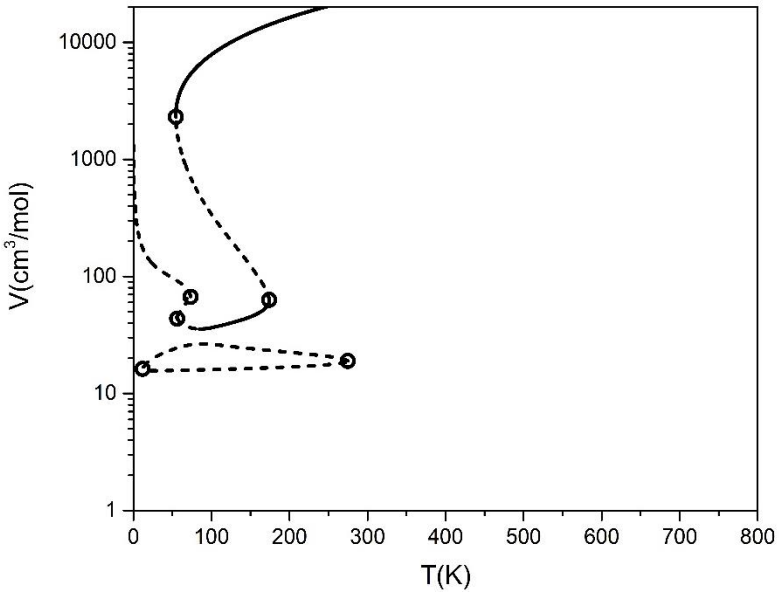

Figure 4.5 Molar volume of methane (cm^3/mol) (log-scale) versus temperature (K) at 1 atm using soft SAFT EOS. Dash curves indicate non-physical regions. Open circles indicate turning points.

From the previous figure, it is obvious that the physical branch has four turning points while the middle branch has two turning points. These turning points exist at 11.89, 54.29, 56.21, 73.3, 174.02 and 225.16 K. This number of turning points would cause the availability of several roots starting from one up to 7 depending on the specified temperature. For example, at 60 K, the soft SAFT EOS exhibits 7 roots as illustrated in **Table 4.8**. **Figure 4.6** illustrates the bifurcation diagrams of the lower branches.

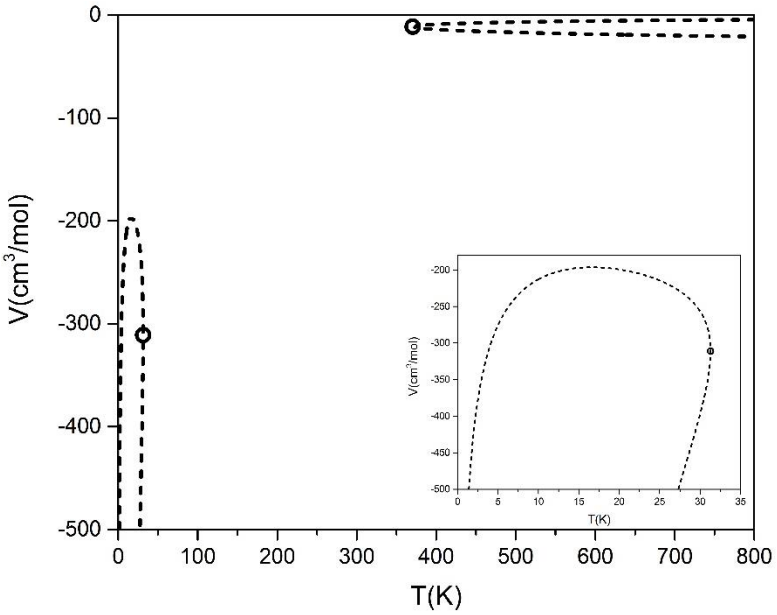

Figure 4.6 Negative region of molar volume for methane (cm^3/mol) versus temperature (K) at 1 atm using soft SAFT EOS. Open circle indicate turning point.

From the previous figure, two lower branches exist where each one of them has only one turning point. These turning points exist at 32.37 and 370.36 K. **Table 4.13** lists the molar volume roots of methane at 60 K and 1 atm:

Table 4.8 Molar volume roots for methane at 60 K and 1 atm using soft SAFT EOS.

Molar Volume Root Number	**Value (cm^3/mol)**
V_1	3793.6
V_2	1242.2
V_3	88.16
V_4	48.56
V_5	39.80
V_6	24.91
V_7	15.76

Unlike PC-SAFT and CK-SAFT EOSs, it is not possible to find the poles for soft SAFT EOSs because it is not in the form of polynomial over polynomial in terms of molar volume.

Finally, in simplified SAFT EOS, the physical branch exists only in the bifurcation diagram except at temperature lower than 2 K where a lower branch exists. **Figure 4.7** illustrates the bifurcation diagram of the positive molar volume of this version generated for methane at 1 atm.

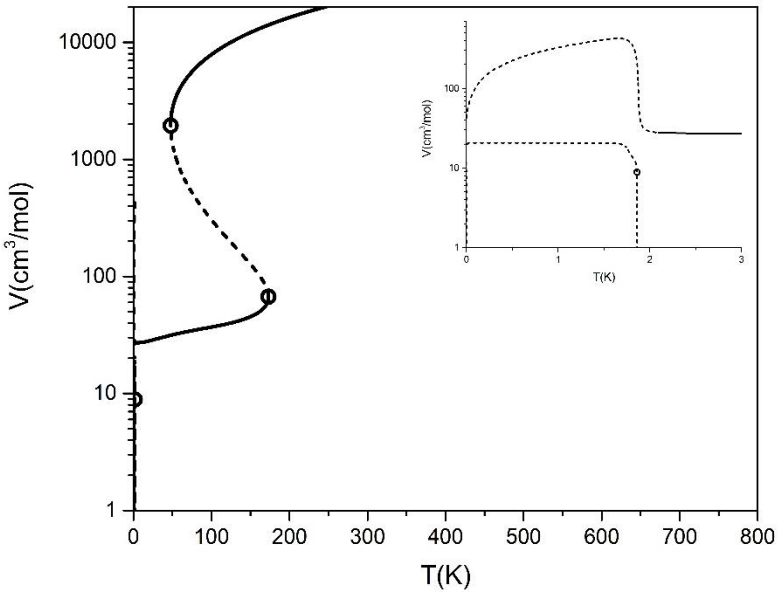

Figure 4.7 Molar volume of methane (cm^3/mol) (log-scale) versus temperature (K) at 1 atm using simplified SAFT EOS. Dash curves indicate non-physical regions. Open circles indicate turning points.

From the previous figure, it is obvious that the physical branch has two turning points while the lower branch has one turning point. These turning points exist at 1.86, 47.73 and 173.1 K. This number of turning points would cause the availability of several roots starting from one up to 3 depending on the specified temperature. For example, at 150 K, the simplified SAFT exhibits 3 roots. **Figure 4.8** illustrates the lower branch.

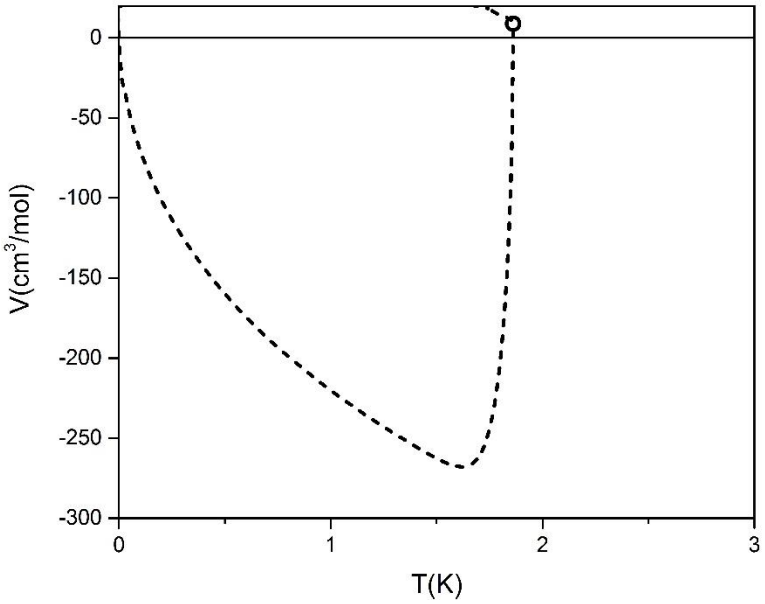

Figure 4.8 Lower branch molar volume values for methane (cm^3/mol) versus temperature (K) at 1 atm using soft SAFT EOS. Dash curves indicate non-physical regions. Open circle indicate turning point.

From the previous figure, the lower branch of simplified SAFT has only one turning point at 1.86 K. **Table 4.9** lists the molar volume roots of methane at 72 K and 1 atm:

Table 4.9 Molar volume roots for methane at 150 K and 1 atm using simplified SAFT EOS.

Molar Volume Root Number	**Value (cm^3/mol)**
$\mathbf{V_1}$	12153.4
$\mathbf{V_2}$	127.1
$\mathbf{V_3}$	45.28

In addition to the previous roots, two poles exist having values of 13.84 and -5.80 cm^3/mol which are located after the third molar volume root.

4.3 Effect of Pressure

The effect of pressure was evident in **Chapter 3** when the turning points in cubic EOSs became one at the critical pressure. Thus, the pressure is a main parameter that would affect the number of multiple volume roots and cause a change in the behavior of the bifurcation diagrams. Therefore, it is important to explore this effect in each SAFT EOS and to see how this would affect all the available branches.

Firstly, to study the effect of pressure in PC-SAFT EOS, **Figure 4.9** is plotted for the molar volume vs. temperature for nitrogen at different pressures including 1, 10 and 100 atm. The purpose of the selection of these values is to cover a wide range from low to high pressures including a value above the critical pressure of nitrogen which is 48.34 atm.

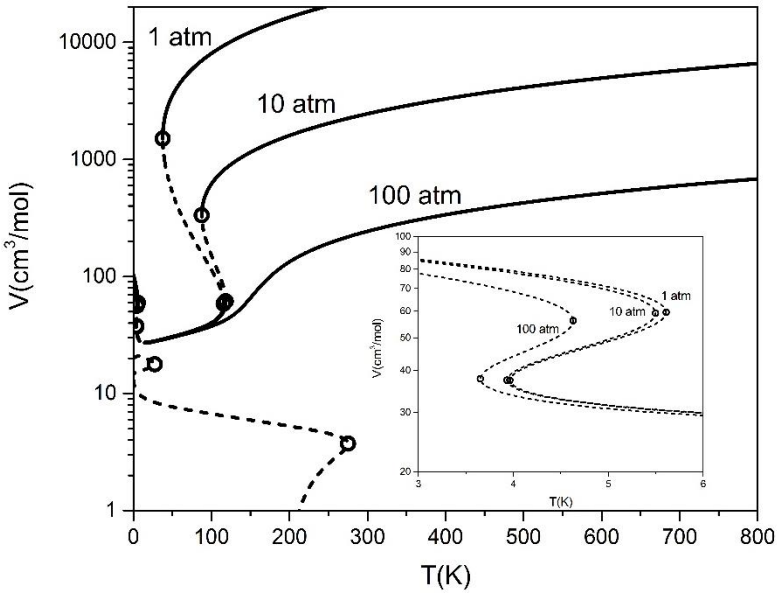

Figure 4.9 Molar volume of nitrogen (cm^3/mol) (log-scale) versus temperature (K) at 1, 10 and 100 atm using PC-SAFT EOS. Dash curves indicate non-physical regions. Open circles indicate turning points.

It is apparent from the figure that the upper branch is sensitive to the change of pressure. In a similar manner like what was found for cubic EOS, the gap representing by the dash curve between the two turning points, which are located at temperature above 50 K, gets shorter as comparison between 1 and 10 atm. However, the two turning points disappear at 100 atm. Indeed, the gap disappears for pressure greater than 46.16 atm which is the critical pressure. The same behavior is detected for the low temperature two turning points as illustrated in the magnified region in **Figure 4.9**. The region between the two turning points is shortened as the pressure is increased. This region is disappeared after passing the pressure value of 1360.38 atm which is found to be another critical pressure as it would be discussed later in section 4.5. Moreover, the whole region is shifted slightly towards the y-axis. However, it is interesting to note that the lower and middle branches are independent of the change of pressure.

Secondly, for the case of CK-SAFT EOS, as in the case of PC-SAFT EOS, the pressure affects the behavior of the physical branch by shortening the mechanically unstable regions which brings the two ends turning points closer to each other till the critical pressure where they combined into one point. After passing the critical pressure, this point disappears. However, the other branches in CK-SAFT EOS have small deviations unlike the non-physical branches in PC-SAFT EOS as illustrated clearly in the magnified regions in **Figure 4.10**.

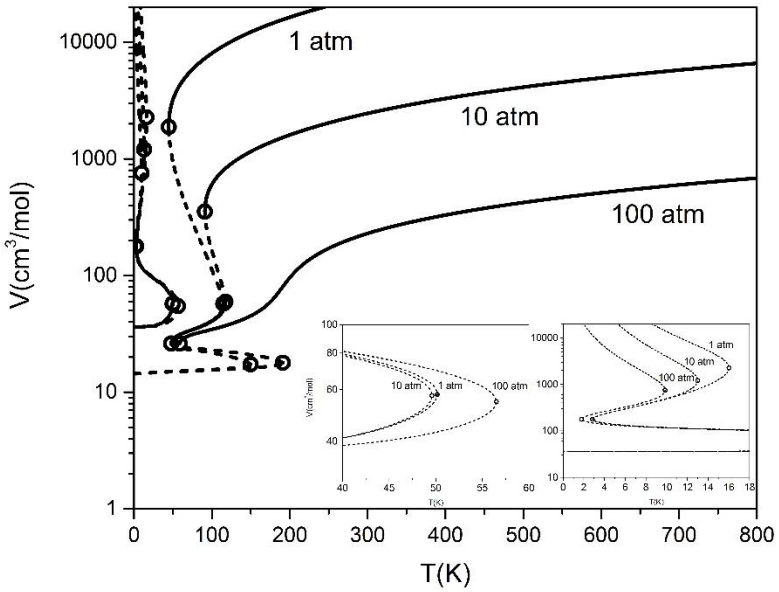

Figure 4.10 Molar volume of nitrogen (cm^3/mol) (log-scale) versus temperature (K) at 1, 10 and 100 atm using CK-SAFT EOS. Dash curves indicate non-physical regions. Open circles indicate turning points.

From the previous figure, the physical branch has been affect the most which caused by increasing the pressure. One of mechanically unstable regions disappeared after passing the pressure of 47.52 atm which is the pressure of the critical point. The right hand side magnified region illustrates that this part of the upper branch is getting closer to the y-axis with increasing the pressure. The left hand side magnified region illustrates that this part started to get closer as in the case of 10 atm, but after that it gets away from the y-axis as in the case of 100 atm.

Thirdly, the effect of increasing the pressure in soft SAFT EOS is the same as in PC-SAFT EOS. The physical branch is the only branch affected as illustrated in **Figure 4.11**.

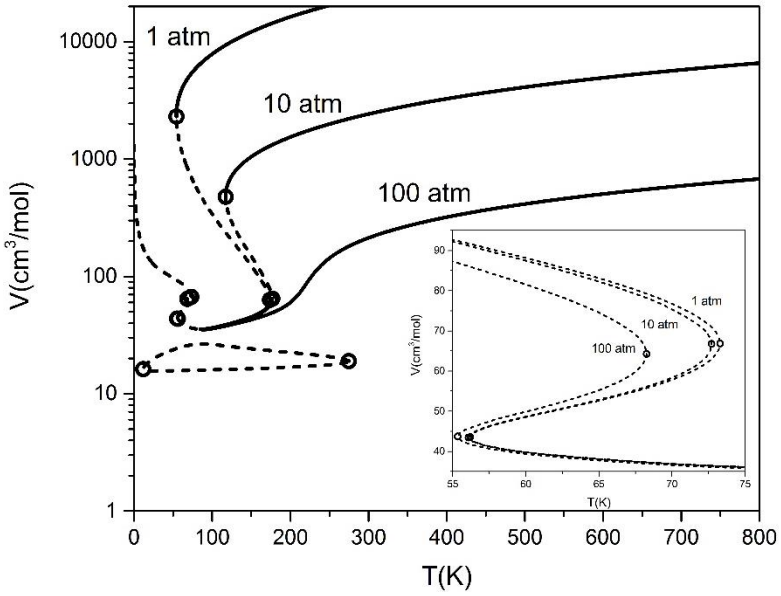

Figure 4.11 Molar volume of methane (cm^3/mol) (log-scale) versus temperature (K) at 1, 10 and 100 atm using soft SAFT EOS. Dash curves indicate non-physical regions. Open circles indicate turning points.

From the previous figure, the physical branch is the only branch which is affected by pressure. One of the mechanically unstable regions disappeared after passing the pressure of 50.60 atm which is the pressure of the critical point.

Finally, pertaining simplified SAFT EOS, similar to PC-SAFT and soft SAFT EOSs, as pressure is increased, the physical branch is affected only as illustrated in **Figure 4.12**.

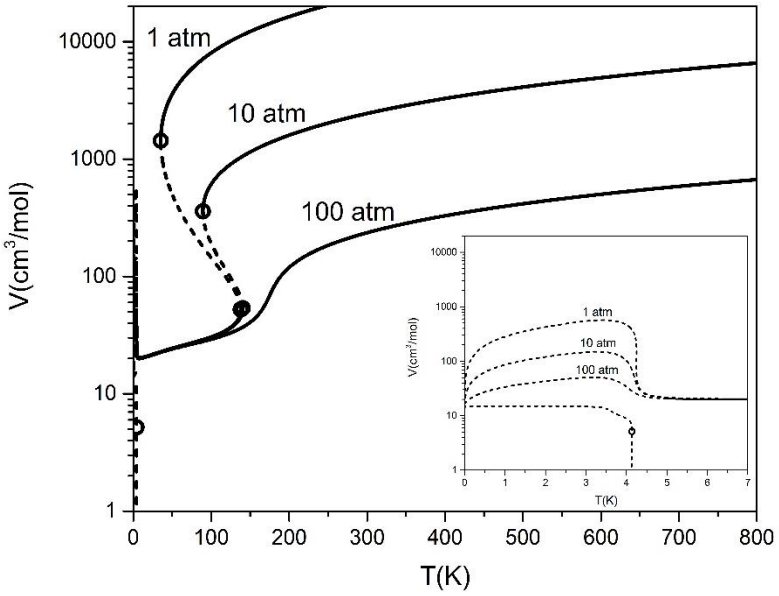

Figure 4.12 Molar volume of methane (cm^3/mol) (log-scale) versus temperature (K) at 1, 10 and 100 atm using simplified SAFT EOS. Dash curves indicate non-physical region. Open circles indicate turning points.

From the previous figure, the physical branch is the only branch which is affected by pressure. The only mechanically unstable region disappeared after passing the pressure of 56.11 atm which is the pressure of the critical point.

4.4 Effect of Model's Parameters

To represent any non-association component in SAFT, three adjustable parameters are used to characterize the components as explained previously in section 2.4. In this section, the bifurcation diagrams for different spherical components are compared to show the effect of the model's parameters on the branches.

Firstly, starting with PC-SAFT EOS, **Figure 4.13** compares the bifurcation diagrams of methane and nitrogen at 1 atm.

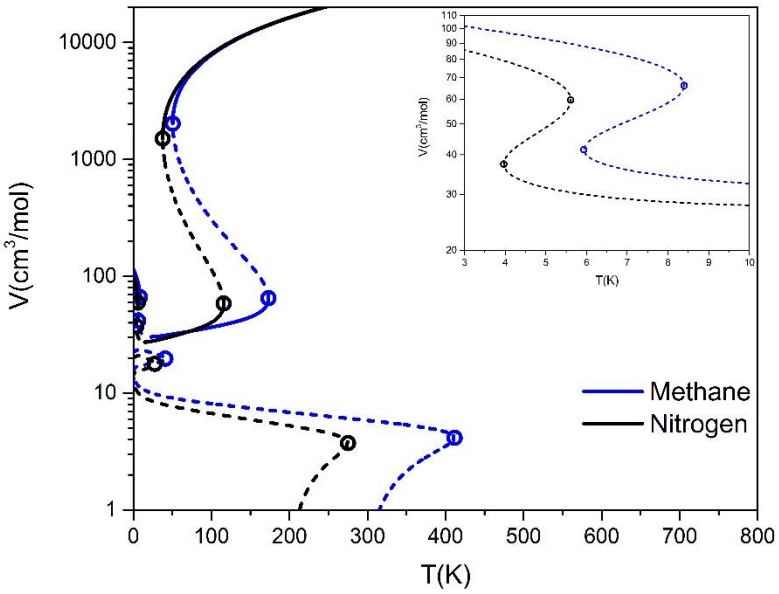

Figure 4.13 Molar volume of methane and nitrogen (cm^3/mol) (log-scale) versus temperature (K) at 1 atm using PC-SAFT EOS. Dash curves indicate non-physical regions. Open circles indicate turning points.

The previous figure illustrates clearly a shift in temperature due to change in segment energy "ε/k" and in molar volume due to change in segment diameter "σ" for all branches. **Table 4.10** lists the parameters of the two components with absolute difference is given:

Table 4.10 PC-SAFT EOS parameters for nitrogen and methane.

	Nitrogen	**Methane**	**Absolute Difference**
$\boldsymbol{m}$ **(-)**	1	1	0
$\boldsymbol{\sigma}$ $\boldsymbol{(m^{-8})}$	3.5767	3.7039	0.1272
$\boldsymbol{\varepsilon/k}$ **(K)**	100.28	150.03	49.75

Figure 4.14 illustrates another comparison between nitrogen and hydrogen. The latter has the smallest segment diameter and energy. The integration constant for hydrogen is 0.241 which is an exceptional case (Economou, 2002).

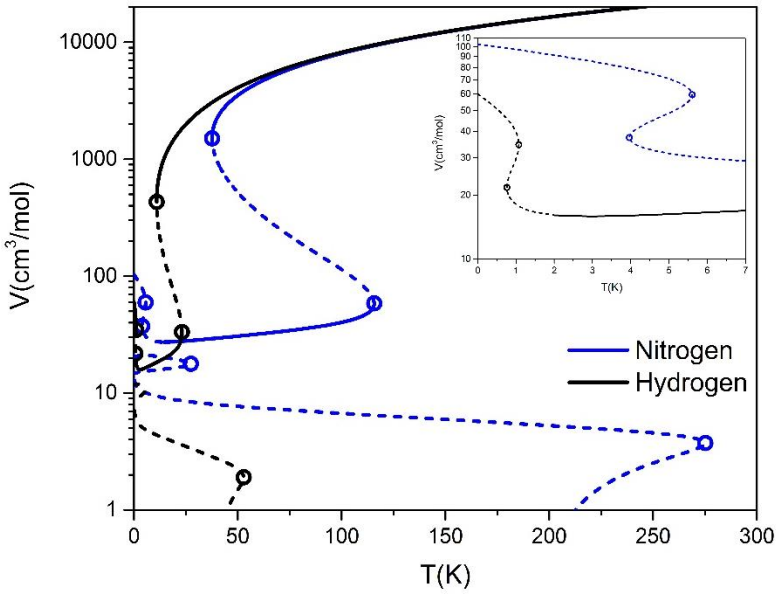

Figure 4.14 Molar volume of nitrogen and hydrogen (cm^3/mol) (log-scale) versus temperature (K) at 1 atm using PC-SAFT EOS. Dash curves indicate non-physical regions. Open circles indicate turning points.

The previous figure illustrates clearly large shift in temperature due to large change in segment energy "ε/k" and in molar volume due to change in segment diameter "σ" for the all branches. **Table 4.11** lists the parameters of the two components with absolute difference is given:

Table 4.11 PC-SAFT EOS parameters for hydrogen (Ghosh et al., 2003) and nitrogen.

	Hydrogen	**Nitrogen**	**Absolute Difference**
$\boldsymbol{m}$ (-)	1	1	0
$\boldsymbol{\sigma}$ $(\boldsymbol{m^{-8}})$	2.9860	3.5767	0.5907
$\boldsymbol{\varepsilon/k}$ (K)	19.278	100.28	81.002
$\boldsymbol{C}$	0.241	0.12	-

The change in integration constant does not contribute directly to the branches' shift. Thus, the absolute difference in the integration constant is not calculated.

Secondly, similar to the case of PC-SAFT EOS, the bifurcation diagrams for methane and nitrogen using CK-SAFT EOS are going to be compared to show the effect of the model's parameters on the branches as illustrated in **Figure 4.15**.

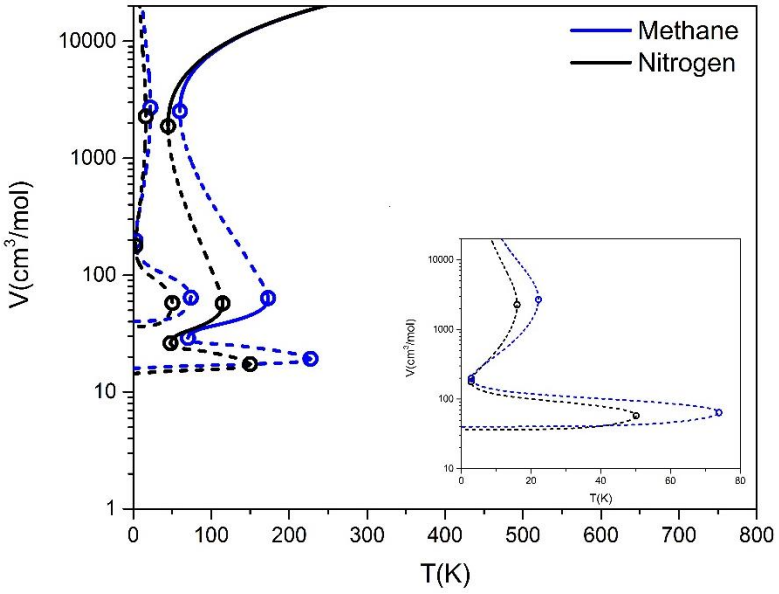

Figure 4.15 Molar volume of methane and nitrogen (cm^3/mol) (log-scale) versus temperature (K) at 1 atm using CK-SAFT EOS. Dash curves indicate non-physical regions. Open circles indicate turning points.

The previous figure illustrates a shift in temperature due to change in segment energy "u^o/k" and in molar volume due to change in segment volume "v^{oo}" for all branches. The two shifts are also shown clearly in the magnified region. **Table 4.12** lists the parameters of the two components with absolute difference is given:

Table 4.12 CK-SAFT EOS parameters for nitrogen and methane (Haung and Radosz, 1990).

	Nitrogen	**Methane**	**Absolute Difference**
$\boldsymbol{m}$ (-)	1	1	0
$\boldsymbol{v^{oo}}$ (ml/mol)	19.457	21.576	2.119
$\boldsymbol{u^o/k}$ (K)	123.53	190.29	66.76
$\boldsymbol{e/k}$ (K)	3	1	-

The change in the well depth of the potential (e/k) does not contribute directly to the branches' shift. Therefore, the absolute difference in the well depth of the potential is not calculated.

Thirdly, pertaining soft SAFT EOS, there is no available parameter to compare different spherical components with methane.

Finally, in simplified SAFT EOS, the bifurcation diagrams for methane and argon are compared to show the effect of the model's parameters on the branches as illustrated in **Figure 4.16**.

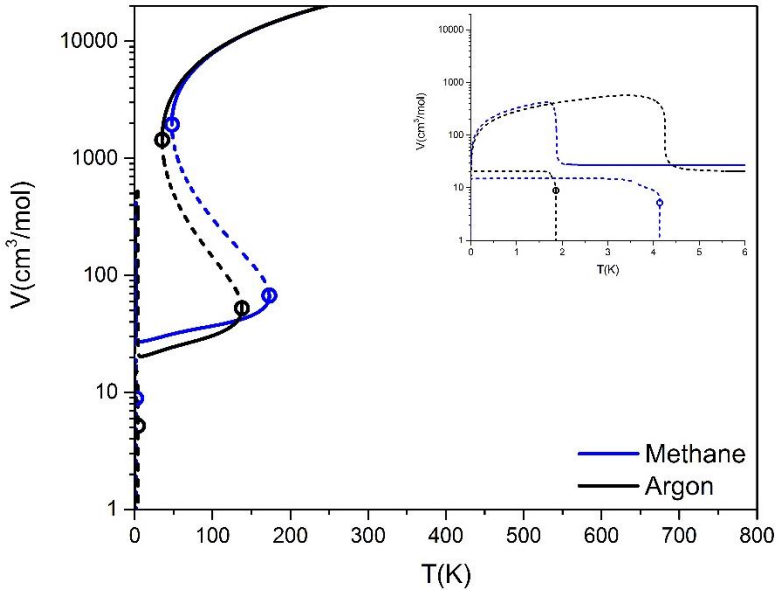

Figure 4.16 Molar volume of methane and argon (cm^3/mol) (log-scale) versus temperature (K) at 1 atm using simplified SAFT EOS. Dash curves indicates non-physical region. Open circles indicate turning points.

The previous figure illustrates a shift in temperature due to change in segment energy "u^o/k" and in molar volume due to change in segment volume "v^{oo}" for all branches. **Table 4.13** lists the parameters of the two components along with the integration constant and "e/k":

Table 4.13 Simplified SAFT EOS parameters for argon and methane.

	Argon	**Methane**
$\boldsymbol{m}$ (-)	1	1
$\boldsymbol{v^{oo}}$ (ml/mol)	16.807	23.137
$\boldsymbol{u^o/k}$ (K)	66.765	82.141
$\boldsymbol{C}$	0.27447	0.35521
$\boldsymbol{e/k}$ (K)	-4.1292	-1.8608

4.5 Critical Points

It is stated in section 4.2 that the existence of critical points is related to regions between two turning points. These regions are known to be mechanically unstable regions. As the pressure is increased, these regions are shortened and they vanished at the critical pressures. Closer to the critical pressures, the two turning points are found to be almost combined into one point. This point is indeed a suitable initial guess for solving the set of **Equations (3.8, 3.9 and 3.10)** in which each critical point has to satisfy. The initial guess is inserted along with the equations in a Mathematica© command called "*FindRoot*" to get the corresponding critical point. The same way is used to calculate all the critical points presented in this chapter.

Firstly, the initial guess points used to find the critical points for methane using PC-SAFT EOS are shown in **Figures (4.17, 4.18 and 4.19)**. The number of critical points for methane using PC-SAFT EOS are found to be three as follows:

1) The first point: T_c=191.40 K, P_c=46.16 atm and V_c=108.3 cm^3/mol.

2) The second point: T_c=3.098 K, P_c=1360.38 atm and V_c=48.47 cm^3/mol.

3) The third point: T_c=50.96 K, P_c=9081.09 atm and V_c=21.19 cm^3/mol.

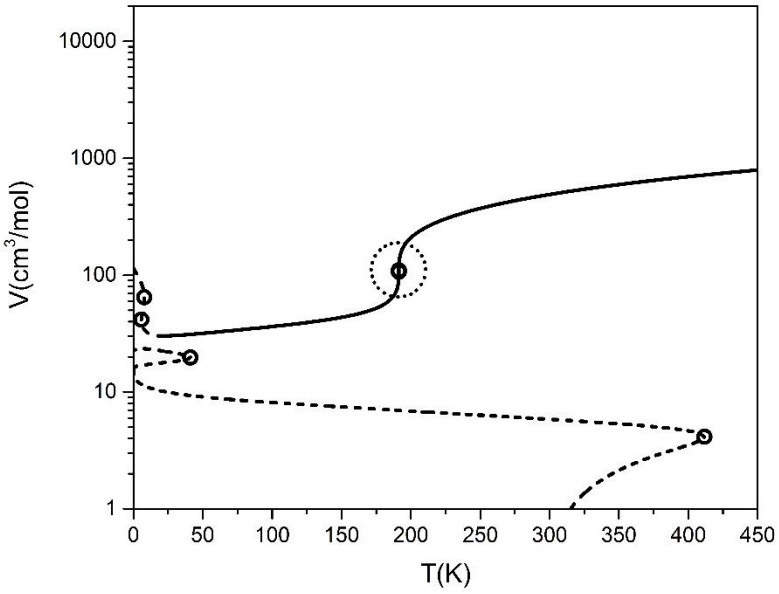

Figure 4.17 Molar volume of methane (cm^3/mol) (log-scale) versus temperature (K) at 46.139 atm using PC-SAFT EOS. Dash curves indicate non-physical region. Open circles indicate turning points. Dot circle illustrates the initial guess of the first critical point.

In the previous figure, the dot circle illustrates the initial guess point used to get the first critical point in the previous list. This critical point is the physical and experimentally well-known critical point. **Figure 4.18** illustrates the second initial guess point.

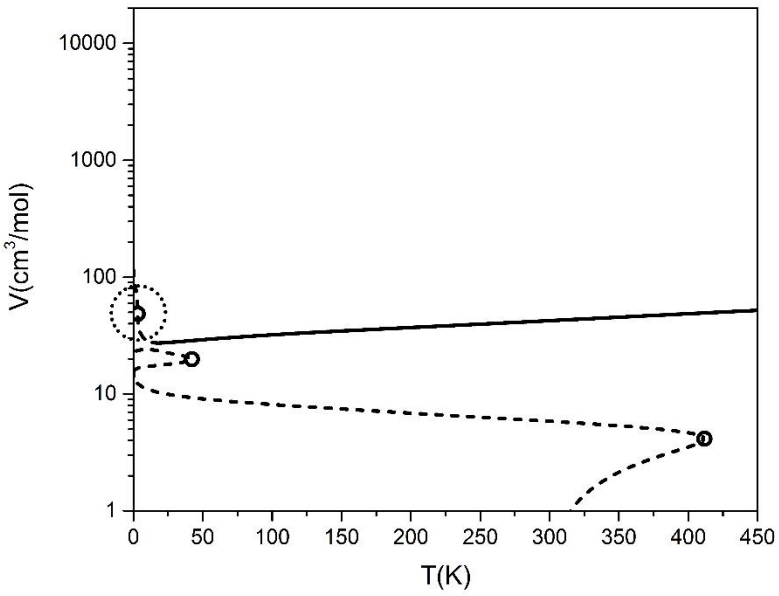

Figure 4.18 Molar volume of methane (cm^3/mol) (log-scale) versus temperature (K) at 1359 atm using PC-SAFT EOS. Dash curves indicate non-physical region. Open circles indicate turning points. Dot circle illustrates the initial guess of the second critical point.

In the previous figure, the dot circle illustrates the initial guess of the second critical point in the previous list. This critical point has not been reported by Privat et al. (2010). **Figure 4.19** illustrates the third initial guess point.

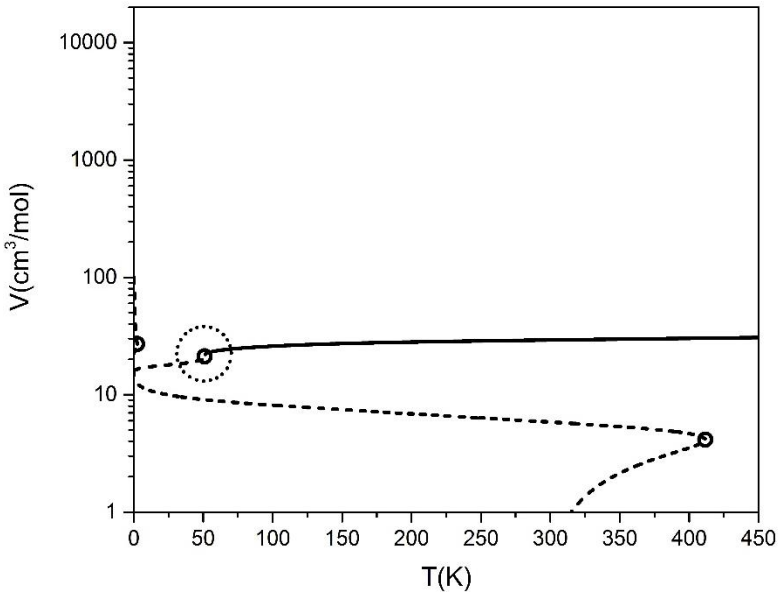

Figure 4.19 Molar volume of methane (cm^3/mol) (log-scale) versus temperature (K) at 9077.9 atm using PC-SAFT EOS. Dash curves indicate non-physical region. Open circles indicate turning points. Dot circle illustrates the initial guess of the third critical point.

In the previous figure, the dot circle illustrates the initial guess of the third critical point in the previous list. This critical point has been reported by Privat et al. (2010) as additional critical point. However, there is no mechanically unstable region corresponding to this critical point in **Figure 4.1**. **Figure 4.20** illustrates a bifurcation diagram at lower pressure than shown in **Figure 4.19**.

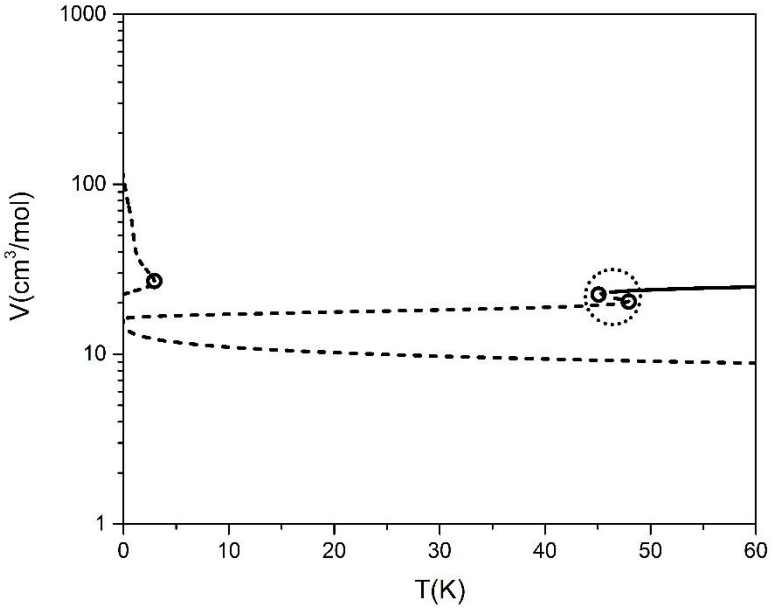

Figure 4.20 Molar volume of methane (cm^3/mol) (log-scale) versus temperature (K) at 7000 atm using PC-SAFT EOS. Dash curves indicate non-physical region. Open circles indicate turning points. Dot circle illustrates the third mechanically unstable region.

From the previous figure, the third mechanically unstable region is illustrated. This new region started at 2000.8 atm as illustrated in **Figure 4.21**.

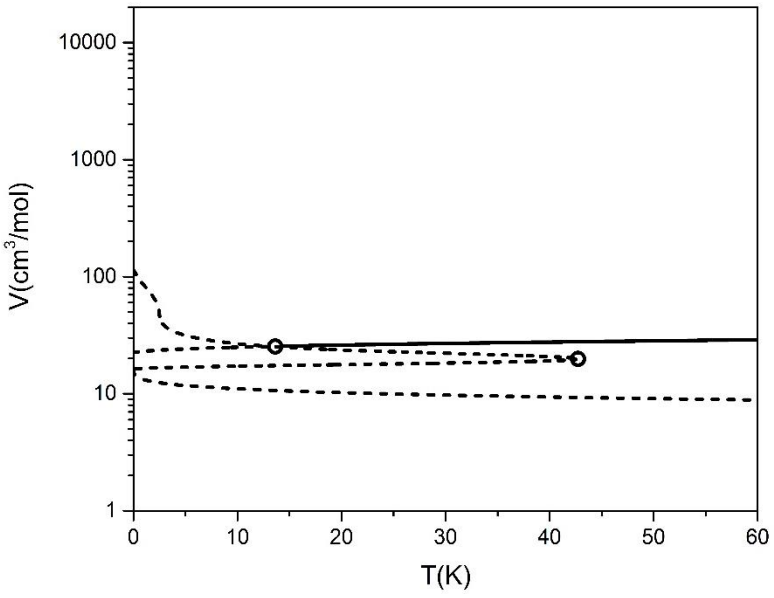

Figure 4.21 Molar volume of methane (cm^3/mol) (log-scale) versus temperature (K) at 2000.8 atm using PC-SAFT EOS. Dash curves indicate non-physical region. Open circles indicate turning points.

From the previous figure, a combination between the upper and middle branches formed a new mechanically unstable region and two new turning points but not clearly shown because they are exactly on the same point. **Figure 4.20** shows clearly three turning points at 7000 atm in the demonstrated region while **Figure 4.22** shows only one turning point at 1500 atm in the same region. This is an evidence of having two more turning points after passing the touching pressure of 2000.8 atm. Another situation pertaining the combination behavior is available also in the next chapter.

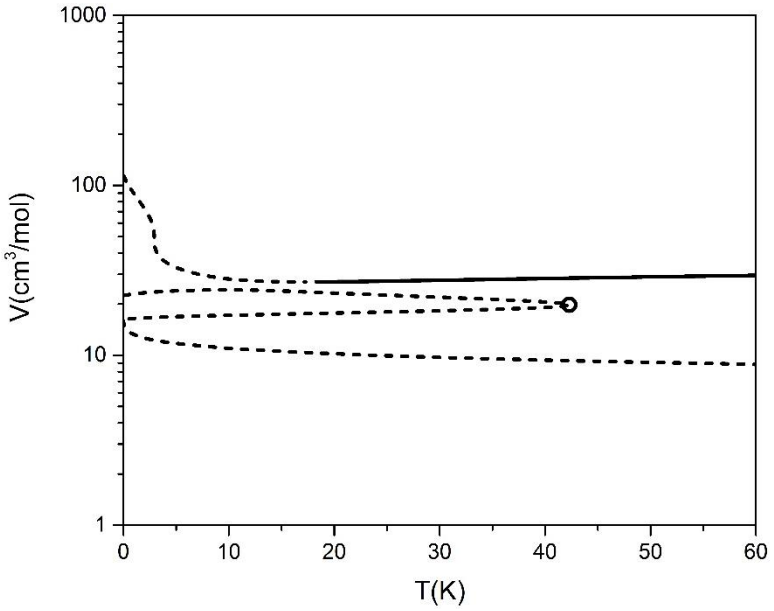

Figure 4.22 Molar volume of methane (cm^3/mol) (log-scale) versus temperature (K) at 1500 atm using PC-SAFT EOS. Dash curves indicate non-physical region. Open circles indicate turning points.

The following table compares the critical points for methane using PC-SAFT EOS of this work with the reported by Privat et al. (2010):

Table 4.14 Critical points for methane using PC-SAFT EOS obtained in this work compared with Privat et al. (2010).

Critical Points		(Privat et al., 2010)	This Work	Absolute Difference
First	T_c (K)	191.40	191.40	0.00%
	P_c (bar)	46.75	46.77	0.04%
	η_c	0.1429	0.1429	0.00%
Second	T_c (K)	-	3.098	-
	P_c (bar)	-	1378.41	-
	η_c	-	0.3305	-
Third	T_c (K)	50.96	50.96	0.00%
	P_c (bar)	9198.22	9201.41	0.03%
	η_c	0.7559	0.7559	0.00%

As it is stated in the case of PC-SAFT EOS, from bifurcation diagrams point of view, the critical points are the points where the two ends of a mechanically unstable region combined. The combined point can be easily figured out by focusing on the corresponding branch while increasing the pressure. Then, this point which has the coordination of (T_c, P_c, V_c) is used as initial guess to solve the **Equations 3.8, 3.9 & 3.10** simultaneously. The number of critical points for methane using CK-SAFT EOS is found to be two as follows:

1) The first point: T_c=192.17 K, P_c=47.52 atm and V_c=95.71 cm^3/mol.

2) The second point: T_c=242.85 K, P_c=32217.1 atm and V_c=20.48 cm^3/mol.

Secondly, the following table compares the critical points for methane using CK-SAFT EOS of this work with the reported by Polishuk (2010):

Table 4.15 The critical points for methane using CK-SAFT EOS obtained in this work compared with the reported by Polishuk (2010).

Critical Point		**(Polishuk, 2010)**	**This Work**	**Absolute Difference**
First	**T_c (K)**	192.17	192.17	0.00%
	P_c (bar)	48.15	48.15	0.00%
	η_c	-	0.1638	-
Second	**T_c (K)**	242.85	242.85	0.00%
	P_c (bar)	32643.7	32644.0	0.00%
	η_c	-	0.7535	-

Thirdly, in the case of methane using soft SAFT EOS, it is similar to CK-SAFT EOS where the number of critical points is two as follows:

1) The first point: T_c=193.4 K, P_c=50.60 atm and V_c=100.1 cm^3/mol.

2) The second point: T_c=320.9 K, P_c=24194.9 atm and V_c=20.71 cm^3/mol.

The following table compares the first critical point of methane obtained in this study with the reported by Llovell et al. (2004):

Table 4.16 The first critical point for methane using soft SAFT EOS obtained in this work compared with the reported by Llovell et al. (2004).

Critical Point		(Llovell et al., 2004)	This Work	Absolute Difference
First	T_c (K)	193.3	193.4	0.05%
	P_c (MPa)	5.10	5.13	0.59%
	D_c (mol/dm^3)	9.93	9.99	0.60%

Finally, for simplified SAFT EOS, only one critical point is found for methane which has the coordinates of: T_c=195.7 K, P_c=56.11 atm and V_c=101.2 cm^3/mol.

4.6 Comparisons

In section 4.2, one of the main purposes was to generate the bifurcation diagrams of spherical molecules for four SAFT versions to figure out the effect of the number of branches and turning points on the multiple molar volume roots problem through different SAFT versions. The focus of the current section is to compare the obtained results in section 4.2 among different SAFT versions. This section is very useful before stating the conclusions of the whole chapter in the coming section.

Three comparisons are going to be held in this section. The first comparison illustrated in **Figure 4.23** demonstrates how the physical branches for spherical molecules are generated using van der Waals, Peng-Robinson, PC-SAFT, CK-SAFT, soft SAFT and simplified SAFT EOSs. This comparison is very important to show how much SAFT versions agree about the physical behavior. Moreover, this comparison is very helpful to note any non-physical behavior in the physical branches. The second

comparison in **Table 4.17** is a quantitative comparison which shows the number of branches, turning points, critical points and maximum number of molar volume roots in each of van der Waals, PC-SAFT, CK-SAFT, soft SAFT and simplified SAFT EOSs. Moreover, at the last column, **Table 4.17** gives whether the physical branch is the only affected branch by increasing the pressure or not. Finally, the last comparison in the section is illustrated in **Table 4.18**. It compares the first (physical) critical point for methane among van der Waals, PC-SAFT, CK-SAFT, soft SAFT, simplified SAFT models with the experimental critical point. The purpose of this comparison is to show that the presented critical points for many components using SAFT EOS in this chapter are not accurate and they need to be corrected. These corrections are well known in the literature. The following figure illustrates the first comparison.

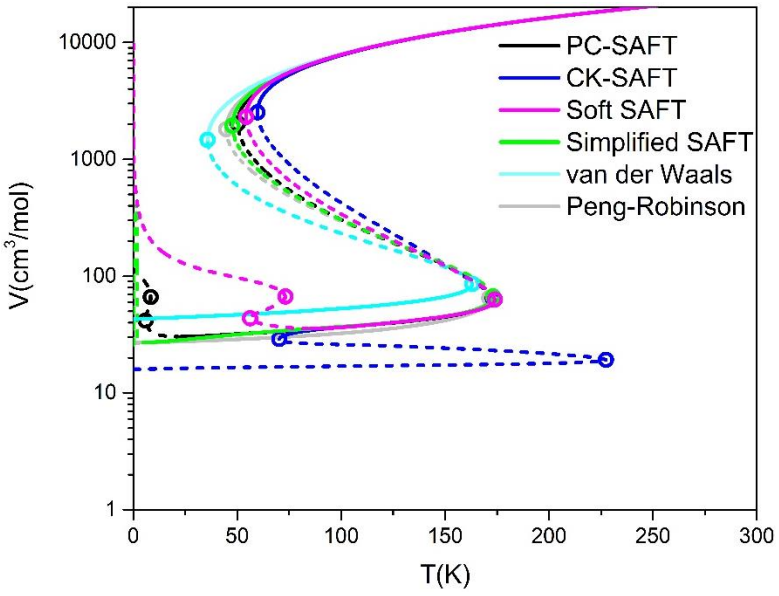

Figure 4.23 A comparison among the physical branches of the PC-SAFT, CK-SAFT, soft SAFT, simplified SAFT, van der Waals and Peng-Robinson EOSs for methane at 1 atm. Dash curves indicate non-physical regions. Open circles indicate turning points.

From the previous figure, all the models are showing the same behavior in the gas phase. By going to the solid phase, CK-SAFT and soft SAFT are going to lower and higher values respectively. The simplified SAFT and Peng-Robinson are matching each other even at very low temperature. At 25 K, the PC-SAFT EOS deviates upwards to values higher than the van der Waals EOS. There is not matching between any two EOSs in mechanically unstable region which may cause critical points to be different. The following table illustrates the second comparison:

Table 4.17 A comparison among the number of branches, turning points, critical points, maximum number of roots and the effect of pressure of van der Waals, PC-SAFT, CK-SAFT, soft SAFT and simplified SAFT for the case of methane.

Model	**Number of Branches**	**Number of Turning Points**		**Number of Critical Points**	**Maximum Number of Roots**	**Branches Affected by Changing Pressure**
		Before the First Critical Point	**After the First Critical Point**			
van der Waals	1	2	0	1	3	Physical
PC-SAFT	3	8	6	3	7	Physical
CK-SAFT	3	8	6	2	9	All
Soft SAFT	4	8	6	2	7	Physical
Simplified SAFT	2	3	1	1	3	Physical

In the previous table, van der Waals cubic EOS is presented to show that SAFT EOS versions have much more number of branches, turning points, critical points and maximum molar volume roots than cubic EOSs. Focusing on SAFT EOS versions for the case of methane, soft SAFT EOS is shown to have highest number of branches among SAFT version while simplified SAFT has the lowest. PC-SAFT, CK-SAFT and soft SAFT have the same number of turning points which is higher than the number of turning points in simplified SAFT. PC-SAFT EOS has the highest number of critical points while simplified SAFT has the lowest. CK-SAFT EOS has the highest maximum number of molar volume roots while simplified SAFT has the lowest. CK-SAFT EOS is the only model in which the non-physical branches is also affected by increasing the pressure. **Table 4.18** illustrates the third comparison:

Table 4.18 A comparison between the critical point given by van der Waals, PC-SAFT, CK-SAFT, soft SAFT and simplified SAFT EOSs with the experimental values for the case of methane.

Model	**T_c (K)**	**P_c (atm)**	**V_c (cm^3/mol)**
Experimental	190.56	45.39	98.34
van der Waals	192.70	46.20	128.3
PC-SAFT	191.40	46.16	108.3
CK-SAFT	192.17	47.52	95.71
Soft SAFT	193.41	50.60	100.1
Simplified SAFT	195.68	56.11	101.2

4.7 Conclusions

In this chapter, PC-SAFT, CK-SAFT, soft SAFT and simplified SAFT EOSs were explored through bifurcation and stability analysis for the simplest case of spherical molecules to investigate the multiple molar volume roots problem.

In section 4.2, the bifurcation diagrams were generated for the four SAFT versions and the criteria for selecting the physical root explained in section 3.3 was applied. Firstly, for the case of methane using PC-SAFT EOS, it was found that there were three branches where one of them represents the physical behavior except at very low temperature. The other two branches were below the physical branch. In addition, it was found that the maximum number of roots that PC-SAFT can exhibits was seven molar volume roots. Secondly, for the same component using CK-SAFT EOS, it was found that there were three branches where one of them represented the physical behavior except at higher temperature than the in the case of PC-SAFT EOS. Moreover, it was found that CK-SAFT exhibited up to nine molar volume roots. The molar volume roots at some state conditions using CK-SAFT EOS were compared with the reported in the literature. This work molar volume roots showed good match with the reported by Aslam and Sunol (2006) except at higher molar volume roots. However, this work results showed good match for all ranges of molar volume with the reported by Koak et al (1999). Thirdly, for the case of soft SAFT EOS, the number of branches were four branches where one of them represented the physical behavior unless lower than a temperature similar to the case of CK-SAFT EOS. The maximum number of roots that soft SAFT can exhibit were seven molar volume roots. Finally, for the case of simplified

SAFT EOS, the number of branches was found to be two only. The second branch existed only at very low temperature. So, at higher temperature, simplified SAFT was found to behave like any cubic EOS in which the number of roots were up to three molar volume roots only.

In section 4.3, the effect of pressure on the branches of PC-SAFT, CK-SAFT, soft SAFT and simplified SAFT EOSs were explored. For all these versions, the mechanically unstable regions were shortened by increasing the pressure bringing the two ends turning points closer to each other till the point where they were combined into one point. This point was investigated to be the critical point. The non-physical branches were independent of pressure except for the case of CK-SAFT EOS in which all the branches including the non-physical branches were pressure dependent.

In section 4.4, the effect of PC-SAFT, CK-SAFT, soft SAFT and simplified SAFT EOSs parameters on the bifurcation diagrams were investigated by generating the diagrams for different components. It was clear that the segment diameter or volume interfere the diagram by shifting them along the molar volume axis. Moreover, the segment energy was found to affect the diagrams by shifting them along the temperature axis.

In section 4.5, the criteria of calculating the critical points explained in **Chapter 3** was implemented on the four SAFT versions. The number of critical points for PC-SAFT EOS was found to be three where two of them were reported by Private et al (2010) while the third point was reported in this work for the first time. CK-SAFT and soft SAFT

EOSs showed two critical points while simplified SAFT EOS showed only one critical point like any cubic EOS.

In section 4.6, three comparisons were held to emphasis on the similarity and differences among the studied models. In the first comparison where the physical branches for van der Waals, Peng-Robinson, PC-SAFT, CK-SAFT, soft SAFT and simplified SAFT EOSs were plotted in one figure, it was shown that the four SAFT versions agreed in the gas and liquid region but differed in the mechanically unstable region and the low temperature regions. In the second comparison where the number of branches, turning points, critical points, maximum number of molar volume roots and the pressure dependency of the branches were compared, simplified SAFT EOS showed minimum number of branches, turning points, critical points and maximum number of molar volume roots among the studied SAFT versions in this chapter.

In the next chapter, the implemented bifurcation and stability analysis for spherical molecules in this chapter is going to be extended for the chain molecules. Spherical molecules are the simplest components to study and few components are under this category. All the other components are affected by the covalent bonds among their segments. Thus, adding the chain term to the SAFT terms is crucial and the effect of adding the chain term to the bifurcation diagrams is one of the objectives of this thesis. The next chapter is going to cover the chain components starting from short chain molecules to longer chain molecules to investigate the effect of having longer chain on the bifurcation diagrams.

CHAPTER 5

Bifurcation and Stability Analysis for Chain Molecules using the SAFT EOS

5.1 Introduction

In **Chapter 4**, the bifurcation and stability analysis were applied successfully to PC-SAFT, CK-SAFT, soft SAFT and simplified SAFT EOSs for spherical molecules. In this chapter, the bifurcation and stability analysis is extended to the chain molecules. Hence, the segment number "m" does not equal one. The effect of adding the chain term on the multiple molar volume roots is studied. Similar to Chapter 4, the multiple volume roots and critical points obtained using PC-SAFT, CK-SAFT, soft SAFT and simplified SAFT EOSs will be compared to those obtained in the literature whenever it is possible. The same analysis of **Chapter 4** is going to be applied in this chapter. The same sections arrangement of **Chapter 4** is also used.

5.2 Bifurcation Diagrams for SAFT EOS

The importance of studying the bifurcation diagrams was explained in section 4.2. In this section, the number of branches and hence molar volume roots is different from spherical molecules because of the new added chain term. The effect of adding the chain term is going to be explored in this section for PC-SAFT, CK-SAFT, soft SAFT and simplified SAFT EOSs.

Firstly, the PC-SAFT EOS in the case of ethane has four branches in which only one of them includes the physical behavior which is the upper branch. One of the middle branches is added by the chain term. It is located in the range of 10-20 cm^3/mol in **Figure 5.1** and seems to be connected with the next upper and next lower branches at T=0 K. The non-physical behavior at lower temperature in the physical branch exists also after adding the chain term. **Figure 5.1** illustrates the bifurcation diagram of the PC-SAFT EOS for the case of ethane.

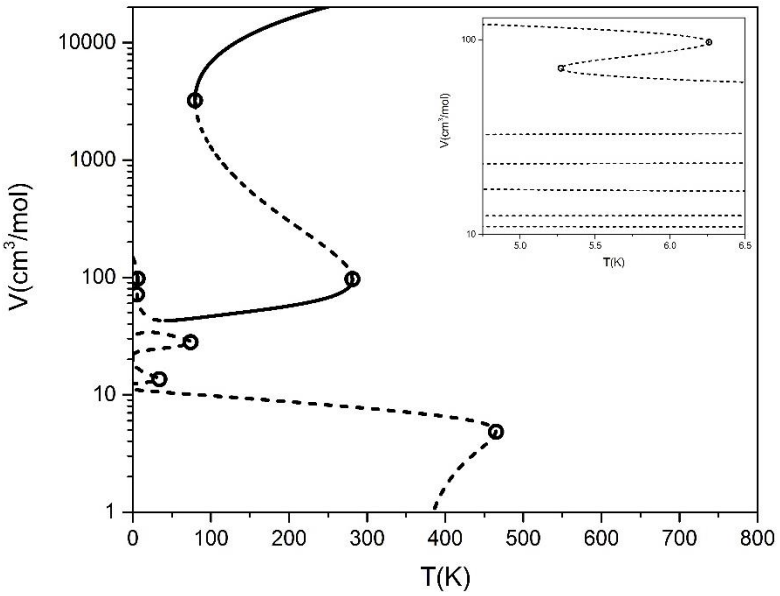

Figure 5.1 Molar volume of ethane (cm^3/mol) (log-scale) versus temperature (K) at 1 atm using PC-SAFT EOS. Dash curves indicate non-physical regions. Open circles indicate turning points.

From the previous figure, it is obvious that the physical branch has four turning points while the lower and two middle branches have one turning point for each. These turning points exist at 5.27, 6.26, 33.88, 74.05, 79.79, 281.28 and 465.21 K. This number of turning points would cause the availability of several roots starting from one up to 9 roots

depending on the specified temperature. For example, at 7 K, the PC-SAFT exhibits 9 roots where one of them is a negative root as illustrated in **Figure 5.2**.

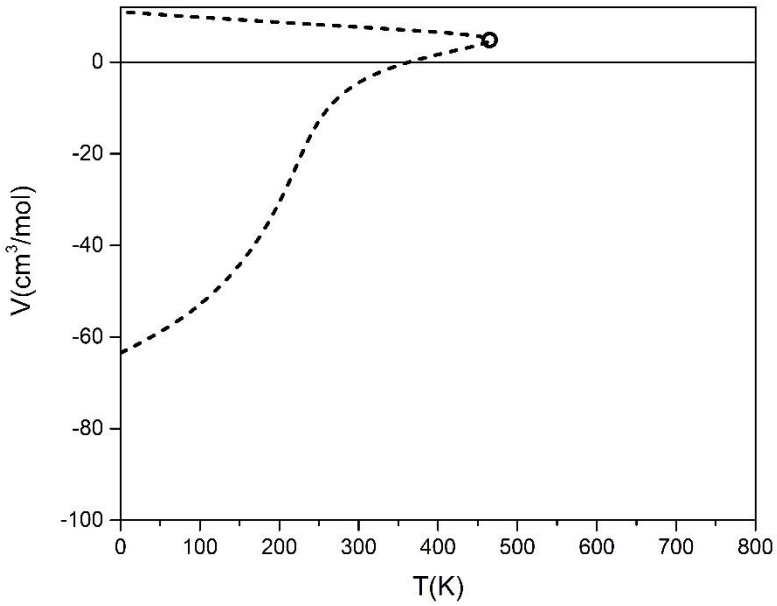

Figure 5.2 Lower branch molar volume region of ethane (cm^3/mol) versus temperature (K) at 1 atm using PC-SAFT EOS. Open circle indicates a turning point.

Figure 5.2 illustrates that the lower branch has one turning points at 465.21 K. **Table 5.1** lists the values of the roots at 7 K and 1 atm:

Table 5.1 Molar volume roots for ethane at 6 K and 1 atm using PC-SAFT EOS.

Molar Volume Root Number	**Value (cm^3/mol)**
V_1	106.7
V_2	87.47
V_3	62.70
V_4	32.89
V_5	23.19
V_6	16.76
V_7	12.47
V_8	10.95
V_9	-62.97

In addition to the roots at 7 K, it is found that two poles exist. The first pole is located between V_5 and V_6 and has the value of 22.10 cm^3/mol. The second pole is located between V_7 and V_8 and has the value of 11.05 cm^3/mol. The number of roots may differ at another temperature. For example at 20 K, **Figures 5.1 & 5.2** illustrate that the number of roots is seven. These roots are listed in **Table 5.2** (45.65, 34.14, 23.99, 14.96, 12.78, 10.75 and -61.75 cm^3/mol). It is important to select the physical root among these roots. The same analysis applied in **Chapter 4** is conducted on these roots as shown in **Table 5.2**. It is clear that the smallest root is negative which could be ignored. The mechanical stability test would show that the second and fifth roots (34.14 and 12.78 cm^3/mol) are not stable. If the reduced densities are obtained for the remaining roots, it would be clear that three roots (23.99, 14.96 and 10.75 cm^3/mol) could also be ignored due to their

values which are higher than the maximum physical value. The material stability test would show that only one root is stable and physical. This root is 45.65 cm^3/mol.

Table 5.2 The analysis for finding the physical root for ethane at 20 K and 1 atm using PC-SAFT EOS.

#	Value (cm^3/mol)	Mechanical Stability		Reduced Density		Gibbs Free Energy	
		Value	Result	Value	Result	Value	Result
V_1	45.65	-249.0	Stable	0.48	Physical	-104	Stable
V_2	34.14	1578.7	Unstable	-	-	-	-
V_3	23.99	$-5*10^5$	Stable	0.92	Non-Physical	-	-
V_4	14.96	$-3*10^7$	Stable	1.5	Non-Physical	-	-
V_5	12.78	$5*10^8$	Unstable	-	-	-	-
V_6	10.75	$-4*10^9$	Stable	2.1	Non-Physical	-	-
V_7	-61.75	-	-	-	-	-	-

In the previous table, it is clear that the physical root is available in the upper branch. Therefore, this indicates that the lower and middle branches are not physical branches.

The maximum number of roots for the case of ethane using PC-SAFT EOS was nine as shown in **Table 5.1**. However, PC-SAFT EOS may show more than nine roots for longer chain molecules. Starting from n-heptane, two new lower branches exist as illustrated in **Figure 5.3**.

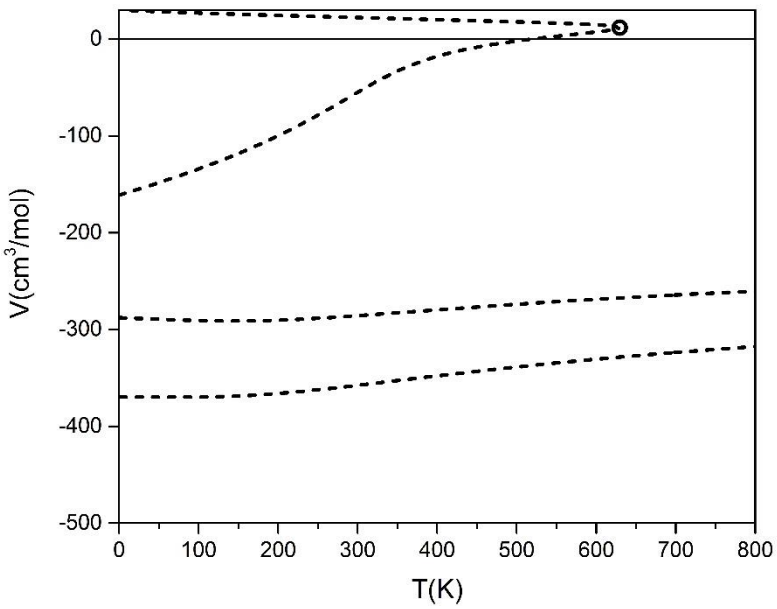

Figure 5.3 Lower branches molar volume region of heptane (cm^3/mol) versus temperature (K) at 1 atm using PC-SAFT EOS. Open circle indicates a turning point.

From the previous figure, the two new branches for n-heptane are below the lower branch without having any turning point. PC-SAFT EOS in the case of n-heptane may exhibit up to 11 roots as listed in **Table 5.3** at 6 K and 1 atm.

Table 5.3 The molar volume roots for heptane at 6 K and 1 atm using PC-SAFT EOS.

Molar Volume Root Number	**Value (cm^3/mol)**
V_1	402.4
V_2	294.1
V_3	156.5
V_4	90.02
V_5	63.12
V_6	47.42
V_7	34.67
V_8	29.94
V_9	-159.7
V_{10}	-288.0
V_{11}	-369.9

In addition to the roots at 6 K, four poles exist. The first pole is located between V_5 and V_6 which has the value of 60.48 cm^3/mol. The second pole is located between V_7 and V_8 which has the value of 30.24 cm^3/mol. The third pole is located between V_{10} and V_{11} which has the value of -345.7 cm^3/mol. The last pole is located after V_{11} which has the value of -390.8 cm^3/mol.

The lower branches roots for n-decane were not considered in the work of Privat et al. (2010). In the latter study, it is illustrated that the number of reduced density roots for n-decane at 135 K and 0.01 bar are five roots. However, it is found to be nine, i.e. four more roots, as illustrated in **Table 5.4**:

Table 5.4 A comparison of the number of reduced density roots for n-decane at 0.01 bar and 135 K obtained in this work using PC-SAFT EOS compared with the reported by Privat et al. (2010).

Reduced Density Root Number	(Privat et al., 2010)	This Work	Absolute Difference
η_1	-	2.3229	-
η_2	0.79043	0.79043	0.00%
η_3	0.70870	0.70870	0.00%
η_4	0.51255	0.51255	0.00%
η_5	$5.6560*10^{-3}$	$5.6560*10^{-3}$	0.00%
η_6	$7.5017*10^{-5}$	$7.4990*10^{-5}$	0.00%
η_7	-	-0.20610	-
η_8	-	-0.22898	-
η_9	-	-0.47525	-

In the study of Privat et al. (2010), the missed branches were the lower branches as explained before. The corresponding reduced density roots are 2.3229, -0.20610, -0.22898 and -0.47525. It is clear that these four roots are not physical reduced density values.

Secondly, after adding the chain term to CK-SAFT EOS, it is expected to have at least one more molar volume root over the spherical molecules at any specific temperature. In fact, the solver illustrates a new value around 10.38 cm^3/mol for ethane at 100 K and 1 atm but when this value was evaluated in the model it gave a function value of -0.42 which is not small enough to be considered as a root. **Figure 5.4** illustrates the diagram of ethane at 1 atm using CK-SAFT EOS:

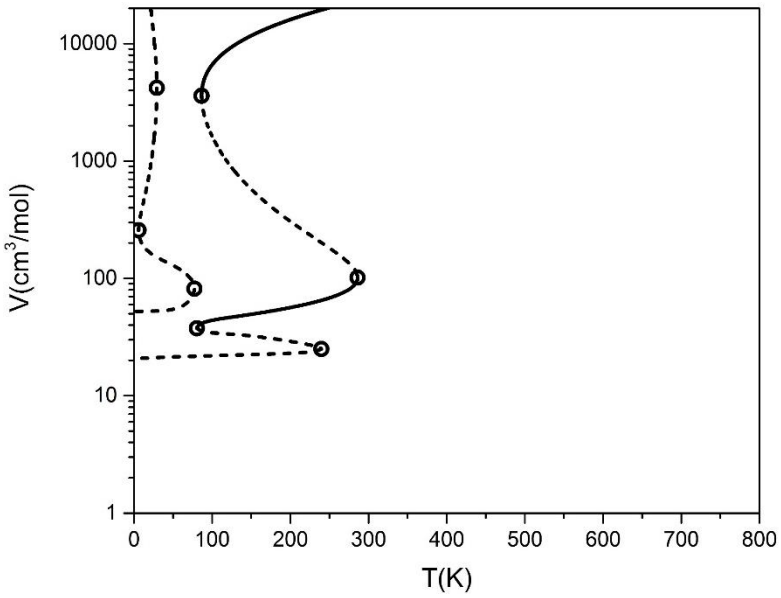

Figure 5.4 Molar volume of ethane (cm^3/mol) (log-scale) versus temperature (K) at 1 atm using CK-SAFT EOS. Dash curves indicate non-physical regions. Open circles indicate turning points.

As was discussed before, there is no effect of adding the chain term on the number of roots, branches and turning points. From the previous figure, it is obvious that the physical branch has four turning points while the upper branch has three turning points. These turning points exist at 5.8, 29.24, 77.27, 80.45, 86.5, 239.64, and 286.01 K. This number of turning points would cause the availability of several roots starting from one up to 7 depending on the specified temperature. For example, at 100 K, the CK-SAFT exhibits 7 roots where two of them are negative roots as illustrated in **Figure 5.5**.

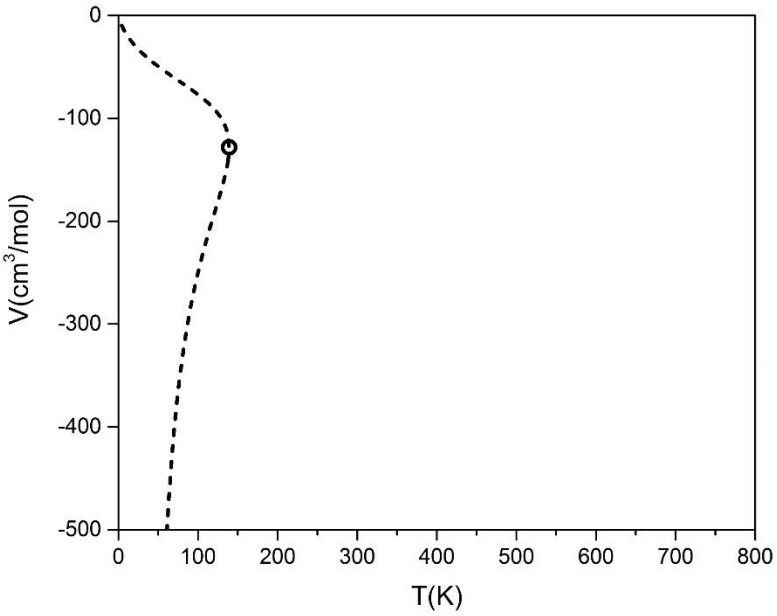

Figure 5.5 Negative molar volume region of ethane (cm^3/mol) versus temperature (K) at 1 atm using CK-SAFT EOS. Open circle indicates a turning point.

From the previous figure, the lower branch of CK-SAFT EOS has only one turning point at 139.08 K. **Table 5.5** shows seven molar volume roots of ethane at 72 K and 1 atm while this number might not be the same for other state conditions:

Table 5.5 Molar volume roots for ethane at 100 K and 1 atm using CK-SAFT EOS.

Molar Volume Root Number	**Value (cm^3/mol)**
$\mathbf{V_1}$	6631.7
$\mathbf{V_2}$	1623.1
$\mathbf{V_3}$	43.98
$\mathbf{V_4}$	34.36
$\mathbf{V_5}$	21.94
$\mathbf{V_6}$	-76.79
$\mathbf{V_7}$	-250.3

In addition to the roots at 100 K, two poles exist between V_5 and V_6 having molar volume values of 20.76 and 10.38 cm^3/mol.

The CK-SAFT EOS turning points obtained in this work seem to be not the same as the points look like in the work of Aslam and Sunol (2006). This can be investigated by comparing the number of roots obtained in this work with the reported by Aslam and Sunol (2006) as illustrated in the following table for propane at 3 bar and 250 K:

Table 5.6 A comparison of the number of roots for propane at 3 bar and 250 K obtained in this work using CK-SAFT EOS compared with the reported by Aslam and Sunol (2006).

Reduced Density Root Number	**(Aslam and Sunol, 2006)**	**This Work**	**Absolute Difference**
$\boldsymbol{\eta_1}$	0.851	-	-
$\boldsymbol{\eta_2}$	0.748	-	-
$\boldsymbol{\eta_3}$	0.352	0.332	0.00%
$\boldsymbol{\eta_4}$	0.047	0.061	30%
$\boldsymbol{\eta_5}$	0.007	0.004	40%

In **Table 5.6**, Aslam and Sunol (2006) reported five roots in this case while it was shown to be three in this work. The third roots in the two studies are very close to each other while the fourth and fifth roots are quite different. However, two roots are not available in this work because of the small variance in the lower turning point of the physical branch. Reduced density values of 0.81 and 0.79 are reported at the same value of pressure but at 242 K.

Thirdly, after adding the chain term to soft SAFT EOS, a new upper branch exists and the lower closed loop split into two connected loops. The connection curve continues to higher temperature. **Figure 5.6** illustrates the positive branches for ethane at 10 atm. The magnified region shows clearly the low temperature non-physical region of the physical branch in addition to the two loops.

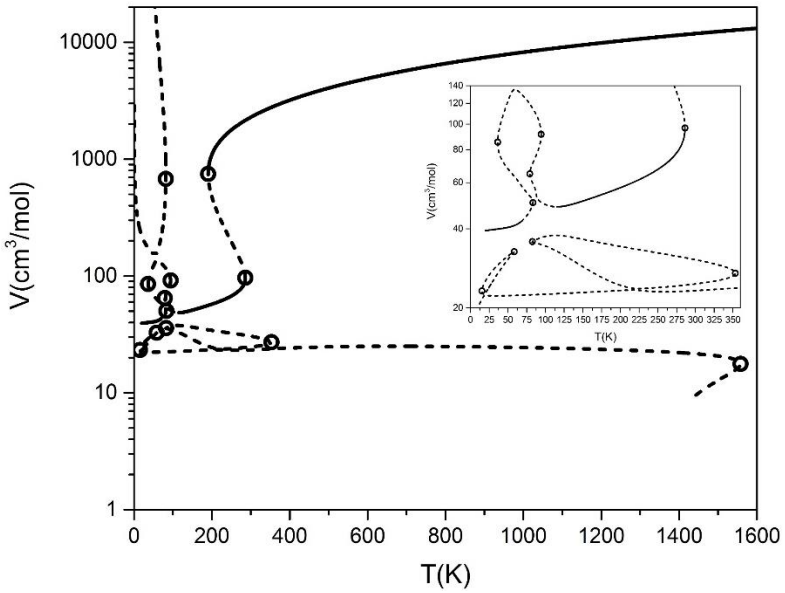

Figure 5.6 Molar volume of ethane (cm^3/mol) (log-scale) versus temperature (K) at 10 atm using soft SAFT EOS. Dash curves indicate non-physical regions. Open circles indicate turning points.

From the previous figure, it is obvious that the physical branch has six turning points while the upper branch and lower branches have one and five turning points respectively. These turning points exist at 15.36, 36.27, 58.37, 79.1, 81.73, 82.02, 83.37, 94.23, 190.6, 286.03, 353.22 and 1557.96 K. This number of turning points would cause the availability of several roots starting from one up to 10 depending on the specified temperature. For example, at 57 K, the soft SAFT exhibits 10 roots where two of them are negative roots as illustrated in **Figure 5.7**.

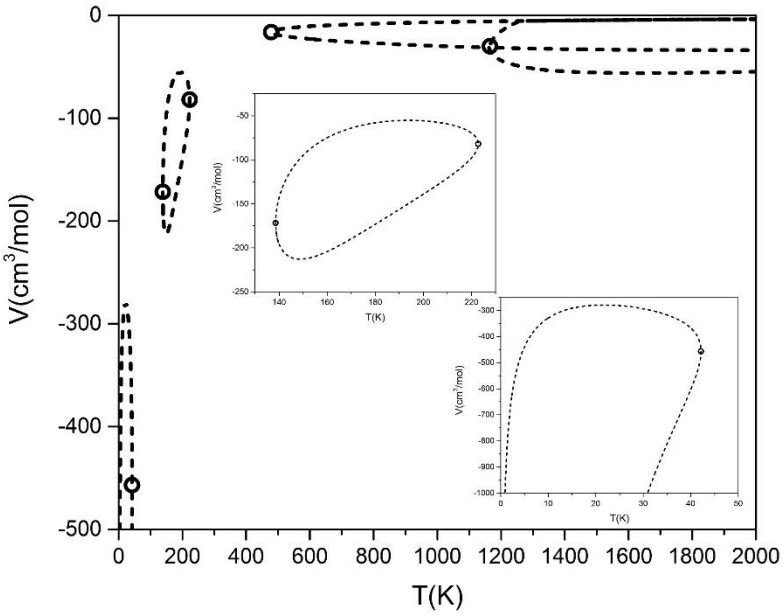

Figure 5.7 Negative molar volume region of ethane (cm^3/mol) versus temperature (K) at 10 atm using soft SAFT EOS. Open circles indicates turning points.

From the previous figure, three lower branches exist where two of them has two turning points each while the lowest branch has only one turning point. These turning points exist at 42.14, 138.57, 222.82, 478.62 and 1165.14 K. The two magnified regions in **Figure 5.7** illustrate the turning points of the two lowest branches. **Table 5.7** lists the molar volume roots of ethane at 57 K and 1 atm:

Table 5.7 Molar volume roots for ethane at 57 K and 1 atm using soft SAFT EOS.

Molar Volume Root Number	**Value (cm^3/mol)**
$\mathbf{V_1}$	147230
$\mathbf{V_2}$	411.6
$\mathbf{V_3}$	286.3
$\mathbf{V_4}$	180.6
$\mathbf{V_5}$	103.3
$\mathbf{V_6}$	78.8
$\mathbf{V_7}$	75.33
$\mathbf{V_8}$	57.10
$\mathbf{V_9}$	-1155.0
$\mathbf{V_{10}}$	-1441.7

Unlike PC-SAFT and CK-SAFT EOSs, it is not possible to find the poles of soft SAFT EOS because it is not in the form of polynomial over polynomial in terms of molar volume.

Finally, after adding the chain term to simplified SAFT EOS, a new middle branch exists. This branch continues to higher temperatures. **Figure 5.8** illustrates the bifurcation diagram of the positive molar volume of this version generated for ethane at 1 atm.

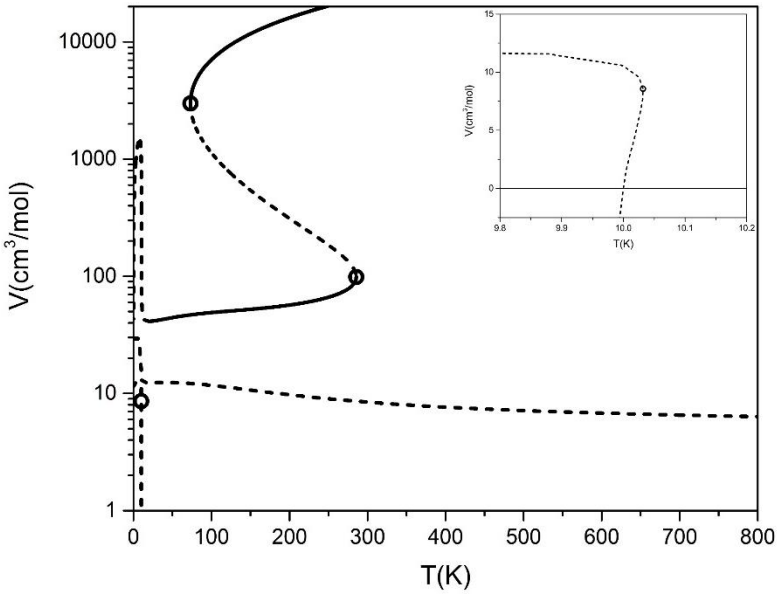

Figure 5.8 Molar volume of ethane (cm^3/mol) (log-scale) versus temperature (K) at 1 atm using simplified SAFT EOS. Dash curves indicate non-physical regions. Open circles indicate turning points.

From the previous figure, it is obvious that the physical branch has two turning points while the lower branch has only one turning point. These turning points exist at 10.03, 73.13 and 285.67 K. This number of turning points would cause the availability of several roots starting from one up to 4 depending on the specified temperature. For example, at 200 K, the simplified SAFT EOS exhibits 4 roots. **Figure 5.9** illustrates the lower branch.

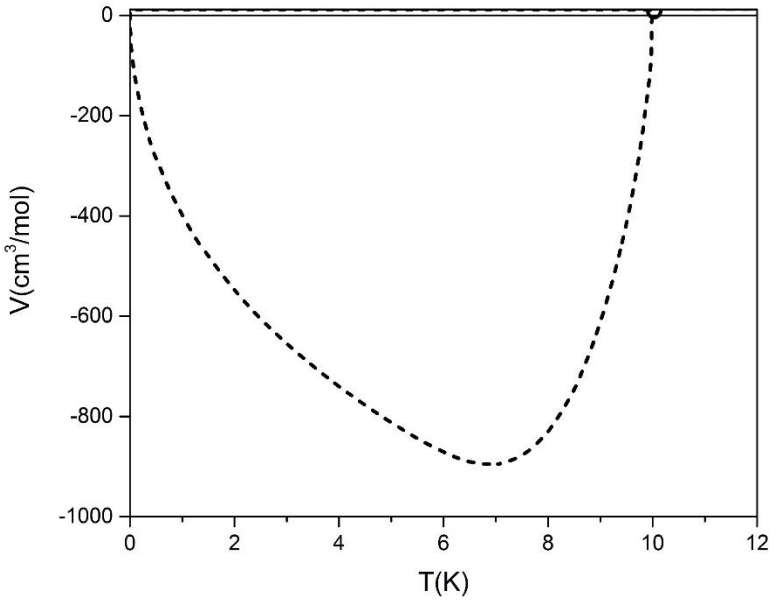

Figure 5.9 Negative molar volume region of ethane (cm^3/mol) versus temperature (K) at 1 atm using simplified SAFT EOS. Open circle indicates a turning point.

From the previous figure, the lower branch of simplified SAFT EOS has only one turning point at 10.03 K. The number of roots at 200 K is four due to the existence of the new continued branch. **Table 5.8** lists the molar volume roots of methane at 200 K and 1 atm:

Table 5.8 The volume roots for ethane at 200 K and 1 atm using simplified SAFT EOS.

Molar Volume Root Number	**Value (cm^3/mol)**
$\mathbf{V_1}$	16069.6
$\mathbf{V_2}$	311.2
$\mathbf{V_3}$	56.78
$\mathbf{V_4}$	9.74

In addition to the number of roots listed in the previous table, three poles exist. The first pole is located between V_3 and V_4 which has the value of 18.58 cm^3/mol. The other two are located after V_4 which have the values of 9.29 and -6.02 cm^3/mol.

The maximum number of roots that simplified SAFT EOS can exhibit for the case of n-pentane is also four as illustrated in **Table 5.9**. However, Lucia and Luo (2002) reported five compressibility factor roots for n-pentane at 10 bar and 360 K as illustrated in the following table:

Table 5.9 A comparison of the number of roots for n-pentane at 10 bar and 360 K obtained in this work with the reported by Lucia and Luo (2002).

Compressibility Factor Root Number	**(Lucia and Luo, 2002)**	**This Work**	**Absolute Difference**
Z_1	0.7402	0.7403	0.01%
Z_2	0.2341	0.2340	0.04%
Z_3	0.0430	0.0431	0.23%
Z_4	0.0107	-	-
Z_5	0.00604	0.00604	0.00%

From the previous table, all the compressibility roots listed for this work are similar to the roots reported by Lucia and Luo (2002) except for the fourth root. When this root was evaluated in the model, it gave a large value of 3.2×10^8 which indicates that this is not a root.

5.3 Effect of Pressure

Similar to the case of spherical molecules, the effect of pressure is a main parameter that would affect the number of molar volume roots and cause the behavior of the bifurcation diagrams to be changed. In this section, the effect of pressure is going to be studied after the chain term was added to PC-SAFT, CK-SAFT, soft SAFT and simplified SAFT EOSs.

Firstly, starting by studying the effect of pressure on PC-SAFT EOS, **Figure 5.10** is plotted for the molar volume vs. temperature for ethane at different pressures including 1, 10 and 100 atm. The purpose of the selection of these values is to cover a wide range from low to high pressures including a value above the critical pressure of ethane which is 50.97 atm.

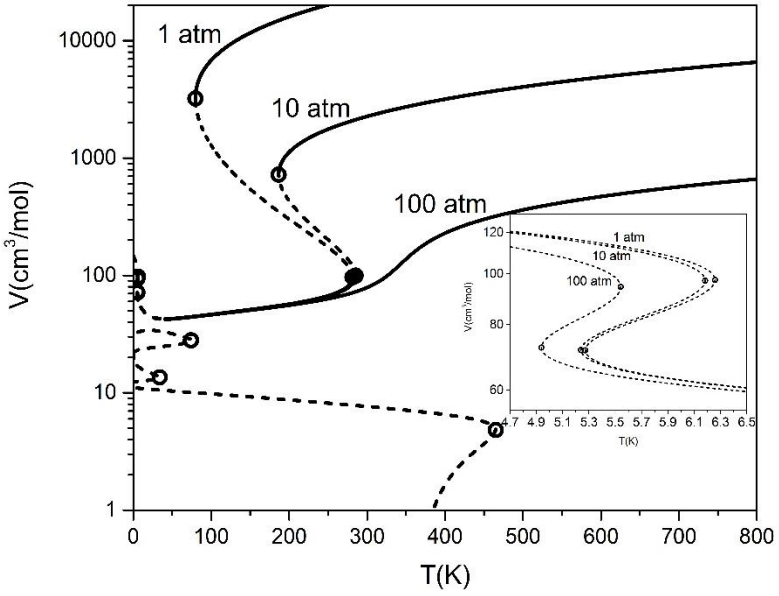

Figure 5.10 Molar volume of ethane (cm^3/mol) (log-scale) versus temperature (K) at 1, 10 and 100 atm using PC-SAFT EOS. Dash curves indicate non-physical regions. Open circles indicate turning points.

Similar to the case of spherical molecules, the effect of increasing the pressure on the bifurcation diagrams is obvious on the physical branch only. The mechanically unstable regions are shortened till the point where the two ends turning points combined into one point which is the critical point. The magnified non-physical region of the physical branch is showing also a shift to the molar volume axis. This region is disappeared after passing the pressure value of 660.47 atm which is found to be another critical pressure as it would be discussed later in section 5.5.

Secondly, the effect of pressure on n-heptane using CK-SAFT EOS is the similar to the explained behavior in Chapter 4 for spherical molecules as illustrated in **Figure 5.11** for ethane at 1, 10 and 100 atm.

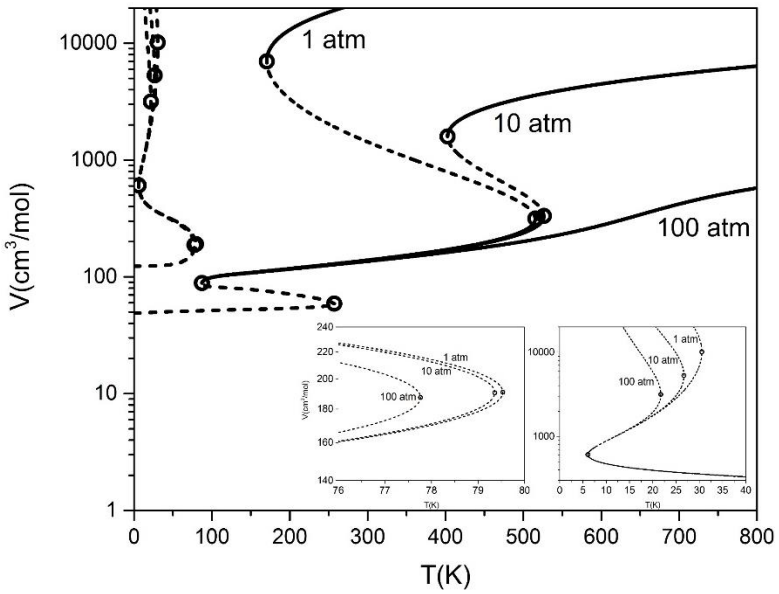

Figure 5.11 Molar volume of n-heptane (cm^3/mol) (log-scale) versus temperature (K) at 1, 10 and 100 atm using CK-SAFT EOS. Dash curves indicate non-physical regions. Open circles indicate turning points.

From the previous figure, the physical branch has the major effect caused by pressure. One of the mechanically unstable regions disappeared after passing the pressure of 59.46

atm which is the pressure of the critical point. The two magnified regions in the previous figure show that the upper non-physical branch is getting closer to the molar volume axis as the pressure is increased.

Thirdly, for the case of soft SAFT EOS, as pressure is increased, the only branch which is affected is the physical branch as illustrated in **Figure 5.12** for ethane at 10 and 100 atm.

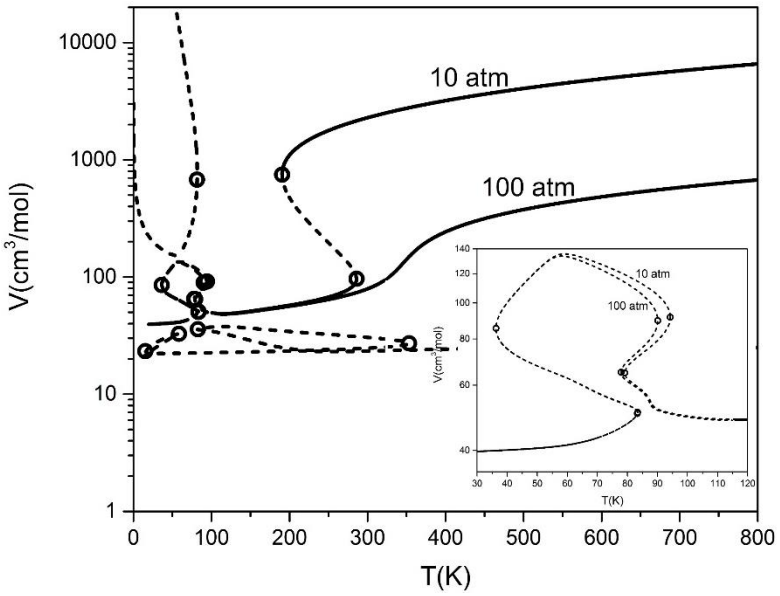

Figure 5.12 Molar volume of ethane (cm^3/mol) (log-scale) versus temperature (K) at 10 and 100 atm using soft SAFT EOS. Dash curves indicate non-physical regions. Open circles indicate turning points.

From the previous figure, the physical branch has the major effect caused by pressure as in the case of spherical molecules. One of the dash lines disappeared after passing the pressure of 56.40 atm which is the pressure of the critical point. The magnified region in the previous figure shows that the non-physical region of the physical branch is getting shrinked also by increasing the pressure.

When the positive branches are plotted at 1 atm, the bifurcation diagram illustrates that the physical branch has been combined with the upper branch as illustrated in **Figure 5.13**.

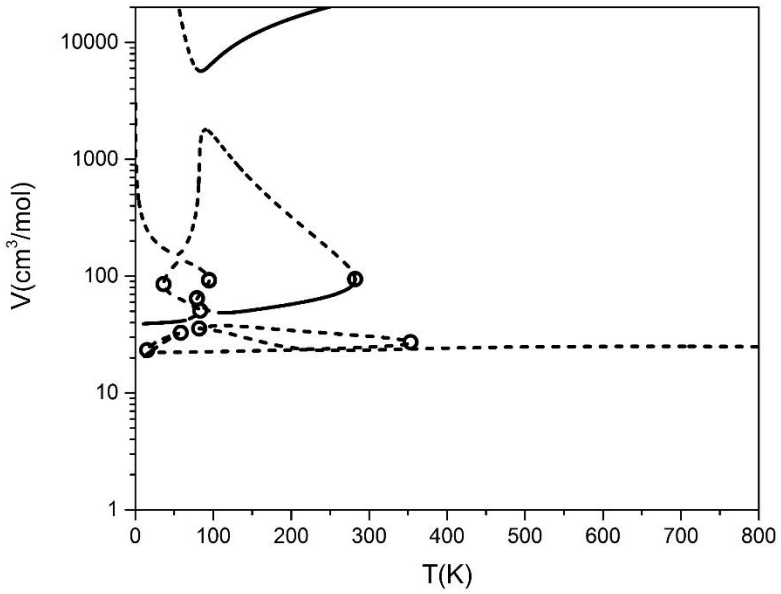

Figure 5.13 Molar volume of ethane (cm^3/mol) (log-scale) versus temperature (K) at 1 atm using soft SAFT EOS. Dash curves indicate non-physical regions. Open circles indicate turning points.

The previous figure shows that the physical behavior in this case is represented by two branches after the combination. Moreover, the region of intersection has no roots.

Finally, as pressure is increased in the case of simplified SAFT EOS, the only branch which is affected is the physical branch as illustrated in **Figure 5.14** for the case of n-pentane at 1, 9.8 and 100 atm.

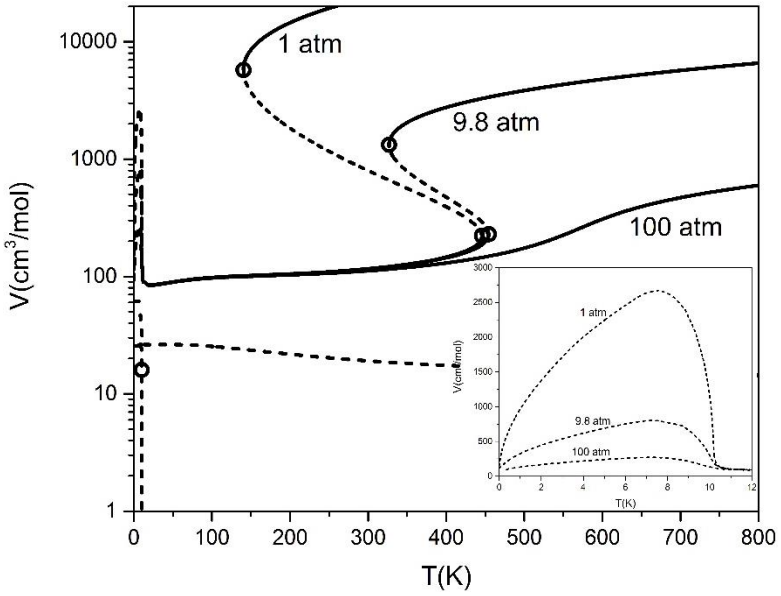

Figure 5.14 Molar volume of n-pentane (cm^3/mol) (log-scale) versus temperature (K) at 1, 9.8 and 100 atm using simplified SAFT EOS. Dash curves indicate non-physical regions. Open circles indicate turning points.

From the previous figure, the physical branch is the only affected by pressure. One of the mechanically unstable regions is disappeared after passing the pressure of 61.26 atm which is the pressure of the critical point. The magnified region shows that the non-physical peak on the physical branch at very low temperature is lowered as the pressure increased.

5.4 Effect of Model's Parameter

Similar to section 4.4, the effect of changing SAFT parameters on the bifurcation diagrams is studied by comparing the bifurcation diagrams for different molecules, but the effect of changing the segment number "m" is introduced because the chain molecules are considered in this chapter.

Firstly, starting with PC-SAFT EOS, the bifurcation diagrams for ethane and propane are compared to show the effect of the model's parameters on the branches as illustrated in **Figure 5.15**.

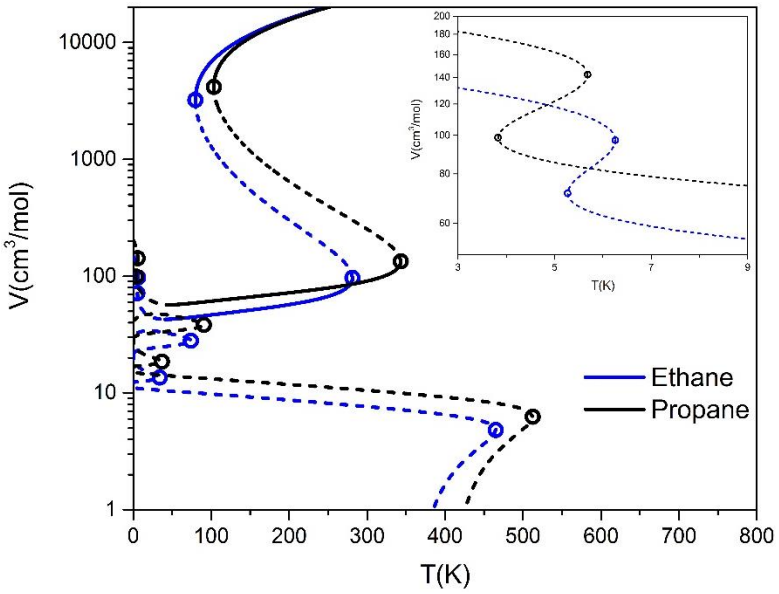

Figure 5.15 Molar volume of ethane and propane (cm^3/mol) (log-scale) versus temperature (K) at 1 atm using PC-SAFT EOS. Dash curves indicate non-physical regions. Open circles indicate turning points.

The previous figure illustrates a shift in temperature due to change in segment energy "ε/k" and in molar volume due to change in segment number "m" and segment size "σ" for all branches. In the magnified region, the non-physical region of the physical branch at low temperature is shifting closer to the molar volume axis unlike the other parts of the branch as the segment number "m" is increased. **Table 5.10** lists the parameters of the two components with absolute difference is given:

Table 5.10 PC-SAFT EOS parameters for ethane and propane adopted from Gross and Sadowski (2001).

	Ethane	**Propane**	**Absolute Difference**
$\boldsymbol{m}$ (-)	1.6069	2.0020	0.3951
$\boldsymbol{\sigma}$ ($\boldsymbol{m^{-8}}$)	3.5206	3.6184	0.0978
$\boldsymbol{\varepsilon/k}$ (K)	191.42	208.11	16.69

When the segment number "m" equals 3.0576 in which the component is n-hexane, the upper and next middle branches are combined with each other forming new two turning points at 44.153 and 59.162 K. These two turning points are splitting the upper and middle branches into "right" and "left" branches. **Figure 5.16** illustrates this case.

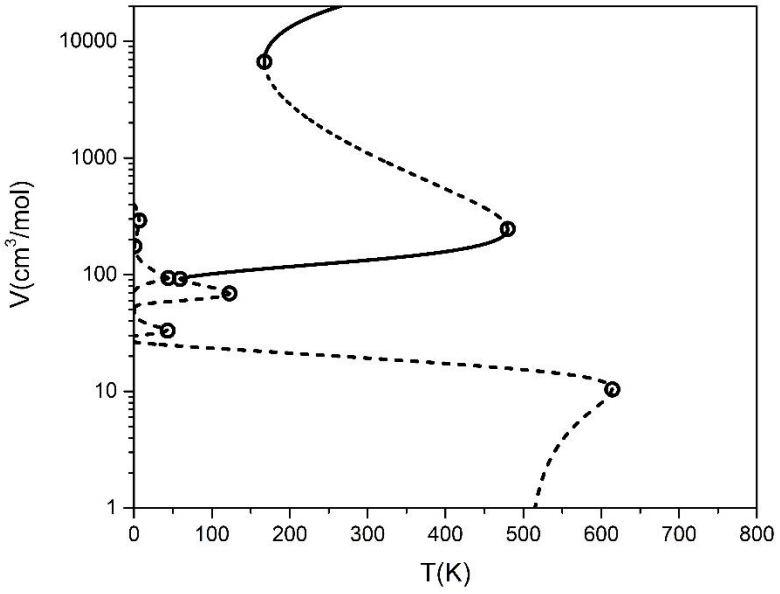

Figure 5.16 Molar volume of n-hexane (cm^3/mol) (log-scale) versus temperature (K) at 1 atm using PC-SAFT EOS. Dash curves indicate non-physical regions. Open circles indicate turning points.

To see the splitting space created by the combination, a closer look to this region is needed. **Figure 5.17** illustrates the space clearly.

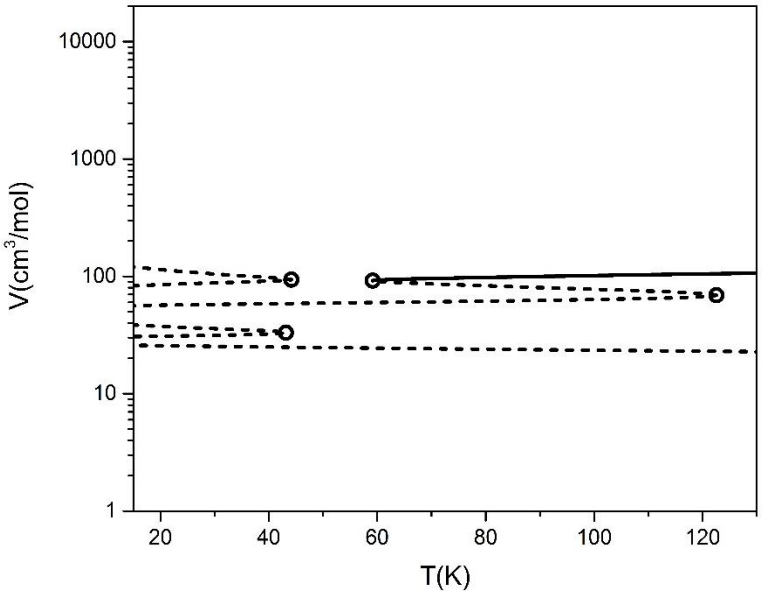

Figure 5.17 Molar volume of n-hexane (cm^3/mol) (log-scale) versus temperature (K) at 1 atm using PC-SAFT EOS. Dash curves indicate non-physical regions. Open circles indicate turning points.

As illustrated in the previous figure, a clear splitting space exists and forming right and left branches. The right branch has new mechanically unstable region. That means the PC-SAFT EOS is able to predict the physical properties of hexane only at a temperature higher than the turning point located at one end of the new mechanically unstable region which has the largest molar volume. This turning point is shifting to higher temperatures as the value of the segment number "m" increases. **Figure 5.18** illustrates how much is the shift for a higher value of the segment number "m".

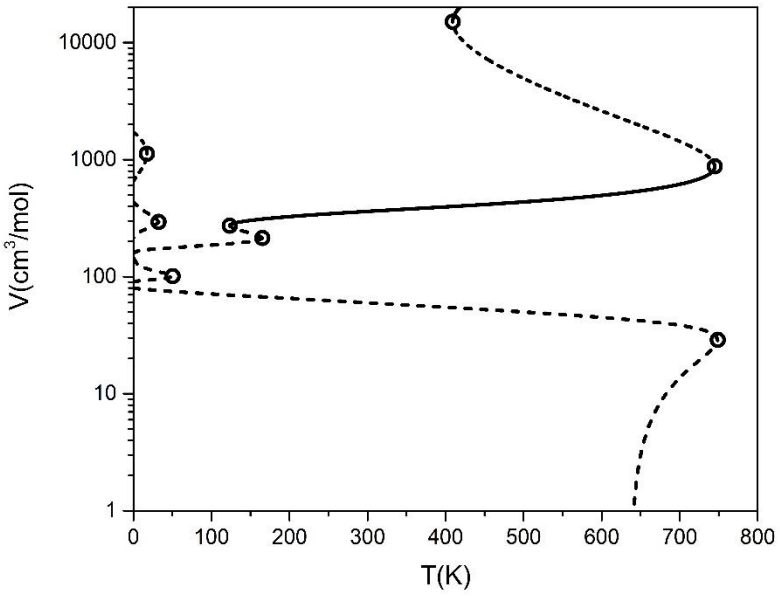

Figure 5.18 Molar volume of n-eicosane (C20) (cm^3/mol) (log-scale) versus temperature (K) at 1 atm using PC-SAFT EOS. Dash curves indicate non-physical regions. Open circles indicate turning points.

Figure 5.18 illustrates clearly that the turning point has a huge shift caused by the high value of the segment number "m". It is noticed that one of the turning points of the left branch at very low temperature disappeared in the range of 400-600 cm^3/mol.

Before studying the effect of model's parameters on other SAFT versions, one caution should be raised about adding the chain term in PC-SAFT EOS for argon. **Figure 5.19** illustrates that the argon with the chain term does not fit the liquid experimental data at 14.8 atm.

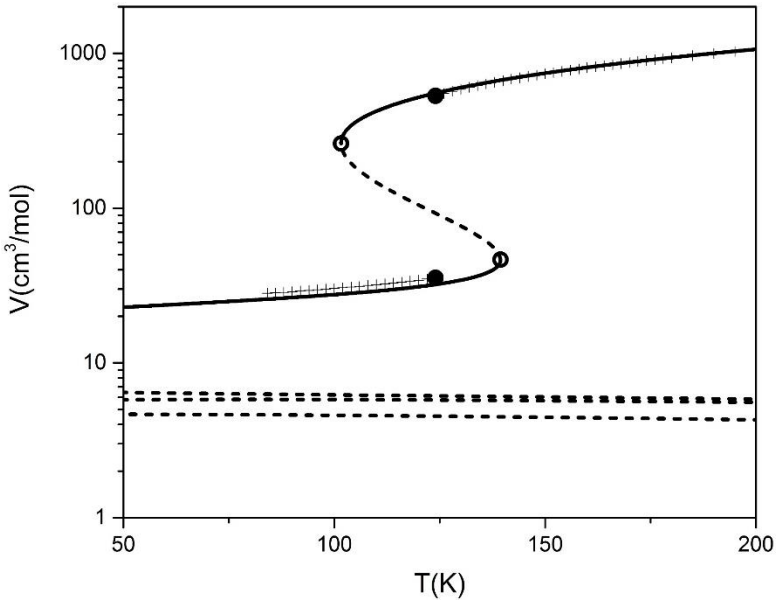

Figure 5.19 Molar volume of argon (cm^3/mol) (log-scale) versus temperature (K) at 14.8 atm using PC-SAFT EOS considering the chain term. Dash curves indicates non-physical regions. Open circles indicate turning points. "+" indicate the experimental data points adopted from Stewart and Jacobsen (1989). Closed circles indicate saturation point.

From the previous figure, the new middle branch illustrated in section 5.2 has been broken into two long branches indicated in **Figure 5.19** in the range of 5.5 and 6.5 cm^3/mol. **Figure 5.20** illustrates that the argon without the chain term perfectly fits.

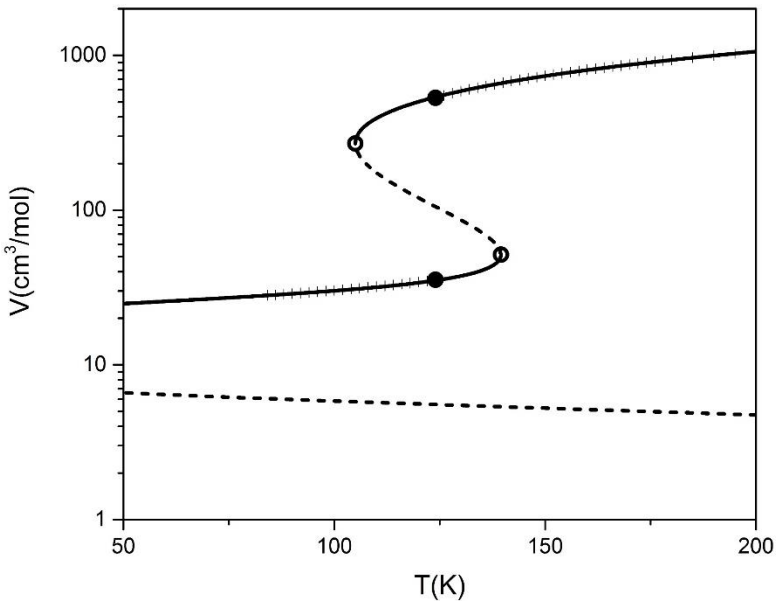

Figure 5.20 Molar volume of argon (cm^3/mol) (log-scale) versus temperature (K) at 14.8 atm using PC-SAFT EOS without considering the chain term. Dash curves indicates non-physical regions. Open circles indicate turning points. "+" indicate the experimental data points adopted from Stewart and Jacobsen (1989). Closed circles indicate saturation point.

Secondly, regarding the effect of changing the components on the bifurcation diagrams using CK-SAFT EOS, the bifurcation diagrams for ethane and n-heptane are compared as illustrated in **Figure 5.21**.

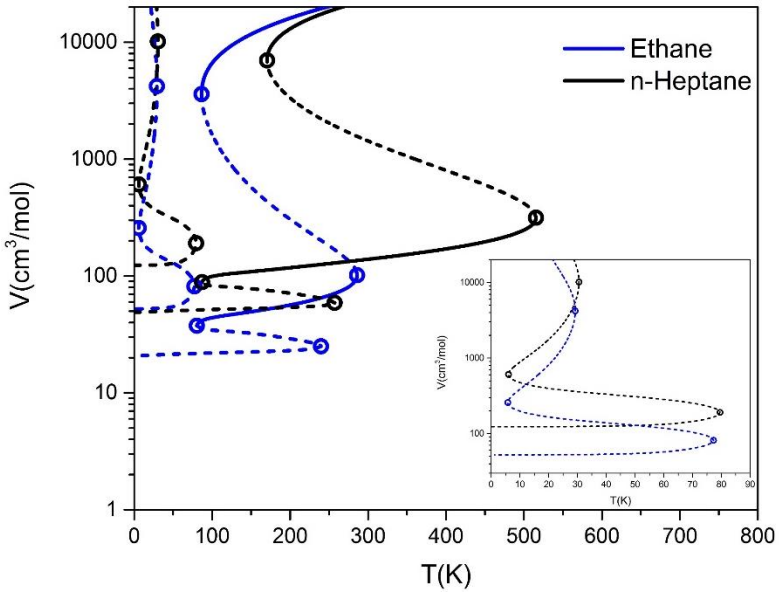

Figure 5.21 Molar volume of ethane and n-heptane (cm^3/mol) (log-scale) versus temperature (K) at 1 atm using CK-SAFT EOS. Dash curves indicate non-physical regions. Open circles indicate turning points.

Figure 5.21 shows a shift in molar volume because of the change in the segment number "m" and segment volume "v^{oo}" and in temperature due to change in segment energy "u^o/k". The magnified region shows that the shift is conducted on the upper branch in the same direction of the other branches. **Table 5.11** illustrates the parameters of ethane and n-heptane for CK-SAFT EOS with absolute difference is given:

Table 5.11 CK-SAFT EOS parameters for ethane and n-heptane adopted from Haung and Radosz (1990).

	Ethane	**n-Heptane**	**Absolute Difference**
$\boldsymbol{m}$ (-)	1.941	5.391	3.450
$\boldsymbol{v^{oo}}$ (ml/mol)	14.460	12.282	2.178
$\boldsymbol{u^o/k}$ (K)	191.44	204.61	13.17

Thirdly, for the case of soft SAFT EOS, the bifurcation diagrams for ethane and n-heptane are compared to show the effect of the model's parameters on the branches as illustrated in **Figure 5.22**.

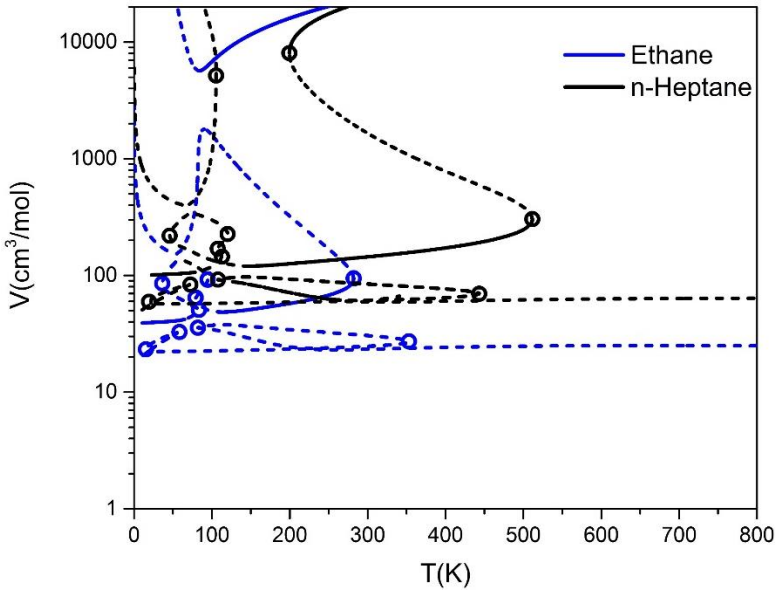

Figure 5.22 Molar volume of ethane and n-heptane (cm^3/mol) (log-scale) versus temperature (K) at 1 atm using soft SAFT EOS. Dash curves indicate non-physical regions. Open circles indicate turning points.

Figure 5.22 illustrates a shift in temperature due to change in segment energy "ε/k" and in molar volume due to change in segment number "m" and segment diameter "σ" for all branches. **Table 5.12** lists the parameters of the two components with absolute difference is given:

Table 5.12 Soft SAFT EOS parameters for ethane and propane adopted from Blas and Vega (1998).

	Ethane	**n-Heptane**	**Absolute Difference**
$\boldsymbol{m}$ (-)	1.5936	3.7256	2.132
$\boldsymbol{\sigma}$ $(\boldsymbol{m^{-8}})$	3.585	3.697	0.112
$\boldsymbol{\varepsilon/k}$ (K)	190.38	240.13	49.75

Finally, pertaining the case of simplified SAFT EOS, the bifurcation diagrams for ethane and n-pentane are compared to show the effect of the model's parameters on the branches as illustrated in **Figure 5.23**.

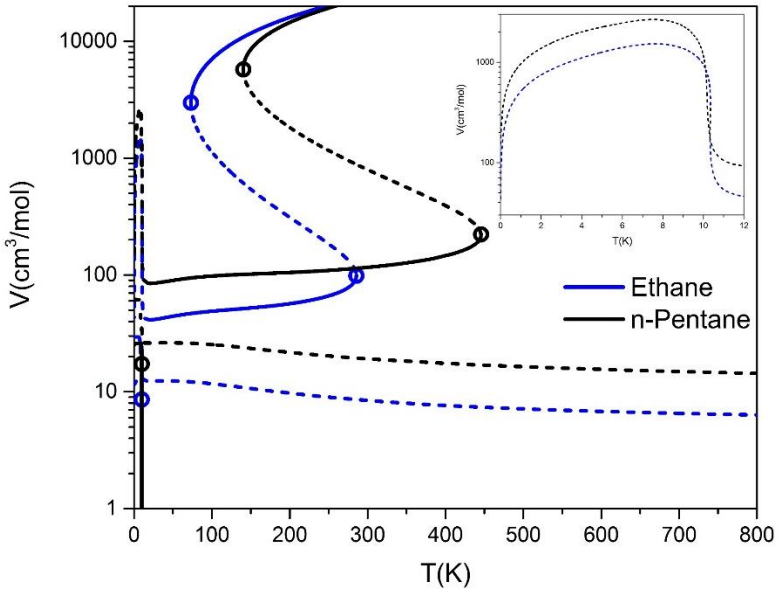

Figure 5.23 Molar volume of ethane and n-pentane (cm^3/mol) (log-scale) versus temperature (K) at 1 atm using simplified SAFT EOS. Dash curves indicate non-physical regions. Open circles indicate turning points.

From the previous figure, there is a shift in temperature due to change in segment energy "u^o/k" and in molar volume due to change in segment number "m". The magnified

region shows that the non-physical region of the physical branch at low temperature shifts in the same direction of the other parts of the physical branch. **Table 5.13** lists the parameters of ethane and n-pentane with absolute difference is given:

Table 5.13 Simplified SAFT EOS parameters for ethane and n-pentane adopted from Fu and Sandler (1995).

	Ethane	**n-Pentane**	**Absolute Difference**
$\boldsymbol{m}$ (-)	2.022	3.708	1.686
$\boldsymbol{v^{oo}}$ $(\boldsymbol{mL})$	16.236	18.574	2.338
$\boldsymbol{u^o/k}$ (K)	90.529	101.56	11.031

5.5 Critical Points

In section 4.5, the critical points for methane using PC-SAFT, CK-SAFT, soft SAFT and simplified SAFT EOSs were reported. Similarly, the critical points for ethane using the same SAFT versions are going to be listed in this sections with some remarks on the number of critical points of chain components in PC-SAFT EOS. Moreover, comparisons with some of the reported critical points for ethane in the literature are going to be illustrated.

Firstly, the number of critical points for ethane using PC-SAFT EOS is found to be also three as follows:

1) The first point: T_c=308.96 K, P_c=50.97 atm and V_c=156.4 cm^3/mol.

2) The second point: T_c=3.5622 K, P_c=660.47 atm and V_c=80.75 cm^3/mol.

3) The third point: T_c=87.403 K, P_c=9619.56 atm and V_c=30.14 cm^3/mol.

The PC-SAFT EOS illustrates three critical points till the disappearance of one of the turning points of the low temperature mechanically unstable region. At this case, PC-SAFT exhibit only two critical points as in the case of n-decane illustrated in **Table 5.14**. This table compares these critical points with the reported by Privat et al. (2010).

Table 5.14 The critical points for n-decane of obtained in this work compared with the reported by Privat et al. (2010).

Critical Point		**(Privat et al., 2010)**	**This Work**	**Absolute Difference**
First	**T_c (K)**	630.57	630.57	0.00%
	P_c (bar)	25.89	25.90	0.04%
	η_c	0.1201	0.1201	0.00%
Second	**T_c (K)**	158.00	158.00	0.00%
	P_c (bar)	5139.77	5141.56	0.04%
	η_c	0.6998	0.6998	0.00%

Secondly, the number of critical points for ethane using CK-SAFT EOS is found to be also two as follows:

1) The first point: T_c=320.61 K, P_c=59.46 atm and V_c=156.4 cm^3/mol.

2) The second point: T_c=254.60 K, P_c=46037.1 atm and V_c=26.59 cm^3/mol.

Table 5.15 compares the critical points for ethane between this work and the work of Polishuk (2010):

Table 5.15 Critical points for ethane obtained in this work using CK-SAFT EOS compared with the reported by Polishuk (2010).

Critical Point		(Polishuk, 2010)	This Work	Absolute Difference
First	T_c (K)	320.61	320.61	0.00%
	P_c (bar)	60.24	60.25	0.02%
	η_c	-	0.1250	-
Second	T_c (K)	254.59	254.60	0.00%
	P_c (bar)	46646.7	46647.1	0.00%
	η_c	-	0.7522	-

Thirdly, the number of critical points for ethane using soft SAFT EOS is found to be also two as follows:

1) The first point: T_c=312.1 K, P_c=56.40 atm and V_c=148.5 cm^3/mol.

2) The second point: T_c=408.1 K, P_c=33205.2 atm and V_c=29.58 cm^3/mol.

The following table compares the first critical point of ethane obtained in this work with the reported by Llovell et al. (2004):

Table 5.16 Critical points for ethane obtained in this work using soft SAFT EOS compared with the reported by Llovell et al. (2004).

Critical Point		(Llovell et al., 2004)	This Work	Absolute Difference
First	T_c (K)	311.0	312.1	0.35%
	P_c (MPa)	5.70	5.71	0.18%
	D_c (mol/dm^3)	6.86	6.73	1.90%

Finally, the critical point for ethane using simplified SAFT EOS was calculated numerically as: T_c=321.0 K, P_c=61.26 atm and V_c=151.5 cm^3/mol.

5.6 Comparisons

Similar to section 4.6, the focus of this section is to compare the obtained results in section 5.2 among different SAFT versions. This section is very useful before stating the conclusions of the whole chapter in the coming section.

Similarly, three comparisons are going to be held in this section. The first comparison illustrated in **Figure 5.24** demonstrates how the physical branches for chain molecules are generated using PC-SAFT, CK-SAFT, soft SAFT and simplified SAFT EOSs. This comparison is very important to show how much SAFT versions agree about the physical behavior. Moreover, this comparison is very helpful to note any non-physical behavior in the physical branches. The second comparison in **Table 5.17** is a quantitative comparison which shows the number of branches, turning points, critical points and maximum number of molar volume roots in each of PC-SAFT, CK-SAFT, soft SAFT and simplified SAFT EOSs. Moreover, at the last column, **Table 5.17** gives whether the physical branch is the only affected branch by increasing the pressure or not. Finally, the last comparison in the section is illustrated in **Table 5.18**. It compares the first (physical) critical point for ethane among PC-SAFT, CK-SAFT, soft SAFT, simplified SAFT models with the experimental critical point. The purpose of this comparison is to show that the presented critical points for many components using SAFT EOS in this chapter are not accurate and they need to be corrected. These corrections are well known in the

literature. The following figure illustrates the first comparison for the case of ethane at 10 atm.

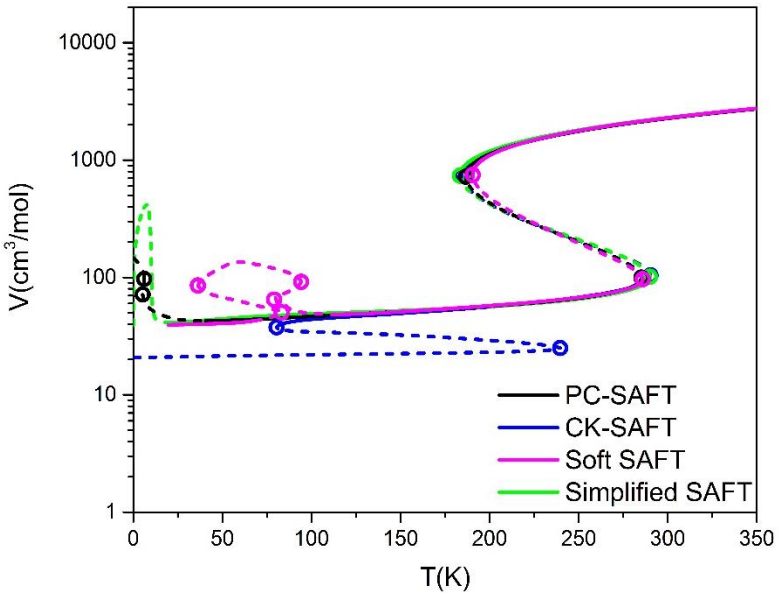

Figure 5.24 A comparison among the physical branches of the PC-SAFT, CK-SAFT, soft SAFT and simplified SAFT EOSs for ethane at 10 atm. Dash curves indicates non-physical regions. Open circles indicate turning points.

Figure 5.24 illustrates that PC-SAFT, soft SAFT and simplified SAFT EOSs are showing the same values of molar volume in the vapor, liquid and solid phases except the non-physical region for each SAFT version. The CK-SAFT EOS illustrates a good match to the previous version but not for the solid region. Below 25 K, the simplified SAFT EOS has a sharp peak while the PC-SAFT EOS goes upward gradually. The soft SAFT EOS has no roots at this region. So, all the versions of SAFT EOS fail below 25 K. The following table illustrates the second comparison for the case of ethane:

Table 5.17 A comparison among the number of branches, turning points, critical points, maximum number of roots and the effect of pressure of PC-SAFT, CK-SAFT, soft SAFT and simplified SAFT for the case of ethane.

Model	Number of Branches	Number of Turning Points		Number of Critical Points	Maximum Number of Roots	Branches Affected by Changing Pressure
		Before the First Critical Point	After the First Critical Point			
PC-SAFT	4	7	5	3	9	Physical
CK-SAFT	3	8	6	2	7	All
Soft SAFT	6	16	14	2	10	Physical
Simplified SAFT	3	3	1	1	4	Physical

In the previous table, soft SAFT EOS is shown to have highest number of branches among SAFT version while simplified SAFT and CK-SAFT EOSs have the lowest. Soft SAFT EOS has the highest number of turning points while simplified SAFT EOS has the lowest. PC-SAFT EOS has the highest number of critical points while simplified SAFT has the lowest. Soft SAFT EOS has the highest maximum number of molar volume roots also while simplified SAFT EOS has the lowest. CK-SAFT EOS is the only model in which the non-physical branches are also affected by increasing the pressure. **Table 5.18** illustrates the third comparison:

Table 5.18 A comparison between the critical points given by PC-SAFT, CK-SAFT, soft SAFT and simplified SAFT EOSs with the experimental values for the case of ethane.

Model	T_c (K)	P_c (atm)	V_c (cm^3/mol)
Experimental	305.3	48.08	145.5
PC-SAFT	309.0	50.97	156.4
CK-SAFT	320.6	59.46	156.4
Soft SAFT	312.1	56.40	148.5
Simplified SAFT	321.0	61.26	151.5

5.7 Conclusions

In this chapter, PC-SAFT, CK-SAFT, soft SAFT and simplified SAFT EOSs were explored through bifurcation and stability analysis for the case of chain molecules to investigate the multiple molar volume roots problem.

Similar to section 4.2, in section 5.2, the bifurcation diagrams were generated for the four SAFT versions and the criteria for selecting the physical root explained in section 3.3 was applied. Firstly, for the case of ethane using PC-SAFT EOS, it was found that there were four branches where one of them represents the physical behavior except at very low temperature which is the upper branch. One middle branch was added by the chain term contributing to the maximum number of molar volume roots by two roots. In addition, it was found that the maximum number of roots that PC-SAFT can exhibits was nine roots. The reduced density roots for n-decane at 0.01 bar and 135 K using PC-SAFT EOS were compared with the reported by Privat et al. (2010). This comparison showed that four more reduced density roots were reported in this work. It was found that the

lower branches were not considered in the study of Privat et al (2010). Secondly, for the same component using CK-SAFT EOS, it was found that the number of branches was three which was the same as in section 4.2 because the new solution added by the chain term was not a root. It was found that it did not satisfy the function perfectly. Moreover, it was found that CK-SAFT EOS exhibited up to seven molar volume roots. This number was higher in the case of spherical molecules because the branches were over each other in specific temperatures. The reduced density roots for propane at 3 bar and 250 using CK-SAFT EOS were compared with the reported by Aslam and Sunol (2006). Molar volume roots reported in this thesis showed good match with the reported by Aslam and Sunol (2006) except at higher molar volume roots. However, the turning points seem to be different between the two studies because two reduced density roots were missed in this comparison while similar roots were found at a temperature closer to the compared value. Thirdly, for the case of soft SAFT EOS, the number of branches were five branches where one of them represented the physical behavior except at low temperature. A new upper branch existed because of adding the chain term. The closed loop presented in section 4.2 for soft SAFT EOS split into two connected loops. The maximum number of roots that soft SAFT EOS can exhibit were ten molar volume roots. Finally, for the case of simplified SAFT EOS, the number of branches was found to be three. The second branch existed only at very low temperature. The new added branch because of the chain term was continued to high temperature.

Similar to section 4.3, in section 5.3, the effect of pressure on the branches of PC-SAFT, CK-SAFT, soft SAFT and simplified SAFT EOSs were explored. For all these versions, the mechanically unstable regions were shortened by increasing the pressure

bringing the two ends turning points closer to each other till the point where they were combined into one point. This point was investigated to be the critical point. The non-physical branches were independent of pressure except for the case of CK-SAFT EOS in which all the branches including the non-physical branches were pressure dependent. In the case of soft SAFT EOS at 1 atm, it was found that the physical branch combined with the next left branch so that the gas and liquid molar volumes were represented by two branches separately.

Similar to section 4.4, in section 5.4, the effect of PC-SAFT, CK-SAFT, soft SAFT and simplified SAFT EOSs parameters on the bifurcation diagrams were investigated by generating the diagrams for different components. It was clear that the segment diameter or volume interfere the diagram by shifting them along the molar volume axis. Moreover, the segment energy was found to affect the diagrams by shifting them along the temperature axis. The effect of the segment number were also investigated, it also shifted the bifurcation diagram along the molar volume axis. For the case of n-hexane using PC-SAFT EOS, a combination between the upper and next middle branches occurred causing two new turning points to exist. The right hand side new turning point temperature is the temperature where PC-SAFT EOS start to represent physical behavior.

Similar to section 4.5, in section 5.5, the criteria of calculating the critical points explained in **Chapter 3** was implemented on the four SAFT versions. The number of critical points for PC-SAFT EOS might be three till the case where one of the turning point of the lower mechanically unstable region disappeared. The critical points for n-decane using PC-SAFT EOS reported in this work and the study of Privat et al. (2010)

were compared. CK-SAFT and soft SAFT EOSs showed two critical points while simplified SAFT showed only one critical point like any cubic EOS.

Similar to section 4.6, in section 5.6, three comparisons were held to emphasis on the similarity and differences among the studied models. In the first comparison where the physical branches for PC-SAFT, CK-SAFT, soft SAFT and simplified SAFT EOSs were plotted in one figure, it was shown that the four SAFT versions agreed in the gas and liquid region but differed in the mechanically unstable region and the low temperature regions. In the second comparison where the number of branches, turning points, critical points, maximum number of molar volume roots and the pressure dependency of the branches were compared, simplified SAFT EOS showed minimum number of branches, turning points, critical points and maximum number of molar volume roots among the studied SAFT versions in this chapter.

In the next chapter, a simple procedure to determine the correct roots without finding all the roots is recommended for PC-SAFT EOS based on the bifurcation and stability analysis of the spherical and chain molecules discussed in **Chapters 4 & 5**. This procedure can be implemented in process simulators to improve the method of solving thermodynamic problems using PC-SAFT EOS.

CHAPTER 6

Solution to Multiple Roots Problem for PC-SAFT EOS

6.1 Introduction

In **Chapters 4 and 5**, bifurcation diagrams with physical root analysis were applied for spherical and chain molecules for PC-SAFT, CK-SAFT, soft SAFT and simplified SAFT EOSs. In the case of PC-SAFT EOS, the physical branch was always the upper branch in the bifurcation diagram of molar volume versus temperature at fixed pressure. Also, the next middle branch was always next to the physical branch and independent of pressure. Based on these two observations, a simple procedure is proposed to locate the roots on the physical branch without finding all the roots. This proposed procedure is important for process simulators to locate the physical root in more efficient manner.

In section 6.2, the bifurcation diagrams for mixtures using PC-SAFT EOS are introduced to show that the two observations figured out for pure components' bifurcation diagrams using PC-SAFT EOS take place also in the bifurcation diagrams in the case of mixtures using the same EOS. Different examples of binary and tertiary mixtures are illustrated under atmospheric and high pressure for verity. The discussion about the poles is ignored in the case of mixtures. In section 6.3, the proposed solution for the multiple molar volume roots in statistical associating fluid theory is explained. This solution is illustrated in all the bifurcation diagrams shown in section 6.2. In section 6.4, the conclusion of this chapter is stated.

6.2 Bifurcation Diagrams for Mixtures via PC-SAFT EOS

The mixing rule used in this chapter is the van der Waals one fluid mixing rule. This mixing rule does not depend on molar volume. So it is expected that the number of branches remains the same as illustrated in section 5.2 for the case of PC-SAFT EOS. **Figure 6.1** illustrates the case for a mixture of 15% ethane and 85% n-eicosane.

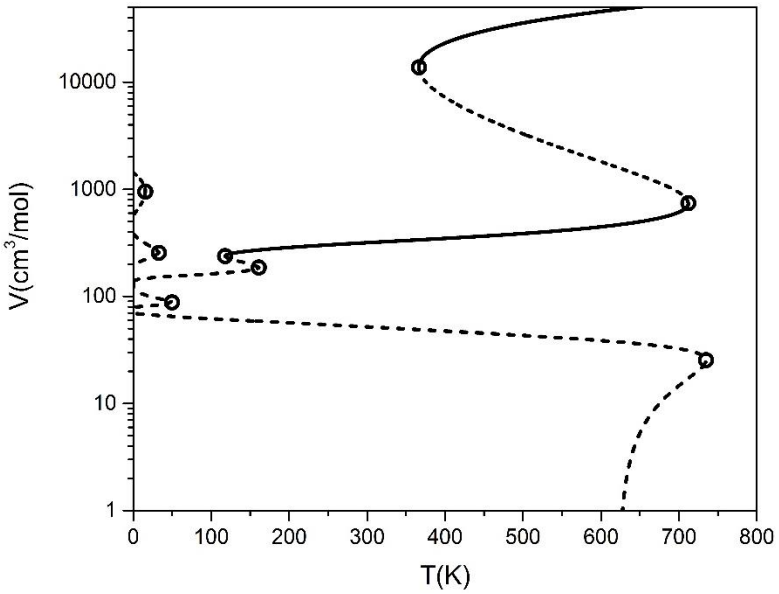

Figure 6.1 Molar volume of a mixture of 15% ethane and 85% n-eicosane (cm^3/mol) (log-scale) versus temperature (K) at 1 atm using PC-SAFT EOS. Dash curves indicate non-physical regions. Open circles indicate turning points.

From the previous figure, the number of branches and turning points are exactly the same as illustrated in section 5.2 for the case of pure n-eicosane using PC-SAFT EOS. The bifurcation diagram of the mixture in **Figure 6.1** is compared with the bifurcation diagrams for the two corresponding pure components as illustrated in **Figure 6.2**.

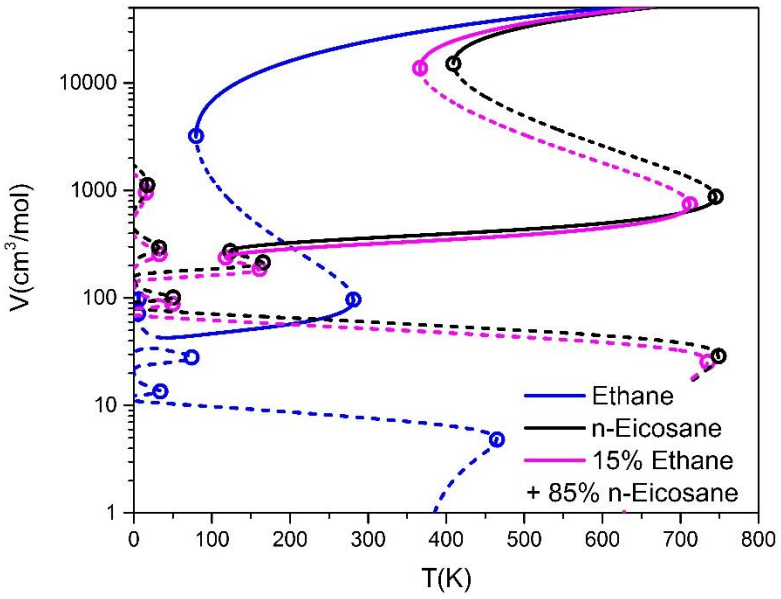

Figure 6.2 A comparison among the molar volume branches of ethane, n-eicosane and the mixture of 15% ethane and 85% n-eicosane using PC-SAFT EOS at 1 atm. Dash curves indicate non-physical regions. Open circles indicate turning points.

From the previous figure, the bifurcation diagram for the mixture of 15% ethane and 85% of n-eicosane is located between the bifurcation diagrams of the corresponding pure components' bifurcation diagrams closer to the n-eicosane bifurcation diagram because the n-eicosane is dominant in the mixture. **Figures 6.3 & 6.4** illustrate the effect of the dominance of the component on the bifurcation diagram of the mixture. **Figures 6.3** illustrates the case for a mixture of carbon dioxide and n-decane where the carbon dioxide is the dominant at high pressure.

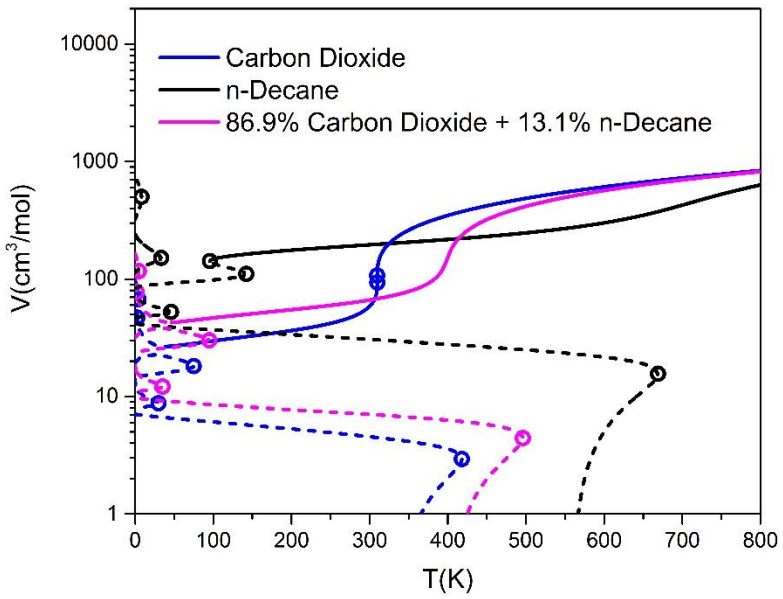

Figure 6.3 A comparison among the molar volume branches of carbon dioxide, n-decane and the mixture of 86.9% carbon dioxide and 13.1% n-decane using PC-SAFT EOS at 79 atm. Dash curves indicate non-physical regions. Open circles indicate turning points.

From the previous figure, the bifurcation diagram of the mixture is similar to the bifurcation diagram of the dominant component with is the carbon dioxide by having one upper branch rather than left and right upper branches like the n-decane. If the composition of n-decane is dominant, for example 76.39%, the bifurcation diagram of the mixture will show the left and right upper branches as illustrated in **Figure 6.4**.

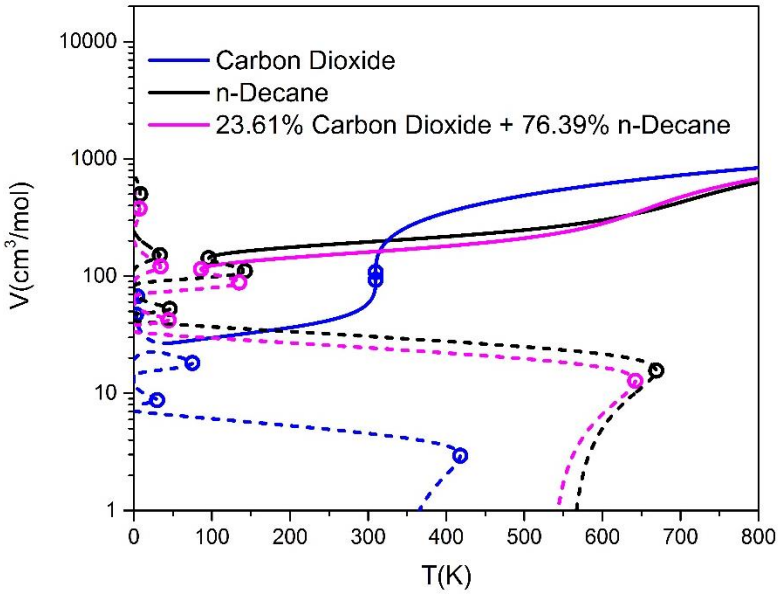

Figure 6.4 A comparison among the molar volume branches of carbon dioxide, n-decane and the mixture of 23.61% carbon dioxide and 76.39% n-decane using PC-SAFT EOS at 79 atm. Dash curves indicate non-physical regions. Open circles indicate turning points.

The previous figures showed that the binary mixture bifurcation diagram is located always between the bifurcation diagrams of the corresponding pure components closer to the dominant component. **Figure 6.5** illustrates the situation is similar in the case of tertiary mixtures.

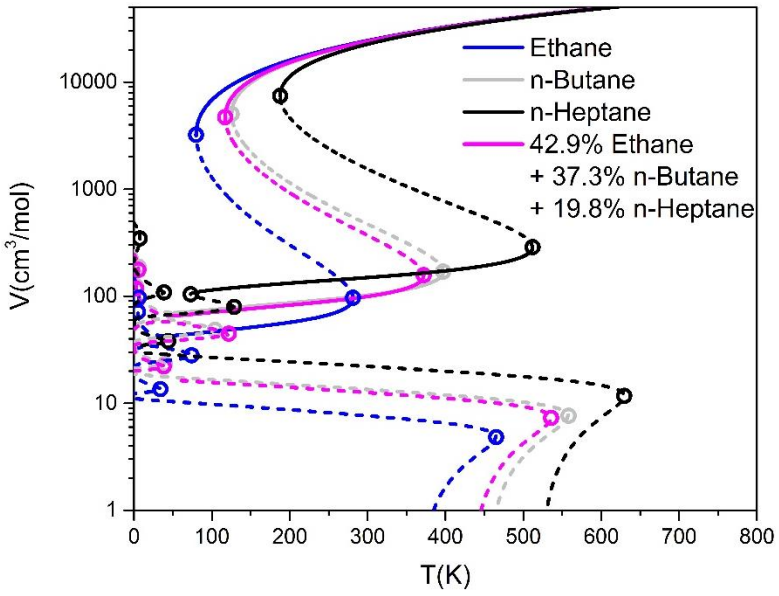

Figure 6.5 A comparison among the molar volume branches of ethane, n-butane, n-heptane and the mixture of 42.9% ethane, 37.3% n-butane and 19.8% n-heptane using PC-SAFT EOS at 1 atm. Dash curves indicate non-physical regions. Open circles indicate turning points.

From the previous figure, the bifurcation diagram of the tertiary mixture is located between the most dominant pure components' bifurcation diagrams. All the previous figures in this section show the two observation stated in the introduction of this chapter.

6.3 Physical Lines

In all the PC-SAFT EOS figures discussed in the **Chapters 4, 5** and the previous sections in this chapter, it was noticed that the physical branch was always the upper branch. Moreover, the next middle branch was independent of pressure, i.e. the maximum molar volume root located on the middle branch is almost constant at any value of pressure for a specific component or mixture. As a result, the "physical line" idea is proposed.

The physical line is a border horizontal line used as indicator for the maximum non-physical root of a component or mixture. All the points used to draw the physical line for many pure components are listed in Appendix A. Fortunately, the physical line can be predicted for any mixture with any composition by taking the arithmetic mean of the data reported in Appendix A for the corresponding pure components. The reported physical lines for pure components with the predicted lines for mixtures are added to **Figures 6.2, 6.3, 6.4 and 6.5** as illustrated in **Figures 6.6, 6.7, 6.8, and 6.9**.

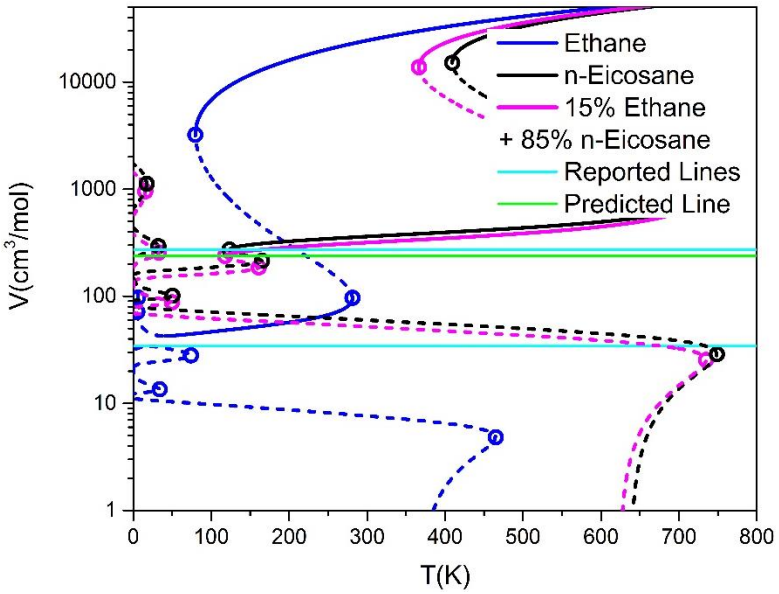

Figure 6.6 A comparison among the molar volume of ethane, eicosane and the mixture of 15% ethane and 85% eicosane using PC-SAFT EOS at 1 atm. Dash curves indicate non-physical regions. Open circles indicate turning points.

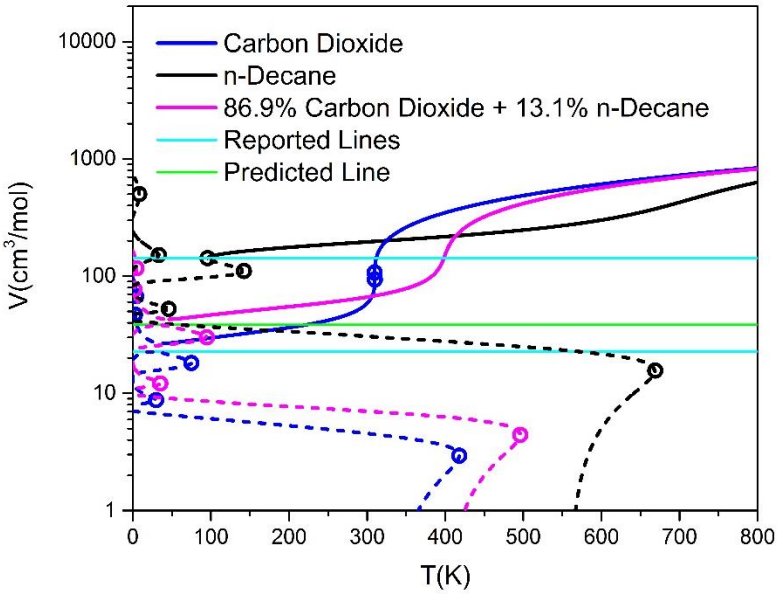

Figure 6.7 A comparison among the molar volume branches of carbon dioxide, n-decane and the mixture of 86.9% carbon dioxide and 13.1% n-decane using PC-SAFT EOS at 79 atm. Dash curves indicate non-physical regions. Open circles indicate turning points. Cyan and green lines are the physical lines.

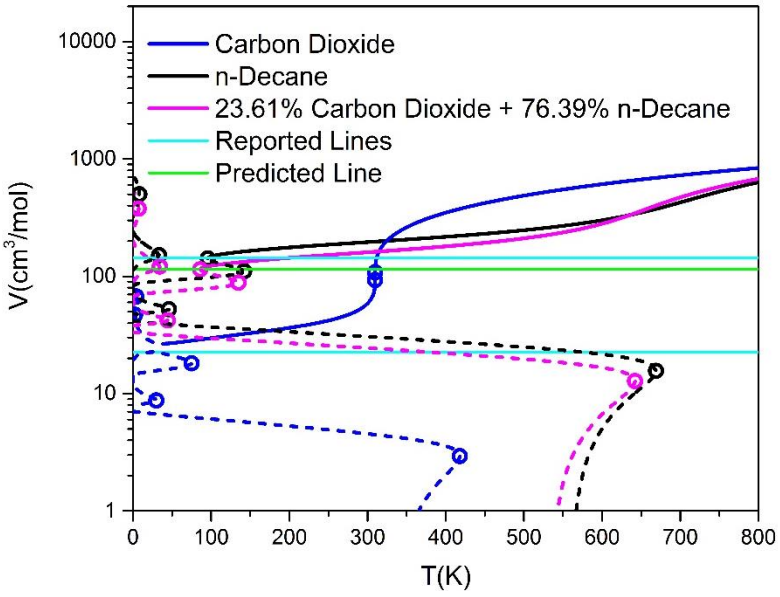

Figure 6.8 A comparison among the molar volume branches of carbon dioxide, n-decane and the mixture of 23.61% carbon dioxide and 76.39% n-decane using PC-SAFT EOS at 79 atm. Dash curves indicate non-physical regions. Open circles indicate turning points. Cyan and green lines are the physical lines.

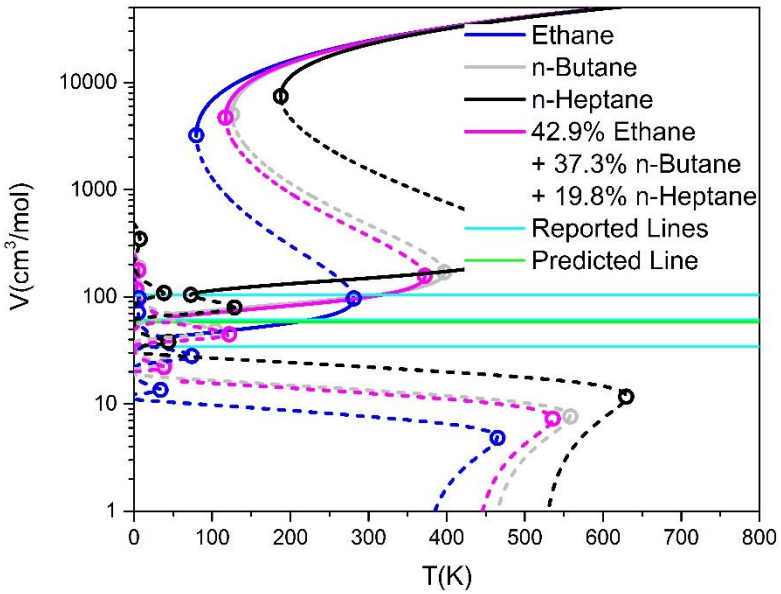

Figure 6.9 A comparison among the molar volume branches of ethane, n-butane, n-heptane and the mixture of 42.9% ethane, 37.3% n-butane and 19.8% n-heptane using PC-SAFT EOS at 1 atm. Dash curves indicate non-physical regions. Open circles indicate turning points. Cyan and green lines are the physical lines.

6.4 Conclusions

In this chapter, the last objective of this thesis was achieved by proposing a simple strategy to assist in locating the physical root without finding all the roots introduced by PC-SAFT EOS and performing the stability calculations. This strategy was proposed after observing that the upper branch in PC-SAFT EOS is always the physical branch and the next middle branch is independent of pressure. Thus, the idea of constructing boarder lines between the cubic EOS similar roots region and the non-physical roots region added by PC-SAFT EOS was very useful to achieve the last objective in the practical ranges of temperature for the studied components. These boarder lines were called “physical lines”. The physical lines were obtained by finding the maximum non-physical root in the middle branch next to the physical branch. The maximum non-physical roots for the components listed in the work of Gross and

Sadowski (2001) were reported in Appendix A. Moreover, the physical line of any mixture of these pure components can be predicted by calculating the arithmetic mean of the physical lines of the pure components.

In the next chapter, the conclusions of the whole thesis are going to be stated. In addition, the recommendations for future work are going to be presented.

CHAPTER 7

Conclusions and Recommendations

7.1 Conclusions

In this thesis, bifurcation and stability analysis were very valuable for studying the behavior of SAFT EOSs especially for the multiple molar volume problem. The bifurcation diagrams generated by arc-length continuation method was very efficient in showing all the branches, turning points, critical points and molar volume roots for spherical and chain molecules among four SAFT EOS versions, namely: PC-SAFT, CK-SAFT, soft SAFT and simplified SAFT EOSs. It was shown that each SAFT version showed different number of branches, turning points, critical points and molar volume roots for the same component and under the same state conditions. Moreover, adding the chain term resulted also in increasing the number of branches, turning points and molar volume roots.

The mechanical and material stability tests along with the calculation of reduced density were used to select the physical roots and hence the physical branches. The observations of the physical branch in PC-SAFT EOS to be always the upper branch and next middle branch to be independent of pressure have leaded to the idea of "physical lines" which is the proposed solution for multiple molar volume roots problem. This solution leads to the physical branch roots in PC-SAFT EOS without finding all the roots and performing the stability analysis.

7.2 Recommendations

The first recommendation for future work is to extend the analysis used in this thesis to polar and associating molecules to investigate the effect of adding each of these two terms on the number of branches, turning points, critical points and molar volume roots. It is also recommended to investigate the three different polar terms of Chapman, Gross and Economou. The study of the effect of the number of associating sites is also recommended.

The second recommendation is to study long chain molecules like polymers which have large segment number "m" especially for the combination of the physical and next middle branches. This study is very important in order to show the ability of PC-SAFT EOS to give physical solutions for these molecules at low temperature.

The third recommendation is to extend the idea of the physical line for simplified SAFT EOS because of having the same explained behavior in PC-SAFT. Studying more SAFT versions using bifurcation analysis is also recommended so more versions might have the same observed behavior.

The fourth recommendation is to study the state conditions where the physical branch showed three roots. The prior estimation of the number of roots exhibited by the physical branch or even cubic EOSs might be useful for thermodynamic calculations.

REFERENCES

Al-Saifi N.M. (2011) Prediction and Computation of Phase Equilibria in Polar and Polarizable Mixtures Using Theory-based EOSs. The university of British Columbia (Vancouver).

Alder B., Young D., Mark M. (1972) Studies in molecular dynamics. X. Corrections to the augmented van der Waals theory for the square well fluid. The Journal of Chemical Physics 56:3013-3029.

Alsaifi N.M., Englezos P. (2011) Prediction of multiphase equilibrium using the PC-SAFT EOS and simultaneous testing of phase stability. Fluid Phase Equilibria 302:169-178.

Aslam N., Sunol A.K. (2006) Reliable computation of all the density roots of the statistical associating fluid theory EOS through global fixed-point homotopy. Industrial & Engineering Chemistry Research 45:3303-3310.

Barker J.A., Henderson D. (1967) Perturbation theory and EOS for fluids. II. A successful theory of liquids. The Journal of Chemical Physics 47:4714-4721.

Binous H., Shaikh A.A. (2014) Introduction of the arc-length continuation technique in the chemical engineering graduate program at KFUPM. Computer Applications in Engineering Education. DOI: 10.1002/cae.21604.

Blas F.J., Vega L.F. (1997) Thermodynamic behaviour of homonuclear and heteronuclear Lennard-Jones chains with association sites from simulation and theory. Molecular Physics 92:135-150.

Blas F.J., Vega L.F. (1998) Prediction of binary and ternary diagrams using the statistical associating fluid theory (SAFT) EOS. Industrial & Engineering Chemistry Research 37:660-674.

Boyle R. (1772) New experiments physico-mechanicall touching the spring of the air. Oxford 1660:299.

Cameretti L.F., Sadowski G., Mollerup J.M. (2005) Modeling of aqueous electrolyte solutions with perturbed-chain statistical associated fluid theory. Industrial & engineering chemistry research 44:3355-3362.

Carnahan N.F., Starling K.E. (1969) EOS for Nonattracting Rigid Spheres. The Journal of Chemical Physics 51:635. DOI: 10.1063/1.1672048.

Chapman W.G., Jackson G., Gubbins K.E. (1988) Phase equilibria of associating fluids - Chain molecules with multiple bonding sites. Molecular Physics 65:1057.

Chapman W.G., Gubbins K.E., Jackson G.R., M. (1989a) SAFT Equation-of-State Solution Model for Associating Fluids. Fluid Phase Equilibria 52:31-38.

Chapman W.G., Gubbins K.E., Jackson G., Radosz M. (1989b) SAFT: Equation-of-State Solution Model for Associating Fluids. Fluid Phase Equilibria: 31-38.

Chapman W.G., Gubbins K.E., Jackson G., Radosz M. (1990) New reference EOS for associating liquids. Industrial and Engineering Chemistry Research 29:1709.

Donohue M., Prausnitz J. (1978) Perturbed hard chain theory for fluid mixtures: thermodynamic properties for mixtures in natural gas and petroleum technology. AIChE journal 24:849-860.

Economou I.G. (2002) Statistical associating fluid theory: A successful model for the calculation of thermodynamic and phase equilibrium properties of complex fluid mixtures. Industrial & Engineering Chemistry Research 41:953-962.

Economou I.G., Donohue M.D. (1991) Chemical, quasi-chemical and perturbation theories for associating fluids. AIChE journal 37:1875-1894.

Economou I.G., Donohue M.D. (1996) EOSs for hydrogen bonding systems. Fluid Phase Equilibria 116:518-529.

Fu Y.-H., Sandler S.I. (1995) A Simplified SAFT EOS for Associating Compounds and Mixtures. Industrial & Engineering Chemistry Research 34:1897-1909. DOI: 10.1021/ie00044a042.

Ghosh A., Chapman W.G., French R.N. (2003) Gas solubility in hydrocarbons—a SAFT-based approach. Fluid Phase Equilibria 209:229-243.

Gross J., Sadowski G. (2001) Perturbed-Chain SAFT An EOS Based on a Perturbation Theory for Chain Molecules. Industrial & engineering chemistry research 40:1244-1260.

Gross J., Sadowski G. (2002) Modeling Polymer Systems Using the Perturbed-Chain Statistical associating fluid theory EOS. Industrial & engineering chemistry research 41:1084-1093.

Gross J., Spuhl O., Tumakaka F., Sadowski G. (2003) Modeling copolymer systems using the perturbed-chain SAFT EOS. Industrial & engineering chemistry research 42:1266-1274.

Guggenheim E. (1945) Statistical thermodynamics of the surface of a regular solution. Trans. Faraday Soc. 41:150-156.

Haung S., Radosz M. (1990) EOS for Small, Large, Polydisperse, and Associating Molecules. Industrial & Engineering Chemistry Research 29:2284-2294.

Kim C.H., Vimalchand P., Donohue M., Sandler S. (1986) Local composition model for chainlike molecules: a new simplified version of the perturbed hard chain theory. AIChE journal 32:1726-1734.

Koak N., de Loos T.W., Heidemann R.A. (1999) Effect of the power series dispersion term on the pressure-volume behavior of statistical associating fluid theory. Industrial & Engineering Chemistry Research 38:1718-1722.

Kontogeorgis G.M., Folas G.K. (2009) Thermodynamic models for industrial applications: from classical and advanced mixing rules to association theories John Wiley & Sons.

Lafitte T., Apostolakou A., Avendano C., Galindo A., Adjiman C.S., Muller E.A., Jackson G. (2013) Accurate statistical associating fluid theory for chain molecules formed from Mie segments. The Journal of chemical physics 139:154504. DOI: 10.1063/1.4819786.

Lee K.-H., Lombardo M., Sandler S. (1985) The generalized van der Waals partition function. II. Application to the square-well fluid. Fluid Phase Equilibria 21:177-196.

Llovell F., Pàmies J.C., Vega L.F. (2004) Thermodynamic properties of Lennard-Jones chain molecules: Renormalization-group corrections to a modified statistical associating fluid theory. The Journal of Chemical Physics 121:10715-10724.

Lucia A., Luo Q. (2002) Binary refrigerant oil phase equilibrium using the simplified SAFT equation. Advances in Environmental Research 6:123-134.

Muller E.A., Gubbins K.E. (2001) Molecular-Based EOSs for Associating Fluids: A Review of SAFT and Related Approaches. Industrial & engineering chemistry research: 2193-2211.

Panayiotou C., Sanchez I. (1991) Hydrogen bonding in fluids: an equation-of-state approach. The Journal of Physical Chemistry 95:10090-10097.

Peng D.-Y., Robinson D.B. (1976) A new two-constant EOS. Industrial & Engineering Chemistry Fundamentals 15:59-64.

Polishuk I. (2010) About the numerical pitfalls characteristic for SAFT EOS models. Fluid Phase Equilibria 298:67-74.

Polishuk I. (2011) Addressing the issue of numerical pitfalls characteristic for SAFT EOS models. Fluid Phase Equilibria 301:123-129. DOI: 10.1016/j.fluid.2010.11.021.

Polishuk I., Mulero A. (2011) The numerical challenges of SAFT EoS models. Reviews in Chemical Engineering 27. DOI: 10.1515/revce.2011.009.

Privat R., Gani R., Jaubert J.-N. (2010) Are safe results obtained when the PC-SAFT EOS is applied to ordinary pure chemicals? Fluid Phase Equilibria 295:76-92. DOI: 10.1016/j.fluid.2010.03.041.

Ramdharee S., Muzenda E., Belaid M. (2013) A review of the EOSs and their applicability in phase equilibrium modeling, International Conference on Chemical and Environmental Engineering.

Sanchez I.C., Lacombe R.H. (1976) An elementary molecular theory of classical fluids. Pure fluids. The Journal of Physical Chemistry 80:2352-2362.

Sandler S.I. (1993) Models for Thermodynamic and Phase Equilibria Calculations Taylor & Francis.

Sherman A. (2011) Dynamical systems theory in physiology. The Journal of general physiology 138:13-19.

Stewart R.B., Jacobsen R.T. (1989) Thermodynamic properties of argon from the triple point to 1200 K with pressures to 1000 MPa. Journal of Physical and Chemical reference data 18:639-798.

Straty G., Tsumura R. (1976) PVT and vapor pressure measurements on ethane. J. Res. Natl. Bur. Stand. (US) A 80:25.

Tang X., Gross J. (2010) Modeling the phase equilibria of hydrogen sulfide and carbon dioxide in mixture with hydrocarbons and water using the PCP-SAFT EOS. Fluid phase equilibria 293:11-21.

Tumakaka F., Sadowski G. (2004) Application of the perturbed-chain SAFT EOS to polar systems. Fluid phase equilibria 217:233-239.

Valderrama J.O. (2003) The state of the cubic EOSs. Industrial & Engineering Chemistry Research 42:1603-1618.

Vargas F.M., Gonzalez D.L., Hirasaki G.J., Chapman W.G. (2009) Modeling Asphaltene Phase Behavior in Crude Oil Systems Using the Perturbed Chain Form of the

Statistical Associating Fluid Theory (PC-SAFT) EOS†. Energy & Fuels 23:1140-1146.

Wertheim M.S. (1984a) Fluids with Highly Directional Attractive Forces. I. Statistical Thermodynamics. Journal of statistical physics 35:19.

Wertheim M.S. (1984b) Fluids with Highly Directional Attractive Forces. II. Thermodynamic Perturbation Theory and Integral Equations. Journal of statistical physics 35:35.

Wertheim M.S. (1986a) Fluids with Highly Directional Attractive Forces. III. Multiple Attraction Sites. Journal of statistical physics 42:459.

Wertheim M.S. (1986b) Fluids with Highly Directional Attractive Forces. IV. Equilibrium Polymerization. Journal of statistical physics 42:477.

Xu G., Brennecke J.F., Stadtherr M.A. (2002) Reliable Computation of Phase Stability and Equilibrium from the SAFT EOS. Industrial & Engineering Chemistry Research 41:938-952.

Yelash L., Muller M., Paul W., Binder K. (2005) Artificial multiple criticality and phase equilibria: an investigation of the PC-SAFT approach. Physical Chemistry 7:3728-32. DOI: 10.1039/b509101m.

Appendix

Maximum Non-Physical Molar Volume Roots Data

Table A.1 Maximum non-physical molar volume roots for the components listed in Gross and Sadowski (2001).

Component	Maximum Non-Physical Molar Volume Root (cm^3/mol)	Component	Maximum Non-Physical Molar Volume Root (cm^3/mol)
Methane	23.45	**n-Nonadecane**	260.5
Ethane	34.14	**n-Eicosane**	272.4
Propane	47.59	**Isobutane**	61.34
n-Butane	61.12	**Isopentane**	75.27
n-Pentane	76.46	**Neopentane**	74.96
n-Hexane	91.84	**2-methylpentane**	91.53
n-Heptane	104.4	**2,2-dimethylbutane**	87.63
n-Octane	117.0	**2,3-dimethylbutane**	87.80
n-Nonane	129.5	**3-methylpentane**	89.76
n-Decane	142.6	**2-methylhexane**	105.0
n-Undecane	156.1	**Cyclopentane**	62.31
n-Dodecane	169.4	**Cyclohexane**	75.34
n-Tridecane	184.1	**Methylcyclopentane**	76.84
n-Tetradecane	194.6	**Methylcyclohexane**	89.91
n-Pentadecane	209.4	**Ethylcyclopentane**	92.64
n-Hexadecane	221.7	**Ethylcyclohexane**	104.8
n-Heptadecane	234.9	**Ethylene**	31.68
n-Octadecane	246.4	**Propylene**	43.32

Table A.1 (cont.) Maximum non-physical molar volume roots for the components listed in Gross and Sadowski (2001).

Component	Maximum Non-Physical Molar Volume Root (cm^3/mol)	Component	Maximum Non-Physical Molar Volume Root (cm^3/mol)
1-butene	56.63	**Carbon disulfide**	39.25
1-pentene	71.39	**Methyl chloride**	32.43
1-hexene	88.38	**Chloroethane**	46.15
1-octene	112.6	**2-chloropropane**	59.17
Cyclopentene	57.94	**1-chlorobutane**	74.41
Benzene	62.12	**Chlorobenzene**	73.79
Toluene	77.43	**Bromobenzene**	78.67
Ethylbenzene	92.37	**Dimethyl ether**	40.73
m-xylene	92.23	**Diethyl ether**	71.04
o-xylene	91.16	**Methyl-n-propyl ether**	68.28
p-xylene	93.47	**Methyl methanoate**	41.65
n-propylbenzene	103.5	**Ethyl methanoate**	56.69
Tetralin	105.1	**n-propyl methanoate**	69.88
n-butylbenzene	118.7	**Ethyl ethanoate**	69.61
Biphenyl	117.1	**n-propyl ethanoate**	82.38
Carbon monoxide	21.37	**n-butyl ethanoate**	95.95
Nitrogen	20.62	**Isopropyl ethanoate**	82.75
Argon	17.90	**Methyl propanoate**	68.90
Carbon dioxide	22.59	**Ethyl propanoate**	82.04
Sulfur dioxide	29.76	**n-propyl propanoate**	94.57
Chlorine	28.71	**methyl butanoate**	81.52

Vitae

Name	:Isa Ataallah Saeed Al Aslani
Nationality	:Saudi
Date of Birth	:10/8/1989
Email	:al3oslani@gmail.com
Address	:King Fahd University of Petroleum and Minerals
Academic Background	:Chemical Engineering